

POLITECNICO DI TORINO

Master of Science in Nanotechnologies for ICTs

Master Thesis

Molecular-FET based Neuromorphic Circuits



Supervisors

Prof. Mariagrazia Graziano

Prof. Gianluca Piccinini

Dr. Fabrizio Mo

Dr. Chiara Elfi Spano

Dr. Yuri Ardesi

Candidate

Vincenzo Di Lorenzo - 276566

April, 2022

To my grandparents.

"The ever accelerating progress of technology and changes in the mode of human life give the appearance of approaching some essential singularity in the history of the race beyond which human affairs, as we know them, could not continue."

John von Neumann

Acknowledgements

I must thank my supervisors and co-supervisors, who were always available to listen at all my ideas and possible solutions during these months.

Then, I would like to thank my friends, who showed a lot of patience and interest listening to my discussions about these topics.

A special thank goes to my family, which always believed in me and made all of this possible.

Abstract

The concept of "Neuromorphic engineering" was coined by Carver Mead at the end of the last century. The idea was to exploit VLSI systems based on MOSFETs to physically emulate the brain dynamics and computational principles. With the technological advancements, this concept has been extended to other kinds of materials and devices, such as phase-change memories, ferroelectric devices, valence change memories, electrochemical metallization cells, nanowire networks, 2D materials, spintronics, and organic materials. The neuromorphic approach can lead to very low power in-memory computing systems, a big advantage compared to technological limitations at the device and architectural design level nowadays. This thesis work aims to explore a spiking neural network implementation based on the molecular technology: the Molecular Field-Effect Transistor (MolFET). Furthermore, the thesis aims in discussing contributions or alternatives with respect to current VLSI silicon-based architectures. The MolFET is one among the so-called beyond-CMOS technologies, based on the idea that a single-molecule can realize an electronic switch, by controlling the electron flow through applied gate voltages, conceptually similar to conventional FETs.

More in general, acting on the chemical structure of the molecule implementing the channel, it is possible to obtain different $I(V)$ characteristics, opening the way to molecular-based IC (resistors, inductors, capacitances, transistors, and so on).

The first part of this work is dedicated to a brief theoretical recap regarding biological neurons and molecular technology. Among the possibilities, a specific molecular transistor, namely the para-Cyclophane (PCP) -based one, is reviewed in detail. It shows NDR (Negative Differential Resistance), which is widely exploited in the following chapters to implement a spiking neuron. Since the PCP-MolFET, thanks to its NDR, can show hysteretic behaviour, this was studied to be exploited to generate the neuron spikes. In the second chapter, some electronic stages based on this device are presented. The stages have been selected under the perspective of using them in neuromorphic systems. The emerging properties regard non-linear responses, the presence of discrete stable states allowed for the system (attractors) and monostable-bistable transitions. In the last chapter, all the results are used to propose a possible realization for MolFET-based neurons, synapses, and networks.

Contents

List of Tables	10
List of Figures	11
List of acronyms and abbreviations	14
Introduction	16
1 Theoretical Background	17
1.1 Beyond CMOS: The molecular technology	17
1.2 Molecules as electronic devices	18
1.2.1 The Landauer's formula	21
1.2.2 The PCP molecule	25
1.3 Introduction to the biological neuron	29
1.3.1 The equivalent circuit model of Hodgkin and Huxley	30
1.3.2 The generation of the action potential	34
1.3.3 The Integrate and Fire model	36
1.3.4 Dendrites	40
1.3.5 Synapses	43
1.3.6 Neural coding	49
1.3.7 Rate Models	51
2 PCP-based MolFET: analysis and applications	53
2.1 The PCP-based MolFET characteristics	53
2.2 A stage presenting non-linear behaviour	59
2.2.1 The hysteresis loop in the $V_{out}(V_{in})$ curves	63
2.2.2 Observations: parallel and cascade of non-linear stages	67
2.3 PCP MolFETs based TRAM	70
2.4 PCP-based MOBILE	73
2.4.1 MOBILE as threshold mechanism	75
2.5 Conclusion	77

3	Artificial neurons based on PCP MolFETs	79
3.1	Molecular-FET based soma	79
3.1.1	The theoretical K-channel	80
3.1.2	Estimation of the time constant τ	83
3.1.3	Patterns of spikes vs constant injected current	85
3.2	Response to the synaptic injection	88
3.2.1	Spiking synapses	88
3.2.2	Introducing the synaptic response	94
4	Conclusions and future works	99
	Appendices	101
A	Matlab: "Integrate and fire" model	103
B	Matlab: n-type hypothetical molecule used as K-channel and for synaptic injection	109
C	Matlab: p-type hypothetical molecule used for synaptic injection	111
	Bibliography	113

List of Tables

1.1	Nernst potentials associated to different ionic species.	33
-----	--	----

List of Figures

1.1	The structure of a molecular transistor.	20
1.2	Sketch reporting a portion of the transmission spectrum inside a fixed bias window.	24
1.3	OPE chemical structure.	25
1.4	PCP chemical structure.	25
1.5	I-V characteristics of the PCP based MolFET.	28
1.6	The equivalent circuit model describing the soma in the Hodgkin and Huxley model.	30
1.7	A section of the phospholipid bilayer.	30
1.8	Schematic generation of an action potential.	35
1.9	The equivalent circuit of the "Integrate and Fire" model.	36
1.10	The generation of the action potentials with the "Integrate and Fire" model. $I_{in} = 1.05$ nA between $t_1 = 40$ ms and $t_2 = 166.7$ ms, $R_{leak} = 100$ MW, $C = 0.1$ nF, $\tau = 10$ ms, $E_{Leak} = -50$ mV, $V_{th} = 10$ mV, $V_{reset} = -70$ mV.	37
1.11	Frequency - Current curve from the integrate and fire model. $R_{leak} = 100$ MW, $C = 0.1$ nF, $\tau = 10$ ms, $E_{Leak} = -50$ mV, $V_{th} = 10$ mV, $V_{reset} = -70$ mV.	39
1.12	Unit for the finite method analysis modeling the dendritic extension.	40
1.13	Two-compartment model circuit.	43
1.14	Representation of the synaptic cleft structure.	43
1.15	Synaptic implementation.	45
1.16	Continuous estimation of the R(t).	50
1.17	Two neurons communicating.	51
1.18	A perceptron.	52
2.1	PCP-based MolFET I-V characteristics, $V_{DS} > 0$ V and $V_{GS} > 0$ V.	54
2.2	PCP-based MolFET I-V trans-characteristics, $V_{DS} > 0$ V and $V_{GS} > 0$ V.	55
2.3	PCP-based MolFET I-V characteristics, $V_{DS} < 0$ V and $V_{GS} < 0$ V.	56
2.4	PCP-based MolFET I-V characteristics, $V_{GS} > 0$ V.	57
2.5	Stage presenting non-linear behaviour.	59
2.6	Load analysis for the PCP-based molFET.	59

2.7	Non-linear behaviour, $V_{GS}=2\text{ V}$	61
2.8	Non-linear behaviour, $V_{GS}=1\text{ V}$	62
2.9	Hysteresis loop in the I-V characteristics, $V_{GS}=2\text{ V}$ and $R_{in}=1\text{ M}\Omega$	63
2.10	Investigation regarding the load resistance required in order to have the hysteresis in the I-V characteristics.	64
2.11	Hysteresis loop in the non-linear PCP-based stage, $V_{GS}=2\text{ V}$ and $R_{in}=1\text{ M}\Omega$	65
2.12	Analysis during time of the hysteresis.	66
2.13	Parallel of non-linear stages based on PCP.	67
2.14	Cascade of non-linear stages based on PCP.	67
2.15	Multiple thresholds observed for a cascade of non-linear stage.	68
2.16	Hysteresis in multiple thresholds observed for a cascade of non-linear stage.	69
2.17	TRAM stage.	70
2.18	Load analysis using a PCP MolFET as load.	71
2.19	Time analysis: V_C vs time starting from different initial conditions.	72
2.20	MOBILE load analysis.	73
2.21	Results for the MOBILE stage: V_C in red, V_{driver} in purple and V_{bias} in green.	74
2.22	Threshold mechanism using PCP molecules.	75
2.23	Load analysis for the MOBILE threshold mechanism.	76
2.24	Results for the MOBILE threshold mechanism.	77
3.1	Implementation of a soma based on NDR.	79
3.2	Hysteresis of the non-linear stage using $V_{mol}=2\text{ V}$ and $Res_{mol}=2\text{ MW}$	81
3.3	I-V characteristics for the hypothetical molecule implementing the K-channel.	81
3.4	Estimation for the equivalent resistance for the PCP molecule before the current peak, $V_{mol}=V_{GS}=2\text{ V}$	83
3.5	RC charging in time of the proposed neuron using: 1) $0\text{ tA} \leq I_{in} \leq 5\text{ tA}$ 2) $I_{in} = 2\text{ tA}$ (Green = V_{out} , Red= V_C , Pink= I_{DS} of the K-channel).	84
3.6	V_C and spike generation in time, injecting $I_{in}=6\text{ tA}$	85
3.7	Patterns generated using $5.25\text{ tA} < I_{dc} < 6\text{ tA}$	86
3.8	Some patterns generated using $7\text{ tA} < I_{dc} < 12\text{ tA}$	86
3.9	f-I curve.	87
3.10	A simple 3-1 SNN.	88
3.11	p-like version of the I-V characteristics for the hypothetical K-channel.	89
3.12	Response to an injected train of spikes.	90
3.13	Response to two injected trains of spikes.	91
3.14	Global current injected from the two trains of spikes.	92
3.15	Response to three injected trains of spikes, 2 excitatory and 1 inhibitory.	93

3.16	Global current injected from the three trains of spikes, 2 excitatory and 1 inhibitory.	93
3.17	Excitatory and inhibitory synapses showing time dependence.	94
3.18	3-1 SNN exploiting synaptic responses.	95
3.19	Example of excitatory post-synaptic current.	96
3.20	Example of inhibitory post-synaptic current.	96
3.21	Example of output pattern.	97

List of acronyms and abbreviations

NDR	Negative Differential Resistance
VLSI	Very Large Scale Integration
MolFET	Molecular Field Effect Transistor
SNN	Spiking Neural Network
IRDS	International Roadmap for Devices and Systems
SOI	Silicon On Insulator
FinFET	Fin Field Effect Transistor
CMOS	Complementary Metal Oxide Semiconductor
HOMO	Highest Occupied Molecular Orbital
LUMO	Lowest Unoccupied Molecular Orbital
HLG	HOMO-LUMO gap
PCP	ParaCycloPhane[2,2]-based
OPE	OligoPhenylEthylene
DQI	Destructive quantum interference effect
LUT	Look-Up-Table
HH	Hodgkin and Huxley
EPSP	Excitatory post-synaptic potential
EPSC	Excitatory post-synaptic current
IPSP	Inhibitory post-synaptic potential
IPSC	Inhibitory post-synaptic current
IRF	Impulse response function
RTD	Resonant Tunneling Diode
TRAM	Tunneling-based Random Access Memory
MOBILE	Monostable-Bistable Transition Logic Element

Introduction

In recent years, a lot of efforts went into the study of a possible hardware implementation able to physically emulate the brain dynamics. There are many reasons behind this choice ([3]). Brain-machine interfaces could be considered, but also physical tools able to provide information which could be used to better understand the brain itself. One of the main reasons that makes (spiking) neuromorphic computing appealing is the very low power consumption: it is known that the brain consumes only 20 W on average in a very small volume. This is a crucial aspect considering nowadays limitations in terms of electronic devices integration and *von-Neumann bottleneck* [4].

Anytime a computer performs some computations, there is a part dedicated to calculation and another part that stores information related to these calculations: the CPU has to ask to the memory the data it needs, then it sends back the results to the memory after processing. During these steps the data travel along the bus, this is the reason behind high dissipation and delays. The collective behaviour of neurons in handling the information relies instead on the so called "in-memory computing" principle, where two distinct parts for memory and computing are not required, but instead they are coexisting in the same block. Finally, the currently state of the art for artificial intelligence is based on software algorithms. The servers used to train these algorithms are highly power consuming, therefore, having the possibility to train the network in real-time, on specific neuromorphic structures, can lead to big advantages.

The aim of this thesis is to explore a possible implementation based on molecular technology, to discuss contributions or alternatives with respect to current VLSI (Very Large Scale Integration) silicon-based architectures.

All the analysis and simulations have been performed using Matlab and Cadence Virtuoso.

Chapter 1

Theoretical Background

1.1 Beyond CMOS: The molecular technology

Talking about "Nanoelectronics systems", the usual reference is the IRDS (International Roadmap for Devices and Systems) [5]. This is a collection of documents that presents the state of the art of electronic technology, therefore, the reference [5] is the starting point of this discussion. It reports a summary of the three possible ways that try to solve current problems related to technology.

For many years technology relies on keeping the transistors scaling. This has led to faster single devices with lower power consumption, however, a chip normally has tens of billions of devices inside of it. This allows the chip to have so many functionalities, even if the overall dissipated power due to leakage effects increases.

The *More Moore* approach tries to follow the same trend of the last decades, introducing possible solutions to keep the scaling (*The Moore's law*) going on, like SOI or FinFETs.

The *More Than Moore* approach instead focuses on the diversification, so that chips integrating many different functionalities can be obtained. This could include analog parts, sensors, biochips and so on.

The *Beyond CMOS* aims to other solutions that could be even better than the CMOS itself. There is no doubt that MOSFETs and FinFETs are very reliable and known technologies, but this does not mean they are necessarily the best ones. Among the families of devices concerning the *Beyond CMOS* solutions there is the molecular technology, based on conduction in 0D systems, that will be introduced in the following.

1.2 Molecules as electronic devices

The idea is to implement any kind of electronic devices by using specifically designed molecules [8]. Under this perspective many advantages could be highlighted:

- Molecules are intrinsically nanoscaled. This feature leads to very compact devices and systems;
- They can be generated using bottom-up approaches, for example by self-assembly, in which molecules naturally arrange themselves driven by chemical mechanisms;
- In principle, very versatile systems can be obtained, since, by selecting the suitable molecules, particular behaviour can be achieved;
- A molecule could have a fast response to external stimuli;
- The current generated by such devices could be in the order of fraction of μA concerning saturation regime and fraction of nA for leakages. From an electronic point of view this implies small power dissipation.

However, molecular systems are very sensitive to process variability and dependability on what happens in the environment. This is normally considered as a disadvantage, but in the context of neuromorphic circuits it could be interpreted as a feature. For example, in [6] and [7], it is explained how a certain degree of electronic noise in the system can allow the correct Hebbian learning mechanism.

Generally speaking, the sources of variability obtainable for molecular technology can be related to:

- Not perfect connections (between the anchoring groups and the compound or the external electrodes);
- An unwanted torsion for the molecular channel;
- Not perfect compound with respect to the one expected from synthesis;
- Different structure for the molecular channel itself (for example, more molecules connected in between the electrodes instead of just a single one).

These devices are also currently difficult to be manipulated and integrated due to technological aspects, moreover, they have complex behaviour to be modeled and described.

In [8] a review of possible applications for molecular electronics has been presented. For example, the basic idea behind a molecular wire is to have a certain compound connected between two external electrodes, called generally donor and acceptor (in analogy with chemistry), using specific anchoring groups. By applying a certain voltage drop across the electrodes a current flowing through the molecular channel will be observed.

In particular, the anchoring groups are specific compounds used in order to interfacing the molecular channel to the external electrodes. In fact, it is very difficult to have the molecule itself directly connected to the electrodes since the compound could not present at the same time the desired characteristics for the conduction and the optimal chemical bonds with the electrodes: this requires to technologically adapt the donor and the acceptor to the molecule. The presence of the anchoring group will have an influence: they have not just a mechanical-chemical role in terms of connections, but they also affect the interaction in terms of current flowing into the channel.

Regarding the molecular channel, a lot of factors can influence the conduction: for example its chemical specie, its length and a possible torsion or rotation between the anchoring groups.

Apart from external influence given by the voltage drop across the electrodes, direct influence on the molecular channel can also be achieved. This is reflected in changes in its behaviour, concerning both the amount and the type of transport. Depending on this, different kind of devices can be designed, such as sensors (for example due to the chemical interaction with some environment) and transistors (for example using a gate electrode). A transistor like this is known as MolFET (Molecular-FET). It is important to notice that, in principle, more effects could be present in the same device. Concerning neuromorphic application, the capacitor is another important device, since it can be used to model the neuron lipid bilayer present in the soma, dendrites and axon. Moreover, it allows to introduce temporal dynamics.

It has to be mentioned that also memristive behaviours have been observed in molecular devices ([9],[10]). Even if this work does not involve the usage of memristors, these devices are considered crucial in order to develop bio-inspired synapses for low power and high integration density VLSI neuromorphic circuits.

Molecular transistors

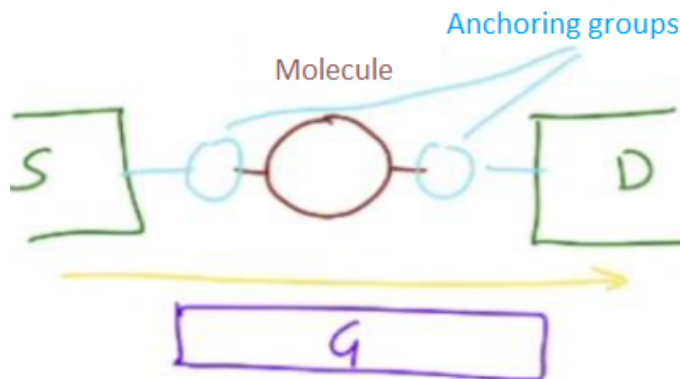


Figure 1.1. The structure of a molecular transistor.

Fig.1.1 shows a sketch of the typical structure of a MolFET. Two electrodes typically made of gold (source and drain, in association with the normal transistor), have in between the molecule making the channel. The molecule is anchored to the electrodes through the anchoring groups exploiting Au-S covalent bonds, which ensure the absence of hopping transport: the transmission of electrons between the electrodes is coherent due to the delocalization introduced by π orbitals. Such coupling is also referred as "strong coupling", a "weak coupling" instead would involve also hopping transport, therefore transport between localized molecular orbitals. Resonant molecules such as Benzene are very important in this context, they allow to have fully delocalized molecular orbitals in which electrons can be shared. This enhances the conduction, making these molecules very important for such technology.

By using gate electrode, the behaviour of the whole system can be changed. As a consequence, also the current. However, the mechanism for the conduction does not change.

The conduction for 0D systems could be explained, in principle, by exploiting a square well approximation. This can allow to have information about the energy levels offered by the molecular channel. However, this does not provide accurate values since a molecule is an arrangement of few atoms, which is not suitable with the square well hypothesis. For this reason, physical ab-initio simulations are used to get information about the allowed energy levels associated to the molecular orbitals with high precision. Then, once a precise estimation for the levels is obtained, they will be used with the model in order to estimate the current passing through the device.

Concerning a molecule, HOMO levels (highest occupied molecular orbital) and LUMO levels (lowest unoccupied molecular orbital) have respectively the role of the valence band and the conduction band considering a solid state analogy. In terms of energy, these levels are separated by the HLG (HOMO-LUMO gap). This is the minimum

energy required from an electron in order to be able to go into a LUMO level starting from a HOMO level. The fact that electrons can be able to go to LUMO levels from HOMO ones is behind the possibility of having conduction inside a molecule. Depending on the HLG, each molecule can present neither conduction or not: the smaller the HLG is, the easier will be the conduction.

1.2.1 The Landauer's formula

The aim of this thesis is not to derive the model used for molecular conduction, therefore only few important results will be presented and commented, however [11] is suggested to get more details about it. The 1.1 refers to the current passing through a dot having a single energy level E_L .

$$I_{DS} = \frac{2q\gamma_1\gamma_2[f(E_L, E_{FS}) - f(E_L, E_{FD})]}{\hbar(\gamma_1 + \gamma_2)} \quad (1.1)$$

q is the electron charge, \hbar is the reduced Planck's constant. This equation considers the difference between the Fermi distributions at the source and drain contacts, with respect to the considered molecular energy level. This difference implies that the current is different from zero only if E_L is between E_{FS} (the Fermi energy at source contact) and E_{FD} (the Fermi energy at drain contact). The energy difference between the two Fermi levels is called "Bias window" and it increases with V_{DS} since $E_{FD} - E_{FS} = -qV_{DS}$, therefore, the E_L must be inside this window to allow the molecule to conduct. If $V_{DS} > 0$ then $E_{FS} > E_{FD}$ and so the electrons will flow from the source to the drain through the energy level E_L . If instead, $V_{DS} < 0$ then $E_{FS} < E_{FD}$, therefore the bias window will still open but the electrons will flow from the drain to the source. The two γ factors specify the strength for the interactions between the considered energy level and the two contacts. Each γ factor is related to a parameter τ called "Escape time" through

$$\gamma = \frac{\hbar}{\tau} \quad (1.2)$$

The escape time expresses the time required for an electron to cross the interface between the related contact and the molecule. This can be seen also as the time required for an electron in the dot to go into the relative electrode. The γ factors are called "Coupling factors", it is clear that the more τ is small and the more the γ will be high. When the γ values are high then it is easier for an electron to move from the relative electrode to the dot and vice versa since the transit times will be very small.

In order to have a generalization for the 1.1 to more energy levels, some density of states is required. $D_{EL}(E)$ can be thought as the description of how E_L is distributed in terms of energy. This is an essential element to have the so called "Transmission

function" $T(E)$ for this specific energy level E_L . In particular:

$$T_{EL}(E) = \frac{\gamma_1 \gamma_2}{\gamma_1 + \gamma_2} D_{EL}(E) \quad (1.3)$$

It is important to remark that these coupling factors are specific for this energy level, with respect to the contacts. In 1.3, E is the electron energy. In particular, if an electron is placed in the discrete level E_L in strong coupling condition, the probability to find it inside the dot will decrease exponentially with time, since it can easily move from the energy level of the dot towards the electrodes. $D_{EL}(E)$ can be defined considering the Fourier transform of the square modulus $|\psi|^2$, where ψ is the wavefunction of the electron. This provides a Lorentzian distribution whose shape depends on how fast is the decay, therefore on the quality of the interaction between the electron and the electrodes.

$$\begin{cases} D_{EL}(E) = \frac{\gamma_{E_L}/(2\pi)}{(E-E_L)^2+(\gamma_{E_L}/2)^2} \\ \gamma_{E_L} = \gamma_1 + \gamma_2 \end{cases} \quad (1.4)$$

A very fast decay corresponds to a quite broad distribution, if instead the decay is slow, then the distribution is narrower. This model in literature is reported as "Broadening of levels", is a very important phenomenon in conduction and basically it is related to the time-energy uncertainty principle. Finally, it can be noticed that if the coupling is low then γ_{E_L} will be small and so the Lorentzian distribution can approximate quite well a delta function, whereas, if the coupling is high, then also broadening effect will have to be considered (this basically depends on the type of technology that is used to connect the dot with the electrodes).

It is easy to extend all of this in the case in which more molecular energy levels are present, in fact, the complete transmission spectrum is the sum of the transmission spectra related to each energy level.

$$T(E) = \sum T_{EL_i}(E) \quad (1.5)$$

There may be different technological aspects influencing the molecular transmission spectrum:

- The length of the molecule used as channel: by adding more resonating molecules to the chain more delocalized π states will be present, this implies more available electrons and so the HLG will reduce. Moreover, as the chain increases, the increased charge inside the molecular orbitals will lead to a shift toward lower energies of the energy peaks. These peaks will result smaller in amplitude since the contacts will be more far away from each other, implying less coupling between the molecules, the anchoring groups and the electrodes. The electrons will find more difficulties to flow in the molecular system, therefore, the overall final situation will depend on the particular case;

- The possibility to have a torsion for the molecule: this introduces a discontinuity in the π bonds due to a misalignment of the molecular orbitals, which implies an impact on the coupling. A rotation of the π bonds will lead to less delocalization which implies more difficulties for the electrons to pass through the molecule;
- The anchoring groups used to connect the channel to the external electrodes: this is due to the difference between the electronegativity of the molecule and the used anchoring group. An atom with high electronegativity tends to attract electrons to it, this reflects in a electronic trap at the extreme of the molecule, so that less electrons will be able to go in. Moreover, the electronic charge which is accumulated at the anchoring groups will produce a potential barrier for other electrons injected from the electrodes.

All the effects from external and direct influences can be gathered as a net energy shift $T(E-U)$ of the complete transmission spectrum.

$$U = U_{V_{DS}} + U_{V_{GS}} + U_{V_{BG}} + U_{CH} \quad (1.6)$$

In 1.6 the main possible types of influences for a MolFET are reported.

- $U_{V_{DS}}$ corresponds to the contribution due to the applied V_{DS} (therefore, V_{DS} opens the bias window but at the same time shifts the transmission spectrum). This can be estimated by exploiting a capacitive model of the quantum dot:

$$U_{V_{DS}} = -q \frac{C_D}{C_S + C_D + C_G + C_{BG}} V_{DS} = -q \frac{C_D}{C_{ES}} V_{DS} = -q\eta V_{DS} \quad (1.7)$$

where q is the electron charge, C_i are the capacitances associated to each contact i and C_{ES} is just the sum of them, called "Electrostatic capacitance". The η factor is called "Voltage division factor" and it indicates the portion of V_{DS} dropping on the drain contact.

It has to be specified that such kind of shift induces also a deformation of the amplitudes of the peaks which is not taking into account in this model, however, simulation tools such as EE-BESD take care of this aspect by exploiting the results provided by ab-initio simulators [12];

- $U_{V_{GS}}$ is the contribution to the shift of the spectrum due to the applied V_{GS}

$$U_{V_{GS}} = -q \frac{C_G}{C_{ES}} V_{GS} = -q\alpha V_{GS} \quad (1.8)$$

$\alpha = \frac{C_G}{C_{ES}}$ in 1.8 is known as "Alpha coupling factor";

- $U_{V_{BG}}$ is the contribution due to a voltage V_{BG} , applied to a second gate, called "Back gate"

$$U_{V_{BG}} = -q \frac{C_{BG}}{C_{ES}} V_{BG} = -q\beta V_{GS} \quad (1.9)$$

$\beta = \frac{C_{BG}}{C_{ES}}$ in 1.9 is known as "Beta coupling factor", basically this electrode is used in order to introduce a sort of offset for V_{GS} ;

- U_{CH} is the contribution due to the so called "Charging effect". This is related to the fact that, when a molecular energy level is used to conduct, the number of hosted electrons inside the dot will change. As a consequence, the whole potential energy of the molecular system will also change. The contribution of the energy shift induced by this phenomenon is to prevent the system to conduct, since the energy levels will be pushed away from the bias window as they approach it. In order to be able to evaluate the right positions for the energy levels, such shifts have to be taken into account using a self-consistent method. This is because the number of electrons N hosted by the molecular levels depends on the potential energy U , but U depends also on N through $U_{CH}=U_0(N-N_0)$ where U_0 is the charging potential due to a single electron.

Summarizing this simple model, once U is found, $T(E-U)$ can be obtained through the molecular transmission spectrum provided by the physical ab-initio results.

It can be used to calculate the current passing into the molecular channel as:

$$I_{DS} = \frac{2q}{\hbar} \int_{-\infty}^{\infty} T(E - U)[f(E, E_{FS}) - f(E, E_{FD})] dE \quad (1.10)$$

The equation 1.10 means that the current is proportional to the integral over the full transmission spectrum of the molecule, shifted by the energy term U , multiplied by the term describing the bias window.

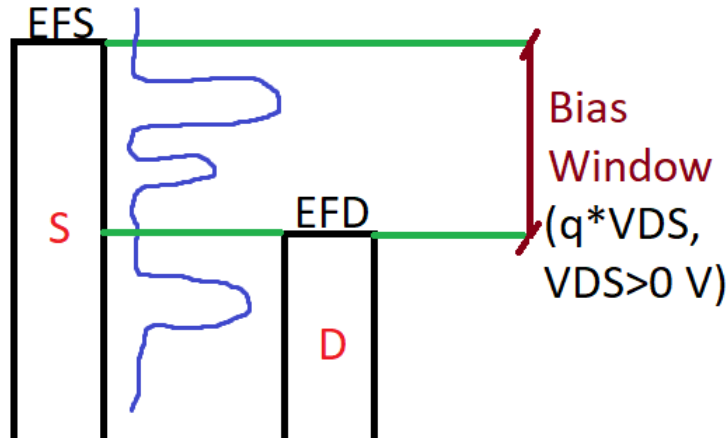


Figure 1.2. Sketch reporting a portion of the transmission spectrum inside a fixed bias window.

Only the portion of the spectrum inside the bias window will mainly contribute to the current (neglecting the tails of the Fermi functions at the contacts). In the example reported in figure 1.2 a positive V_{DS} is used: electrons will flow from source to drain

and a certain I_{DS} will be observed. In particular, the blue curve represents the energy distributed transmission spectrum of the molecule.

Since $E_{FD} - E_{FS} = -qV_{DS}$, the bias window will have amplitude qV_{DS} , $E_{FS} > E_{FD}$ since $V_{DS} > 0$ V.

1.2.2 The PCP molecule

This section is dedicated to the presentation of the ParaCycloPhane[3,3]-based, also known as PCP. It is based on OligoPhenylEthylene, also known as OPE, quite used in the field of molecular electronics.

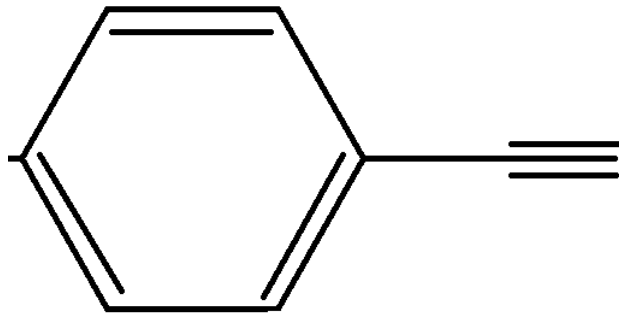


Figure 1.3. OPE chemical structure.

The HLG for OPE is around 3.5 eV, figure 1.3 reports its symbol. It is composed by a Phenylen molecule bonded to a Ethynylene molecule.

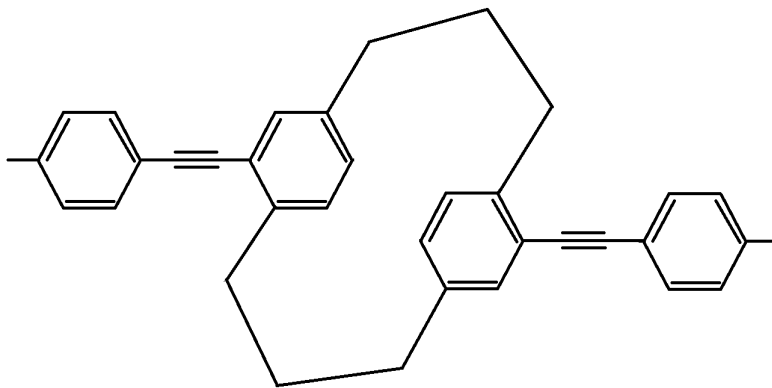


Figure 1.4. PCP chemical structure.

The PCP is made by a chain having two OPE and a block in the middle, based on two Phenyls connected by three molecules of Methylene ($-CH_2-$).

Each connection between the Phenyls in the middle block is also called "Bridge". In this case, having a chain of three molecules of Methylene as each bridge, the notation [3,3] in the full name of the PCP is added. These two molecules of Phenyl are facing each other in the 3D space. This implies a coupling between the delocalized π orbitals, one on top of the first Phenyl and the other on the bottom of the second one. Since the two Methylene bridges are saturated, the only path electrons have for passing from one electrode to the other is through the superposition of the two π states.

This path is interrupted by the so called DQI ("Destructive quantum interference effect", see [13]), generated for some energies by the interaction between the paths given by the bridge and the π orbitals overlap: this is translated in a relevant reduction of the transmission spectrum, which limits drastically the current passing through the PCP. Due to DQI high ratio I_{ON}/I_{OFF} are obtainable exploiting PCP molecule, which makes them good candidates for implementing CMOS logic circuits.

Another interesting thing related to the PCP is that its I-V characteristics present a NDR (Negative Differential Resistance). This is due to the distortion of the transmission spectrum related to the shift induced by the applied V_{DS} , jointly with the charging effect. What happens is that, because of the energy distribution of the molecular levels, as the bias window increases, the current will increase, but the energy levels will also tend to "escape" from it. Once the applied V_{DS} is enough to allow the energy levels to shift outside the bias window, the current will drop abruptly.

PCP modeling and characterization

This thesis has its basis on the study performed by the VLSI group of the Electronics and Telecommunication department (DET) at Polytechnic of Turin, which supervises it. In [2], the methodological description used to obtain the I-V characteristic for the PCP based MolFET has been reported and explained.

Using QuantumATK (a semi-empirical physical ab-initio simulation) and the Extended Hückel Theory, the authors were able to extract the I-V molecular characteristics. In particular, QuantumATK is able to compute the I_{DS} current through eq. 1.10 once the geometry and the applied voltages (both V_{DS} and V_{GS}) have been specified. This is performed by a Self-Consistent Field loop, that considers quantum transport coupled with electrostatics. The transmission function 1.5 is derived by this tool exploiting the Non-Equilibrium Green's function method.

The results have been gathered into a Look-Up-Table (LUT) in order to create a proper symbol in Cadence Virtuoso environment, describing each MolFET with VerilogA. Finally, in order to consider the dynamic behaviour of the PCP, this static model based on LUT has been improved introducing proper electrostatic capacitances and escape times as discussed in the previous section, associated to the correspondent metal contact.

- The capacitance C_G is evaluated from the parallel plate approximation, R_G is associated to the total resistance of the gate dielectric;
- The capacitances C_S and C_D are estimated as electrostatic capacitances taking into account the low number of electronic states available for a molecular channel. The electronic state filling can be considered through a quantum contribution to the electrostatic capacitances, called "quantum capacitance" C_q . Once it is known, C_S and C_D can be computed according to the definition $C = \frac{\partial Q}{\partial V}$, considering the charge inside the molecular channel. The escape times are linked to them by

$$R_i = \frac{\tau_i}{C_i}$$

from which it is possible to get an approximation for R_S and R_D .

A Cadence Virtuoso symbol, using the data stored in the LUT and the parameters related to the dynamic behaviour, can be implemented by positioning the proper parallel RC branch at each contact of the MolFET as described in [11].

This work will use the static model of the presented molecule.

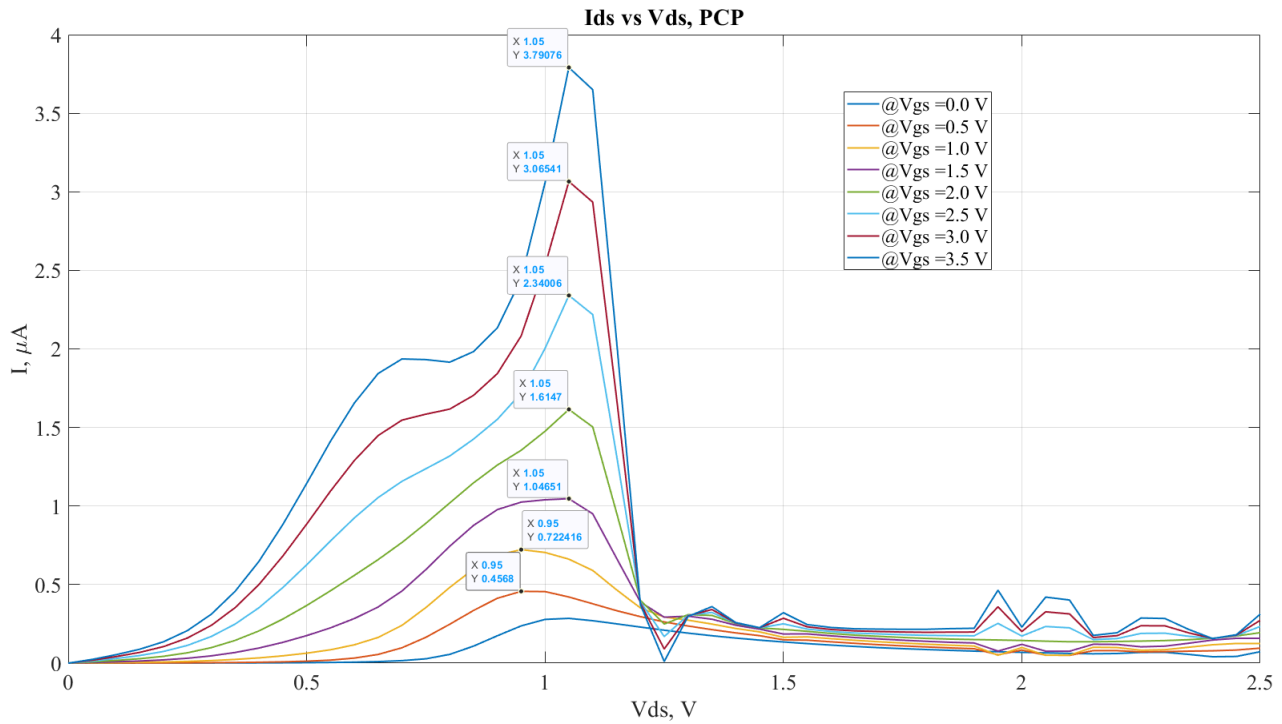


Figure 1.5. I-V characteristics of the PCP based MolFET.

In figure 1.5 the static I-V characteristics of the discussed PCP based MolFET have been reported. This result will be reconsidered and well discussed in successive sections, however, it is important to notice the NDR behaviour due to the escaping of the energy levels from the bias window as the applied potential increases. This will have a crucial application for the proposed molecular neuron, and actually, it is the reason driving this thesis work.

1.3 Introduction to the biological neuron

Once the technological aspects have been introduced, an overview about biological neurons and dynamics is needed in order to understand how it could be possible to employ molecules (and in particular the PCP) to reproduce, at least, some of the properties these systems exhibit. The full theoretical part which is described in this chapter involves concepts coming from [15] and [14].

In this chapter a bottom-up approach will be adopted, the aim is to propose a model for the neuron so that an implementation using electronic components will be suitable. The model which is considered the most biological plausible in neuroscience, is the Hodgkin and Huxley (HH) one. Its description makes use of electrical component to describe the biological neuron, therefore, this is an approach which considers the building of a neuron starting from more basic electronic device instead of thinking about having a single device implementing neural dynamics.

The difficulty in talking about neurons is that there is not just one type, but many different neurons exist. Each class of neurons differ from the other because of the ionic channels they have. These control the flow of current across the cell membrane of the neuron, making possible for it to generate a spike because of the difference in voltage, induced from the charge associated to the ions diffusing through the membrane. Each ionic channel has its own timescale, I-V characteristics, voltage range in which they are sensible: this gives an idea of how much complicate can be thinking about replicating even a single neuron since its behaviour will depend on the collective action of all these ionic channels.

Neuroscience is a very active area in implementing neuromorphic circuits. CMOS implementations, for example, are not just inspired on real effects coming from this area, but really try to physically emulate neurons exploiting sub-threshold regime, which is governed by carriers diffusing into the channel [18]. From the point of view of replicating just the computational principles, the role of molecular technology could bring an important contribution. As discussed in previous section, it is possible, in principle, to obtain any kind of I-V characteristics just synthesizing the right molecule to be used as MolFET. This could be a strategy in order to try to replicate particular I-V behaviour of real ionic channel, without the constrain of use complicated traditional MOSFET architectures. However, it would require a lot of research and effort that a simple master thesis cannot sustain.

The problem becomes even bigger if the physical morphology and extension of the neurons is taken into consideration. It is known that different kind of firing pattern can be obtain by stimulating a neuron (burst, tonic, adapting, and so on) and this depends also on the dendritic extension in the real space.

1.3.1 The equivalent circuit model of Hodgkin and Huxley

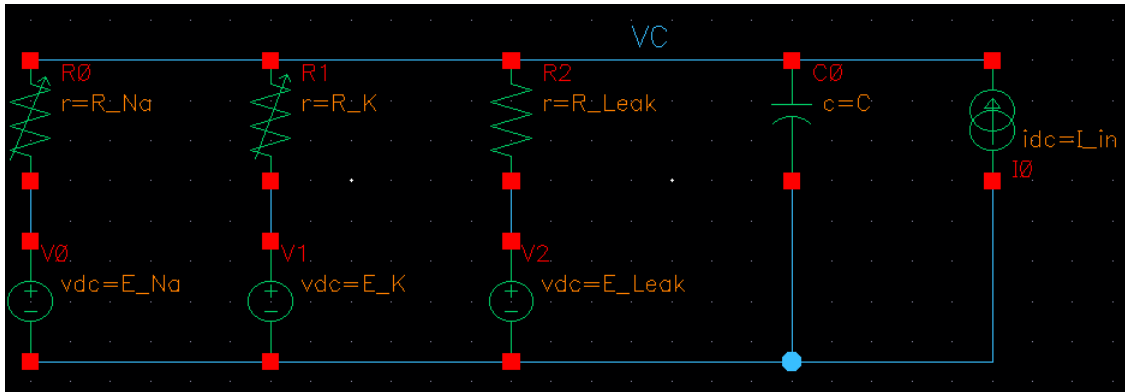


Figure 1.6. The equivalent circuit model describing the soma in the Hodgkin and Huxley model.

Hodgkin and Huxley focused on the study of the squid giant axon in order to understand how neurons generate action potentials, thanks to the interaction of all these different components. In particular, the circuit in figure 1.6 refers just to the soma of the neuron, its nucleus, where the charge is integrated in order to generate a spike. Initially all the dendritic part will be not considered (inside of it the signals propagate until they reach the soma), exactly as the axon (where the generated action potentials propagate to other neurons) and all the synaptic dynamics.

The phospholipid bilayer

The soma can be imagined as a spherical shell made by an insulating organic material, a phospholipid bilayer.

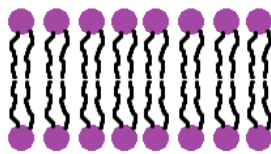


Figure 1.7. A section of the phospholipid bilayer.

Phospholipids are molecules having a polar head on one side a non-polar tail on the other one, this causes the tails of these molecules to be in contact with each other since the whole structure is immersed in a saline solution. These molecules are closely packed together, which avoid ions to pass through the membrane. It is about 23 \AA across. It can be seen as a capacitor separating the outer saline solution from the inner one: this justifies the presence of C in the equivalent circuit in fig.1.6.

The node V_C in particular is referring to the inner part of the neuron, whereas the

bottom common node is referring to the external part. This means that the voltage V_C is the voltage difference between the inside and the outside of the cell, it is called "Membrane Potential". This also means that the current source that connects the outside of the cell to the inside of the cell is injecting charge inside of the neuron. Here comes the first important role of the neuron, leading to the generation of the action potential: the temporal integration of the injected charge.

Leak membrane ionic current

The phospholipid bilayer is not fully insulating, some paths are allowed for the ions to flow from the inside to the outside of the neuron, continuously. The current which is generated in this way is called "Leak current" and it can be modeled using a resistance. Neglecting all the batteries (which will be introduced talking about Nernst potentials) and the variable resistors, an easy first order dynamic circuit is obtained.

$$V_C + R_{Leak}C \frac{\partial V_C}{\partial t} = R_{Leak}I_{in} \quad (1.11)$$

The time constant for such RC circuit is given by $\tau = R_{Leak}C$, the neuron just integrates the inputs over time having a certain leakage in the meanwhile. Having a constant current as input, the solution of the 1.11 is:

$$V_C(t) = (V_C(t_0) - I_{in}R_{Leak})e^{-\frac{t-t_0}{\tau}} + I_{in}R_{Leak} \quad (1.12)$$

As usual, the 1.12 indicates relaxation towards some steady state given by $I_{in}R_{Leak}$. The neuron acts like a filter, it can well respond to inputs slower than τ , so that it has time to relax, but not to inputs which are faster than τ . For this reason, texts refers to the neuron as a low pass filter, and this is its second role.

When the input is a constant current the capacitance keeps integrating, increasing its V_C . In the meanwhile, the leak resistance conducts a current which is proportional to V_C , and so, there will be a time for which a saturation for this voltage drop will be observed. This value V_C has to be enough in order to trigger the mechanism for the action potential generation.

In well-designed neuromorphic circuits, this τ should be around 10 ms in order to be similar to the biological one. This allows to correctly describe the temporal dynamic of biological neurons. Moreover, this is a property only of the membrane.

Considering that $4-5\tau$ are needed in order to reach the steady state, the frequency involved in generating the action potentials results to be in the order of Hz.

Nernst Potentials

Here follows the implementations of the batteries in figure 1.6.

These are needed in order to allow the neuron to change its voltage V_C through the action of the ionic channels. In particular, ionic channels can be seen as voltage-controlled conductances, which connect these batteries to the inner side of the neuron at different times: this is the mechanism behind the generation of an action potential. The reasons why such batteries are present are essentially two:

- The presence of ion-selective channels: these are ionic channels that allow only specific ionic species to pass through them;
- The presence of a concentration gradient between the inside and the outside of the neuron, regarding the specific ionic species allowed to pass through the channel.

What happens is that some ionic charges are able to diffuse from one side of the membrane to the other side. This generates a voltage drop across the phospholipid bilayer which tends to be a barrier for further ionic diffusion. The diffusion process stops when this voltage difference reaches a certain constant value, that's called "Equilibrium Potential" or "Nernst Potential".

This can be modeled using a battery in series to the specific ionic channel it refers to.

In order to derive the value for the Nernst potential, the Boltzmann equation can be used. The probability an ion has to be in a energy state E is proportional to $e^{-\frac{E}{k_B T}}$ where k_B is the Boltzmann constant and T is the temperature.

Considering an ion with charge q in a static electric field, the energy becomes

$E(x) = qu(x)$, where $u(x)$ is the potential at position x . This means that the relation between the probability to find the ion in two different points is:

$$\frac{P(x_1)}{P(x_2)} = \exp\left(-\frac{qu(x_1) - qu(x_2)}{k_B T}\right) \quad (1.13)$$

Due to the huge number of ions, the $P(x)$ may be interpreted as the density of ions at position x , $n(x)$. Secondly, it can be noticed that since $n(x) \propto \exp\left(-\frac{qu(x)}{k_B T}\right)$, if $q > 0$ (as in the case for K^+ and Na^+) then the concentration will be higher where the potential is lower. Therefore, there will be a region with higher potential having less ions, and a region with lower potential having more ions. Associating x_1 to the inner part of the phospholipid bilayer and x_2 as the outer one, from 1.13 follows:

$$\frac{n_{in}}{n_{out}} = \exp\left(-\frac{qV_{in} - qV_{out}}{k_B T}\right) \quad (1.14)$$

From which the voltage difference ΔV after the diffusion can be obtained.

$$\Delta V = V_{in} - V_{out} = \frac{k_B T}{q} \ln \frac{n_{out}}{n_{in}} \quad (1.15)$$

The equation 1.15 refers to the Nernst potential that can be used as voltage for the batteries in the HH model. Considering a single ionic channel at the time, with $T=300$ K, and so $\frac{k_B T}{q}=25$ mV, the results in table 1.1 can be obtained.

Table 1.1. Nernst potentials associated to different ionic species.

Ion	Inner concentration (mmol)	Outer concentration (mmol)	Nernst Potential (mV)
K^+	400	20	-75
Na^+	50	440	55

The meaning of table 1.1 is that when the potassium ionic channel opens, potassium ions will diffuse out of the membrane bringing the voltage drop on it to -75 mV. Also, when sodium ionic channel opens, sodium ions will diffuse in, bringing the voltage drop on the membrane to 55 mV.

These results are the ones obtained by HH studying the giant squid axon, but also for mammalian neurons holds $n_{in} \ll n_{out}$ concerning Na^+ and $n_{in} \gg n_{out}$ concerning K^+ . Moreover, they have been calculated by supposing to have just one kind of ionic channel. In real cells, different kind of ionic channels are simultaneously present and all of them contributes to V_C : this could be kept into account by the more rigorous Goldman equation. It turns out that the neuron has a certain resting potential u_{rest} with a value in between E_K and E_{Na} . This happens in steady state, its value is determined by the equilibrium between the different currents. In figure 1.6, this can be related to E_{Leak} and it results to be -50 mV.

In order to understand the effect of these batteries, a single branch of the circuit in figure 1.6 can be considered. For sake of simplicity, the one having constant conductance can be chosen. Using Kirchhoff's law for the currents:

$$G_{Leak}(V_C - E_{Leak}) + C \frac{\partial V_C}{\partial t} = I_{in} \quad (1.16)$$

Where the quantity $(V_C - E_{Leak})$ is also called "Driving potential" since it basically drives the current passing through the channel (non-selective in this case).

Of course, $G_{Leak} = R_{Leak}^{-1}$.

In presence of constant current, the solution of the equation 1.16 is:

$$V_C(t) = (V_C(t_0) - (E_{Leak} + I_{in} R_{Leak})) e^{-\frac{t-t_0}{\tau}} + (E_{Leak} + I_{in} R_{Leak}) \quad (1.17)$$

Where again, $\tau = R_{Leak} C$. The equation 1.17 is formally equal to the equation 1.12, but this time the steady state takes into consideration also the Nernst potential.

1.3.2 The generation of the action potential

The behaviour of the voltage-controlled time dependent ionic conductances can now be introduced.

Referring again to the figure 1.6, three different conductances can be noticed. A leak resistance R_{Leak} connects the soma to the resting potential, which is the reversal potential E_L , then also the variable sodium and potassium conductances are present, R_{Na} and R_K , connected respectively to E_{Na} and E_K .

Both of them are dependent on time and voltage, in particular, the I-V characteristics are describing the current passing through them as a function of time, once V_C is fixed. The total membrane current is just the sum of all the currents passing through these resistances.

$$\begin{cases} I_m(t) + C \frac{\partial V_C(t)}{\partial t} = I_{in}(t) \\ I_m = I_{Na} + I_K + I_{Leak} \\ I_{Na} = G_{Na}(V_C, t)(V_C - E_{Na}) \\ I_K = G_K(V_C, t)(V_C - E_K) \\ I_{Leak} = G_{leak}(V_C - E_{Leak}) \end{cases} \quad (1.18)$$

From the system reported in 1.18 a qualitative idea about the mechanism generating a spike can be obtained.

1. Initially, both I_K and I_{Na} are very low, in particular $V_C = u_{rest} = E_{Leak}$. This is due to the relaxation through R_{Leak} . In this condition, the neuron is referred as "Polarized", which means that it is inactive.
2. In someway, a certain current is injected into the soma (by an external electrode or through synapses). V_C increases and this is called "Depolarization". The behaviour of I_{Na} with respect to V_C presents a peak, whereas I_K presents a more linear characteristics. Actually, the membrane capacitance is initially charged towards E_{Na} because of this peak.
3. Keeping V_C increasing, I_K increases whereas I_{Na} decreases. In this situation, the capacitance is connected to E_K : V_C decreases again, and this is called "Repolarization", until it becomes negative. Once E_K is approached by V_C , the neuron is referred as "Hyperpolarized", since the potassium reversal potential is lesser than E_{Leak} .
4. At this point both I_{Na} and I_K are very low, therefore V_C can relax again towards E_{Leak} . The time needed to reach the resting potential, starting from the potassium reversal potential, is called "Refractory period". This ensures the impossibility for the generation of further action potentials until the transient ends, since the neuron cannot respond to any incoming stimuli during this time.

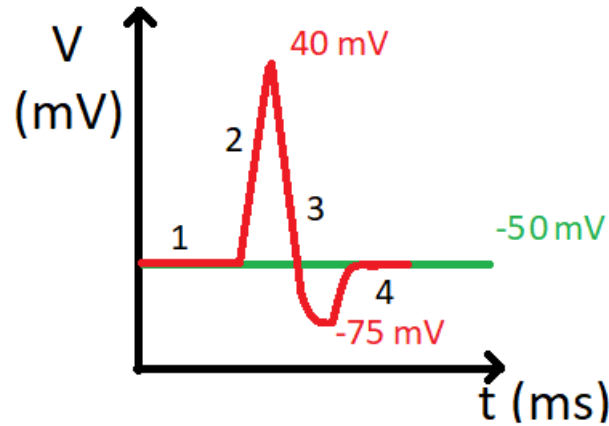


Figure 1.8. Schematic generation of an action potential.

The joint actions of these channels is to produce a spike, having the positive peak around 30-40 mV and the negative peak around -75 mV. This is the generated action potential that will propagate into the axon, impinging on the synapses connecting the axon to the afterwise neurons.

It can be noticed from the system 1.18 that V_C depends on the currents, but the currents depend also on V_C through the ionic conductances. This requires to solve the model using an iterative loop, so that the evolution in time can be observed. Biophysically speaking, the conductances $G_{Na}(V_C, t)$ and $G_K(V_C, t)$ depend on some parameters (voltage dependent) which will be not described here, however, these have been fitted by HH on real experiments keeping into account the precise biological stochastic mechanism used by the ionic channel to open.

For what concerns this work, the important point that has to be highlighted is that, when a certain V_C is reached, one ionic channel starts the mechanism described previously. This establishes a sort of threshold, even if the model of HH doesn't seem to refer to it explicitly, but it is "contained" in the system of equations 1.18.

Once the first ionic channel is activated, the second ionic channel starts to conduct, and when this happens it has to discharge the capacitance so that V_C is reset.

In literature, different kind of electronic devices have been used to replicate the ionic channel behaviour. For example, [16] and [17] explain how memristors could be involved, but also classic CMOS circuits ([18]).

1.3.3 The Integrate and Fire model

In order to simplify the biophysical model proposed by Hodgkin and Huxley, some considerations can be made. There is no doubt that the generation of the action potentials is important, since it allows neurons to communicate each other while performing data compression during time. In fact, the biological neuron spends most of its time at rest, integrating the inputs (analog behaviour), then it fires when needed (digital behaviour).

The most basic "Integrate and Fire" model is based on the idea that what really matters for the information is the presence of the spikes, which are seen just as discrete events at specific times. In particular, the approximation which is introduced regards the presence of a threshold mechanism. This takes into account a sort of equivalent membrane potential V_{th} , for which the mechanism described in the HH framework is triggered. This is also called "Spike threshold".

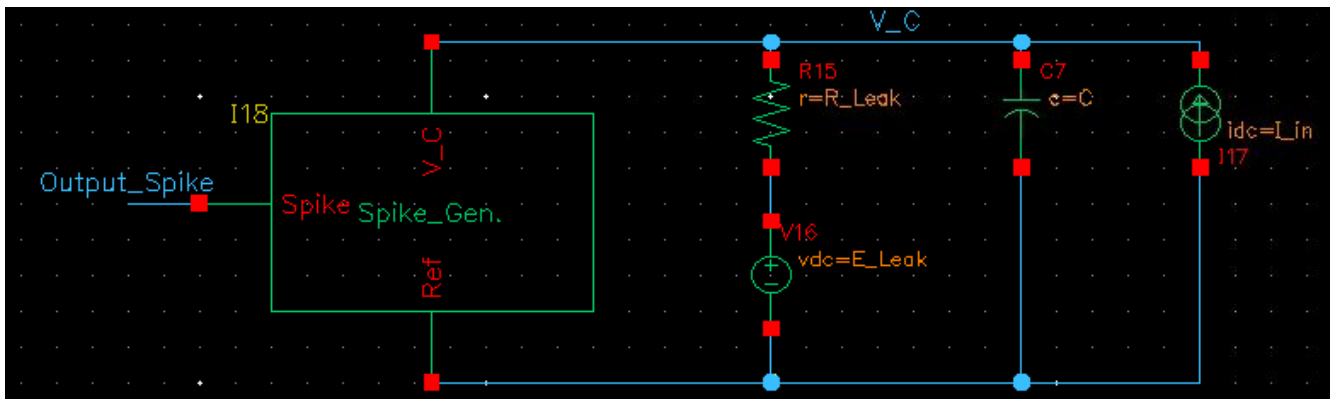


Figure 1.9. The equivalent circuit of the "Integrate and Fire" model.

In fig.1.9 the complex dynamics concerning the ionic channels bringing to the generation of the action potential, described in the previous section, has been substituted with a black box called "Spike generator". The role of the spike generator is just to generate a spike, an event, when the voltage V_C reaches the spike threshold V_{th} , then it has to reset V_C to a value V_{reset} . This is a very simplified version of the HH model, where V_{th} could be associated to the voltage required for the sodium channel to start the spike generation, whereas V_{reset} could be associated to the Nernst potential of the potassium channel.

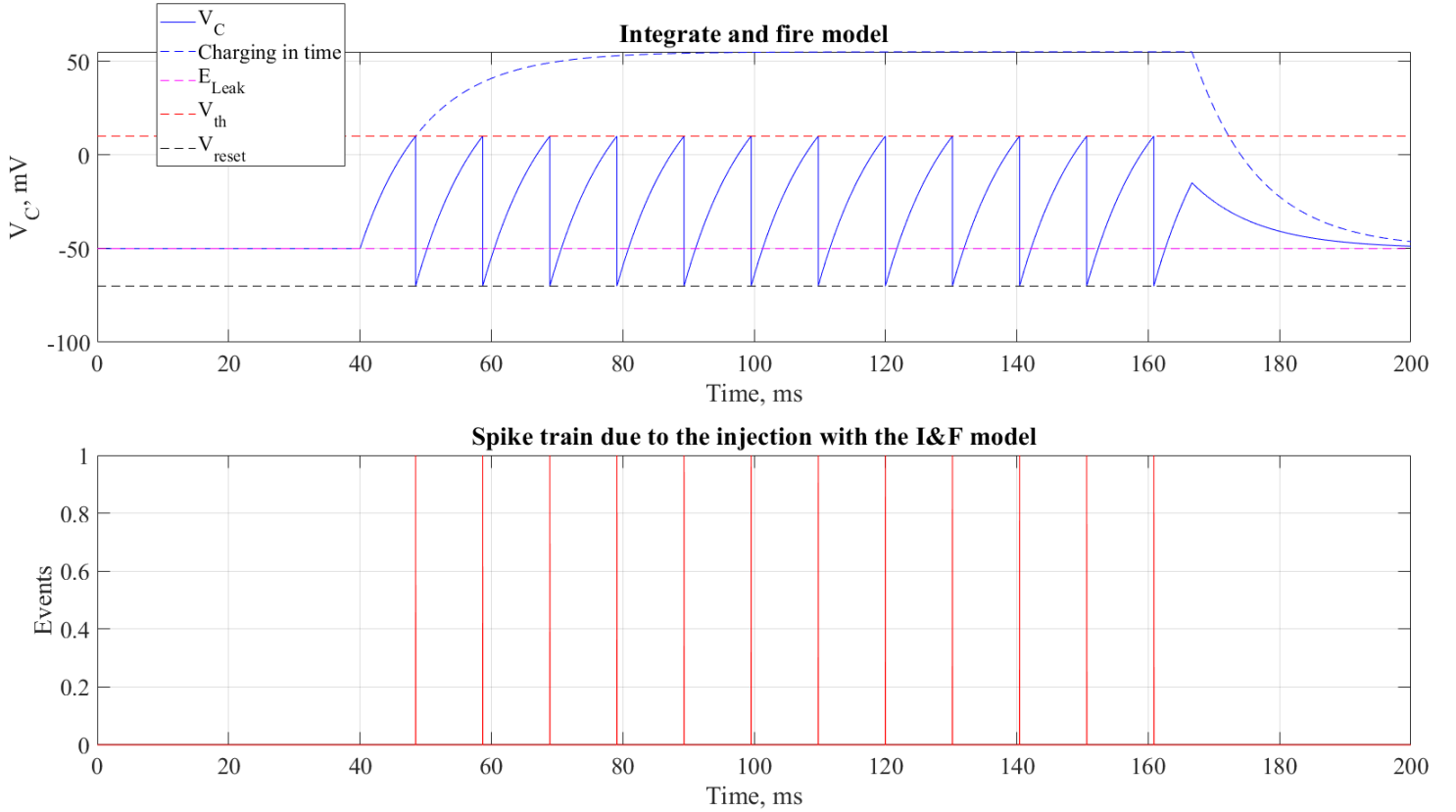


Figure 1.10. The generation of the action potentials with the "Integrate and Fire" model. $I_{in} = 1.05$ nA between $t_1 = 40$ ms and $t_2 = 166.7$ ms, $R_{leak} = 100$ M Ω , $C = 0.1$ nF, $\tau = 10$ ms, $E_{Leak} = -50$ mV, $V_{th} = 10$ mV, $V_{reset} = -70$ mV.

In fig.1.10 the results coming from the integrate and fire model, implemented using Matlab (Appendix A), are shown.

By injecting a constant current into the neuron, the capacitor will charge up until a value $V_{\infty} = E_{Leak} + R_{Leak}I_{in}$ with a certain time constant $\tau = R_{leak}C$ (see eq.1.17). It will fire only if V_C reaches a value greater than V_{th} during this charging, then V_C will be reset to V_{reset} and the process will start again. At the end, V_C will relax to E_{Leak} when the input is removed.

It can be noticed from fig.1.10 that if the total injected current is such that V_{∞} is lesser than V_{th} , then the neuron will never fire a single spike. If instead V_{∞} is greater than V_{th} , then the neuron will start to generate a spike train with a frequency which increases with the injected current. In particular, if the current increases then V_{∞} will increase, therefore V_C will reach V_{th} faster and the time between each spike will decrease.

Considering the time Δt between these events, it is possible to extract an expression describing the frequency at which the neuron fires as a function of the injected current.

$$V_{\infty} = E_{Leak} + R_{Leak}I_{in} = V_{th} \quad (1.19)$$

The eq.1.19 sets the condition for the so called "Rheobase", the minimum current to be injected in order to let the neuron fire.

$$I_{th} = G_{Leak}(V_{th} - E_{Leak}) \quad (1.20)$$

Considering eq.1.17, imposing $V_C(t) = V_{th}$ and $V_C(t_0) = V_{reset}$, the following can be obtained:

$$V_{th} = (V_{reset} - V_{\infty})e^{-\frac{\Delta t}{\tau}} + V_{\infty} \quad (1.21)$$

This means that the initial transition from E_{Leak} to V_{th} , that takes place when $I_{in} \geq I_{th}$, is neglected: the initial condition $V_C(t_0)$ is equal to V_{reset} , therefore at least one spike has already been generated. From eq.1.21, Δt can be derived, leading to:

$$\begin{cases} f = \Delta t^{-1} = (\tau \ln \frac{V_{\infty} - V_{reset}}{V_{\infty} - V_{th}})^{-1} \\ I_{in} \geq I_{th} \end{cases} \quad (1.22)$$

The eq.1.22 describes the so called "Frequency-Current" curve. This can be interpreted as the response the neuron has as a function of the injecting current. The response, in particular, is the frequency of the generated pattern of spikes. The frequency vs current relation only depends on the characteristics of the neuron in exam through the parameters E_{Leak} , R_{Leak} , V_{reset} , V_{th} and C .

The typical shape of the frequency vs current curve has been plotted in fig.1.11. The injected currents are in the order of nA, the frequencies instead are in the order of Hz. If V_{∞} is much greater than V_{reset} and V_{th} , then the relation 1.22 becomes linear.

$$f = \frac{I_{in} - I_{th}}{C(V_{th} - V_{reset})} \quad (1.23)$$

Therefore, in this approximation, it could be said that if the total injected current is lesser than a certain value I_{th} , the neuron will not respond, if instead the total current is greater than it, the neuron will respond linearly with respect to I_{in} .

This approximated behaviour actually resembles a $\text{ReLU}(x) = \max(\theta, x)$ activation function, used in Deep Learning algorithms [28]. The activation functions are used in the so called "Rate models", where the spike trains description is substituted with f-I curves, one for each neuron of the neural network.

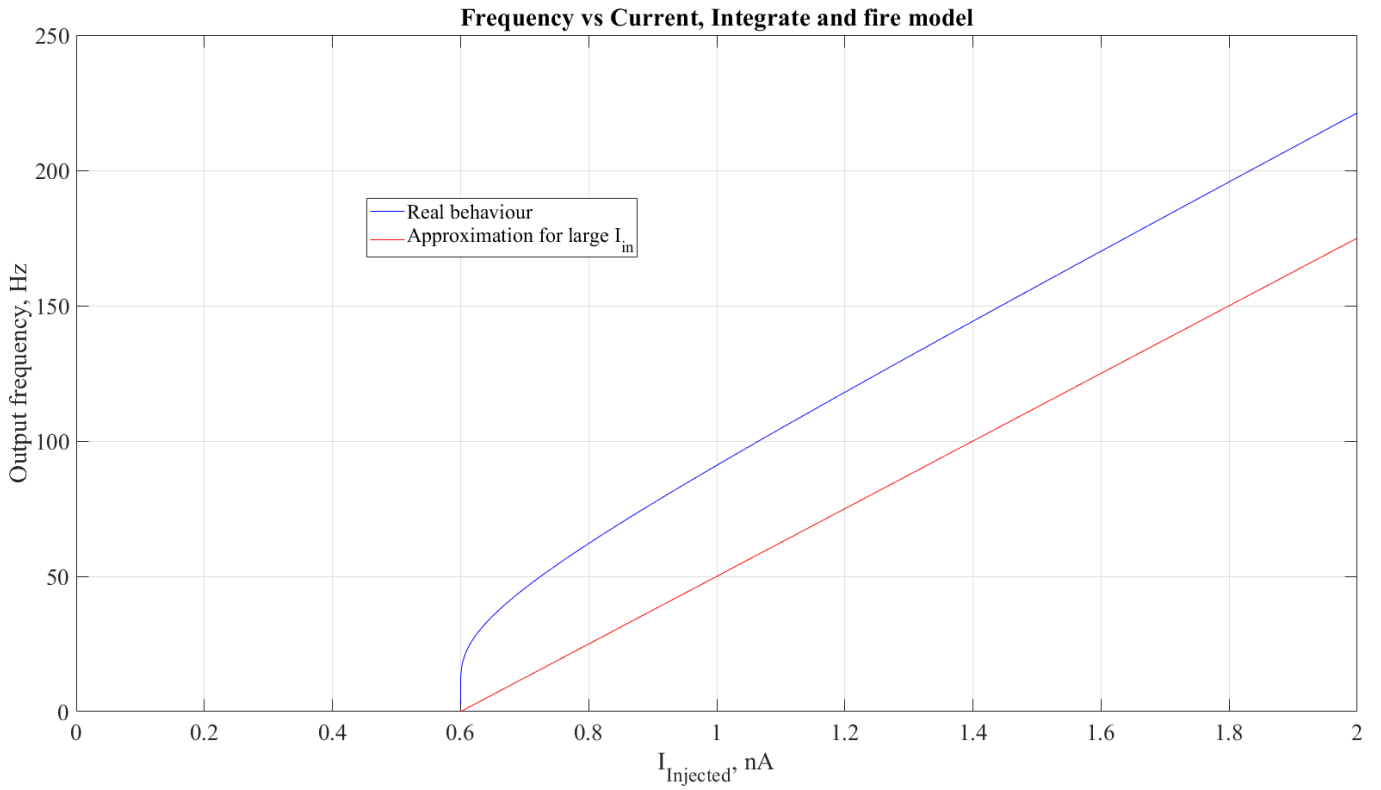


Figure 1.11. Frequency - Current curve from the integrate and fire model. $R_{leak} = 100 \text{ M}\Omega$, $C = 0.1 \text{ nF}$, $\tau = 10 \text{ ms}$, $E_{Leak} = -50 \text{ mV}$, $V_{th} = 10 \text{ mV}$, $V_{reset} = -70 \text{ mV}$.

Normally, the frequency of operation for neurons is in the order of tens of Hz. This is very low if compared to nowadays technologies, however, neural networks compensate such disadvantage with high parallelism, low power consumption because of spike coding and in-memory computing due to the synapses. This suggests that what really matters is not the neuron itself, but the properties of the neural network.

1.3.4 Dendrites

The models reported until now are just for the soma of the neuron. This is the region in which the neuron decides if a spike has to be emitted or not. Different kind of inputs come in, the membrane capacitance integrate them and eventually an action potential is generated.

However, in real neuron, only a few number of inputs are directly injected from the soma. Most of them are injected into the dendrites from the synapses, for example, positioned at some distance with respect to the soma. Once the current is injected it has to propagate along all the dendrites until the soma is reached, this implies attenuation for the traveling signal.

In literature, the complex dendritic arborization is simplified using a single cylinder (see [14]) with radius a . It is possible to demonstrate that, mathematically, this is a good approximation for an extended dendritic part.

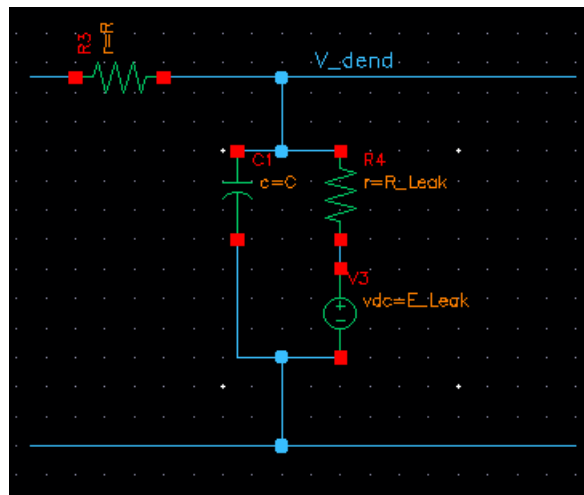


Figure 1.12. Unit for the finite method analysis modeling the dendritic extension.

A finite element analysis is used to model a piece of dendrite. Each of these slices is modeled as a separated circuit: the more the dendritic part is extended in the x axial direction, the more units will be used.

The axial resistance R models the intracellular resistance the input currents find in traveling along the dendrite. This is because this current is confined in a very little space, the bottom node instead refers to the outside of the dendrite, where the volume is larger and any extracellular resistance can be neglected (however, it must be considered to understand how extracellular signals can be recorded).

The membrane can be modeled as done for the soma: a capacitance is used and connected in parallel with the series of a resistance and a battery, referring to non-specific (leak) ionic channels.

The current $I(x, t)$ flowing axially in each piece of the dendrite can be obtained considering $V_{dend}(x, t)$ as the voltage drop on the piece in exam and $V_{dend}(x + \Delta x, t)$ as the voltage drop on the next one.

$$V_{dend}(x, t) - V_{dend}(x + \Delta x, t) = RI(x, t) \quad (1.24)$$

From which:

$$\frac{V_{dend}(x, t) - V_{dend}(x + \Delta x, t)}{\Delta x} = \frac{R}{\Delta x} I(x, t) \quad (1.25)$$

Finally, by taking the limit for $\Delta x \rightarrow 0$:

$$-\frac{\partial V_{dend}}{\partial x} = R_a I(x, t) \quad (1.26)$$

Where $R_a = \frac{R}{\Delta x}$ is the axial resistance per unit length.

Finally, the current entering the membrane can be indicated as $i_m(x, t)$, whereas the injected current can be indicated as $i_e(x, t)$. These are both currents per unit length. By using the Kirchhoff's law for the currents, the following can be obtained:

$$i_m(x, t)\Delta x - i_e(x, t)\Delta x + I(x, t) - I(x - \Delta x, t) = 0 \quad (1.27)$$

By dividing again by Δx and taking the limit to 0:

$$i_m(x, t) - i_e(x, t) = -\frac{\partial I}{\partial x}(x, t) \quad (1.28)$$

And by the equation 1.26, if R_a is constant:

$$\frac{\partial^2 V_{dend}}{\partial x^2} = -R_a \frac{\partial I(x, t)}{\partial x}(x, t) \quad (1.29)$$

From which the following is obtainable:

$$\frac{1}{R_a} \frac{\partial^2 V_{dend}}{\partial x^2}(x, t) = i_m(x, t) - i_e(x, t) \quad (1.30)$$

The only missed element now is $i_m(x, t)$, the current per unit length entering the membrane. This is modeled again as in the HH soma, as can be seen from figure 1.12.

$$i_m(x, t)\Delta x = C_m \Delta x \frac{\partial V_{dend}}{\partial t}(x, t) + G_m \Delta x (V_{dend}(x, t) - E_{Leak}) \quad (1.31)$$

Where C_m is a capacitance per unit of length, and G_m is a membrane ionic conductance per unit length.

Finally, inserting 1.31 into 1.30 and dividing by G_m , the "Cable equation" can be derived. It describes the propagation of input currents along the dendritic arborization.

$$\lambda^2 \frac{\partial^2 V_{dend}}{\partial x^2}(x, t) = \tau_m \frac{\partial V_{dend}}{\partial t}(x, t) + (V_{dend}(x, t) - E_{leak}) - \frac{1}{G_m} i_e(x, t) \quad (1.32)$$

In particular, $\lambda = (\frac{1}{G_m R_a})^{1/2}$ and $\tau_m = \frac{C_m}{G_m}$. λ is known as "Steady state space constant", it has units of length whereas τ_m is the membrane time constant.

τ_m is still a property of the membrane and it expresses the time needed for the membrane to integrate the injected propagating signals. λ instead is expressing the distance that the signal can travel along the dendritic axial direction before being completely attenuated.

It turns out that the current has an exponential decreasing trend with respect to $|x|/\lambda$. This quantity depends on the space geometry of the neural cell. For this reason, different firing patterns are observed for different cell's geometries. The amount of current coming into the soma that contributes to the action potential generation, is the remaining portion of the current after the attenuation due to the propagation into the dendrites, with respect to the point where it was injected. The more a synapse is close to the soma, the more the injected current will contribute to the integration.

Multi-compartment model

Concerning neuromorphic circuits, some implementation of the so called "Multi-compartment model" can be found in literature (see [18], for example).

The cable equation is really a powerful tool, providing intuition about how impulses propagate into the dendritic part starting from some position where they are injected. However, other approximations are used to simplify such kind of description. The multi-compartment model considers the dendritic arborization as a series of parallel capacitor-resistor combinations, where each parallel is connected to the next one through a resistance, exactly as in figure 1.12.

Each parallel provides an independent section of the dendrite, also the soma has been modelled in such a way. In this view, ionic conductances describing ionic channels can be added as a parallel branch to the section, as for the synapses.

A simple and clear example can be done by using the so called "Two-compartment model", which is a sort of extreme simplification of the multi-compartment model: it just considers the whole dendritic part as a section and the soma as another one, connected by a resistance.

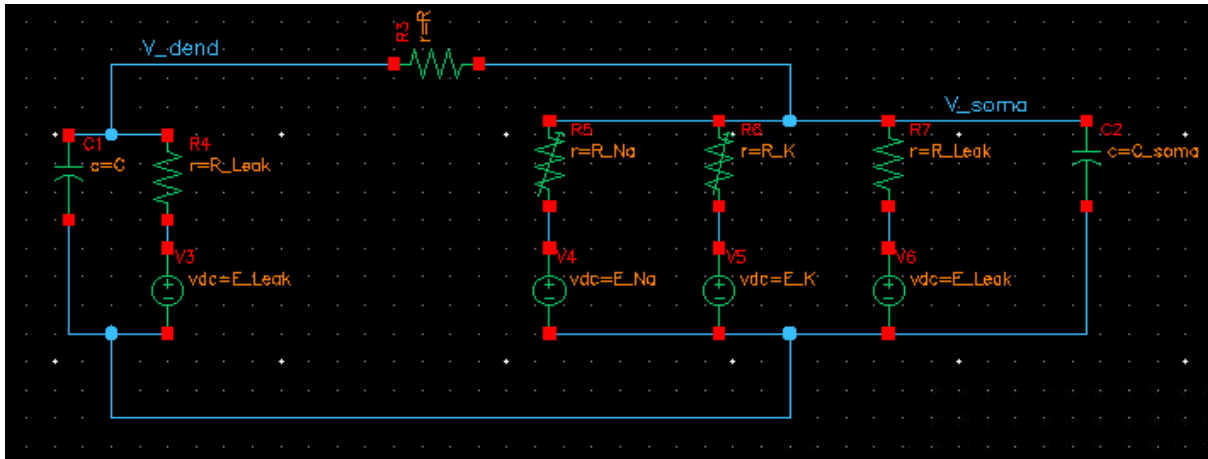


Figure 1.13. Two-compartment model circuit.

The circuit in figure 1.13 could be made more complex by adding synapses on both the soma and the dendrites (or only one of them), dendritic ionic channels, injected current directly on the soma or on the dendrites, and so on.

1.3.5 Synapses

Most of the input currents come into the neuron being injected on the dendritic arbor. This structure offers a very large area, allowing a lot of synapses to contact a neuron. In this section, the neuron injecting a certain current into another one will be referred as "pre-synaptic neuron" whereas, the one receiving the input current, will be referred as "post-synaptic neuron".

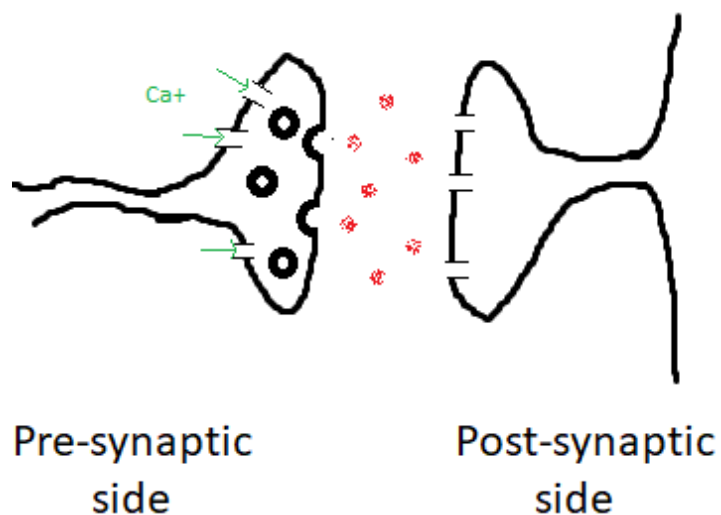


Figure 1.14. Representation of the synaptic cleft structure.

The structure of a chemical synapse (treated in [14]) involves the presence of a nm gap, called "synaptic cleft", which separates one neuron from the other ones. On the pre-synaptic side, the so called "synaptic vesicles" are present, these form a sort of cloud inside the pre-synaptic terminal and are filled by neurotransmitters.

The action potential generated by the pre-synaptic neuron propagates into the axon, reaching the synapse which connects it to the post-synaptic neuron. This leads to the depolarization of the pre-synaptic part, which allows the opening of calcium ionic channel on the pre-synaptic surface. Calcium ions then, are able to flow inside the pre-synaptic terminal, making possible for the vesicles inside of it to flow towards the synaptic cleft. Once the vesicles reach the cleft, they release neurotransmitters.

Electronically speaking, synapses allow neurons to be decoupled. The post-synaptic current is generated by the binding of the neurotransmitters to specific bio-receptors after they diffuse into the cleft. This binding brings to the generation of a input current due to the opening of other ionic channels, then, it will propagated along to the soma. So, the soma is where a sort of compression of the information is done, but if an information is important or not is decided by the synapses which has the role of modulating this information.

Once the post-synaptic channels are opened by the binding of the neurotransmitters, the ionic current passing through them depends on the voltage at which the post-synaptic neural membrane is. This inward current has duration of about 2 ms and its peak depends on the V_C .

The V_C for which the synaptic current is null can be interpreted as the reversal potential of the synapse E_{syn} , in this way, synapses can be introduced in the model as ionic channels where the conductance is modulated by the neurotransmitters released from the pre-synaptic part.

$$I_{syn}(t) = G_{syn}(t)(V_C - E_{syn}) \quad (1.33)$$

From an electronic standpoint, referring to image 1.6, a branch having the series of a variable resistance R_{syn} and a battery E_{syn} has to be added. Moreover, R_{syn} should be controlled by a decoupled pre-synaptic neuron, then, the injected current should be dependent on the membrane potential: in principle, a synapse can be thought as a transistor having V_D and V_S as V_C and E_{syn} , with the pre-synaptic pulses coming on the gate.

Excitatory synapses

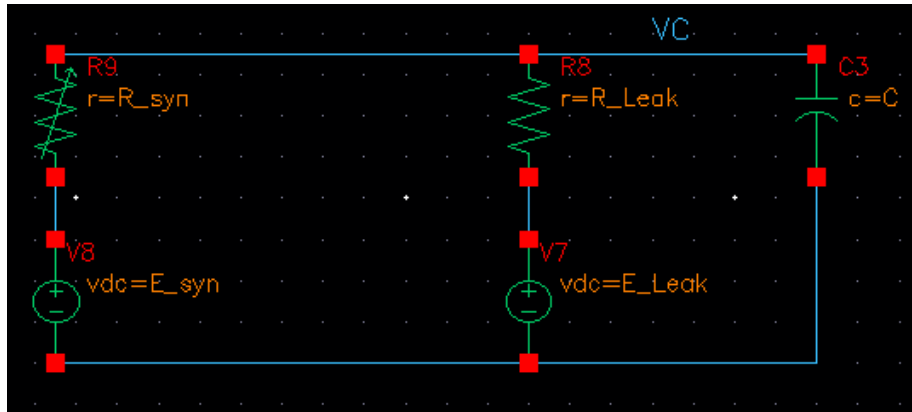


Figure 1.15. Synaptic implementation.

In figure 1.15, a simple leaky soma having a synapse attached to it has been reported. When neurotransmitters arrive, R_{syn} decreases and the capacitance can charge to the value E_{syn} . This means that, in principle, no matter if V_C is greater or lesser than E_{syn} : the membrane potential will always approach the reversal potential of the synapse with a proper current entering ($E_{syn} > V_C$) or exiting ($E_{syn} < V_C$) from the cell. A synapse is said "Excitatory" if its reversal potential E_{syn} is greater than the voltage V_C needed to allow the spiking mechanism. The temporal depolarization due to an excitatory synapse is called "Excitatory post-synaptic potential"(EPSP) whereas the associated ionic current is called "Excitatory post-synaptic current"(EPSC).

Inhibitory synapses

If the reversal potential of the synapse is lesser than the voltage V_C required to the neuron in order to generate a spike, it is said to be an "Inhibitory synapse". It is formally the one reported in figure 1.15, what changes is just the value of E_{syn} . The temporal depolarization due to an inhibitory synapse is called "Inhibitory post-synaptic potential"(IPSP) whereas the associated ionic current is called "Inhibitory post-synaptic current"(IPSC).

Synaptic response to a train of spikes

"Short term memory" will be not treated in this work. In particular, "Synaptic facilitation" and "Synaptic depression" are observed in real neurons. The amplitude of the current coming from a synapse also depends on the "history" of the synaptic activity: if the amplitude of the impulses increases after some activity we talk about facilitation, if instead decreases we talk about depression. Both synaptic facilitation and depression do not persist as for the "Synaptic plasticity" (which is related to long-term learning), but decay in a range between hundreds of ms and few seconds([15]).

In this section, the behaviour of $G_{syn}(t)$ in the equation 1.33 will be discussed. It is possible to demonstrate that the synaptic conductance can be related to the stochastic opening of the post-synaptic channels, due to the binding of the released neurotransmitter with the neuroreceptors [14].

In Magleby-Stevens model for example, two rate constants α and β are considered [14]. In particular, α controls the rate at which a closed channel opens due to the binding of neurotransmitters, whereas β considers their unbinding. They are both probability per unit time.

If P is the probability to have a channel open and N is the total number of released neurotransmitters by a single spike, then $\alpha N(1-P)$ is the rate of probability for a single channel to go from the close state to the open state. Instead, βP will be the rate of probability to go from the open state to the close state. This means that, the probability to have an open channel in time because of a pre-synaptic spike will be given by:

$$\frac{\partial P}{\partial t} = \alpha N(1 - P) - \beta P \quad (1.34)$$

In a simplified view of the Magleby-Stevens model, assuming a very fast binding for the neurotransmitters (α is very high), P can be just considered as a function exponentially decaying in time, with a certain time constant τ_{syn} (see [14]).

$$P(t) = P_{max} e^{-\frac{t}{\tau_{syn}}} \quad (1.35)$$

Associating to each open post-synaptic channel a constant conductance g_R , the synaptic conductance due to a pre-synaptic spike can be obtained as:

$$G_{syn}(t) = g_R N_R P(t) = g_R N_R P_{max} e^{-\frac{t}{\tau_{syn}}} = G_{max} e^{-\frac{t}{\tau_{syn}}} \quad (1.36)$$

Where N_R is the total number of post-synaptic receptors. This means that the spike releases neurotransmitters into the synaptic cleft, they interact with the post-synaptic receptors and then they unbind exponentially.

It has to be noticed that this exponential behaviour of $G_{syn}(t)$ is basically the "Impulse response function" (IRF) of the synapse, this means that if a train of spikes impinging on the pre-synaptic terminal has to be considered, the synaptic conductance will be given by:

$$G_{syn}(t) = \int_{-\infty}^{+\infty} G_{max} e^{-\frac{t'}{\tau_{syn}}} S(t-t') dt' = \int_{-\infty}^{+\infty} K(t') S(t-t') dt' \quad (1.37)$$

It is a convolution between the train of spike $S(t)$ and the IRF $K(t)$, also called Kernel. Using a RC circuit, such synaptic response can be obtained.

Another thing that is noticeable from equation 1.37 is that the behaviour of $G_{syn}(t)$ depends strongly on g_R which is setting a sort of weight for the synaptic response. Due to the temporal coherence of the input spikes, therefore on the synaptic activity, it turns out that the dimension of the channels can change, so they will conduct more or less when neurotransmitters bind with the receptors. This is reflected in a long-term or short-term change of g_R . Considering long-term changes, "Potentiation" (increase of g_R) or "Depression" (decrease of g_R) can be obtained.

Synaptic transmission

Considering the figure 1.15, the current injected by the synapse will depend on the value of $G_{syn}(t)$ and the voltage drop ($V_C(t) - E_{syn}$).

Again, a parallel RC circuit is modeling a leaky soma as described by 1.16. The general solution for the equation 1.16 can be considered, without specifying a form for I_{in} .

$$V_C(t) = (V_C(0) - E_{Leak}) e^{-\frac{t}{\tau_{soma}}} + E_{Leak} + \int_0^{\infty} \frac{e^{-\frac{t'}{\tau_{soma}}}}{\tau_{soma}} I_{in}(t-t') R_{Leak} dt' \quad (1.38)$$

From the equation 1.33, then the following can be obtained:

$$V_C(t) = (V_C(0) - E_{Leak}) e^{-\frac{t}{\tau_{soma}}} + E_{Leak} + \int_0^{\infty} \frac{e^{-\frac{t'}{\tau_{soma}}}}{\tau_{soma}} G_{syn}(t-t') (V_C(t-t') - E_{syn}) R_{Leak} dt' \quad (1.39)$$

The equation 1.39 tells that $V_C(t)$ will be given by a convolution between the synaptic response and the IRF $\frac{e^{-\frac{t'}{\tau_{soma}}}}{\tau_{soma}}$, where $\tau_{soma} = R_{Leak} C$. This consists in a step, decaying with exponential behaviour having time constant τ_{soma} .

When an excitatory synaptic response arrives it will increase V_C up to a certain value (this is a contribution to the depolarization of the neural cell) depending on G_{syn} , E_{syn} and R_{Leak} , then it will decay exponentially. This exponential decay can be interpreted as a "Repolarization" of the cell, since the difference between the membrane potential V_C and the value V_{th} required in order to generate a spike increases.

However, if a second response arrives before V_C has completely decayed, an increase to a second higher value will be observed. The more the frequency of the arriving pre-synaptic spikes, the more $G_{syn}(t)$ will be higher and the more V_C will increase, since all the dynamics will have not sufficient time to relax back. Of course, this is a mechanism depending on both the time constants for the synapse τ_{syn} and the soma τ_{soma} . This is the concept behind the temporal coherence for the arriving spikes. Two spikes which are distant in time will not have so much importance from the point of view of integration, therefore, their contribute will be neglected. If instead they arrive enough close in time, then their importance will be higher. In this context, the importance is quantified by the convolution in equation 1.37.

During this process, considering both excitatory and inhibitory synapses, if V_C is able to reach the V_{th} required for the spike generation mechanism to take place, then the neuron will fire through its axon. The neuron is working just like a voting system, starting from a lot of information it is able to make a data compression through consensus of the inputs, which are weighted by the synapses depending on their "importance".

Finally, it can be noticed from figure 1.15 that when $V_C = E_{syn}$ the current passing through the synapse will be null. This is also known as "Synaptic saturation" and this explains why a synapse conducts lesser and lesser as the membrane potential approaches the synaptic reversal potential.

A mention to memristive devices

The implementation of synapses is a really crucial part for neuromorphic system, since the learning depends on them. Technologically speaking, memristors are considered the best candidates to make good VLSI synapses (see [20]), since they replicate very well dynamics like synaptic plasticity and short-term memory. Moreover, since most of the brain is filled by synapses, memristors are an optimal choice also from the point of view of integration density, due to their nm features and very low power consumption.

1.3.6 Neural coding

In previous sections it has been explained how neurons constitute mixed analog-digital devices, able to convert a general analog signal into a train of spikes. This kind of coding results to be very efficient in terms of power consumption and communication, allowing neural networks to have high parallelism despite the very low frequency of operation if compared with nowadays processors. This means that the key factor behind a spiking neural network is not really the neuron itself, but the way in which the neural network is organized. Through the synapses, neurons can communicate while adapting in time to a specific problem, this implies a co-existence of processing and memory inside the brain. High parallelism and in-memory computing architectures lead the way to the study of neuromorphic circuits, this concept was clear to Carver Mead but more in general also to von Neumann, which tried to deepen the similarities between the computer and the brain in one of his last work in 1957 [1].

Since the spikes are codifying in some way a general analog input provided by the external world, it is important to understand some concepts regarding the correspondence between the two and how the brain handles with it.

Quantifying firing rates

The presence of an extracellular resistance between the soma and the dendrites allows the measure of the so called "Local field potentials", through the usage of electrodes. They are voltage changes related to the neural activity of populations of neurons and depend on how the neurons are organized spatially. Usually, these signals are filtered so that the action potentials generated by a certain behaviour can be emphasized (high-pass filters are used). The spike detection is done by imposing a certain threshold to overcome: if the filtered signal presents some components above the threshold, then they will be considered as spikes given by $\delta(t - t_i)$ where t_i is the time of occurrence of the i th spike. From this analysis it is possible to extract a spike train $\rho(t) = \sum \delta(t - t_i)$, which has units of spikes per second.

The idea is to extract a function R from $\rho(t)$ called "firing rate". In this way, the original behaviour will be codified by a function describing how the frequency of the spike train changes depending on a certain parameter (the so called "Tuning curves").

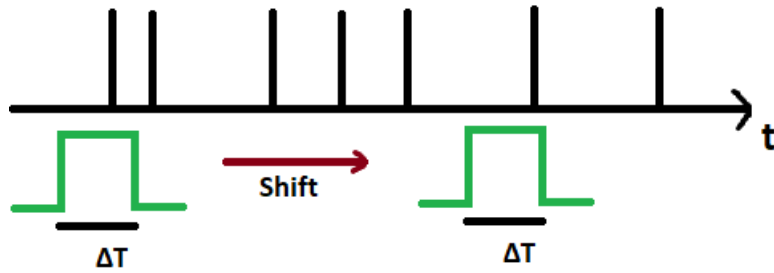


Figure 1.16. Continuous estimation of the $R(t)$.

There are different ways to do so, and the chosen one depends on the specific experiment. However, a continuous measure of firing rate able to provide a function $R(t)$ consists in fixing a certain window with a width ΔT , counting how many spikes are inside the window and then shifting the window of very small time steps. After having shifted the window the process is repeated, this goes on until the whole train of spikes has been fully covered.

$$R(t) = \int_{-\infty}^{\infty} \rho(t - \tau) K(\tau) d\tau \quad (1.40)$$

Mathematically, the operation illustrated in fig.1.16 is described by a convolution between the spike train and a square kernel of width ΔT , as reported in eq.1.40.

More sophisticated techniques could be used to estimate $R(t)$ in a better way, for example by using a Gaussian kernel. The common factor between the different kernels is that the area is normalized to 1. By performing convolution, a weighted temporal average of the spike train is done.

Observation: interesting interlude about neural systems

In the book [1] it is possible to find some notes written by John von Neumann about the comparison between electronic circuits, based on the technology of those years, and the brain. These notes should have been presented at Yale University, for the so called "Silliman Foundation Lectures", but unfortunately he died before completing them. He refers to a class of "mixed" machine types as machines where "each step of the computing procedure combines analog and digital principles". In particular, he talks about the so called "pulse density" system, where each quantity is expressed by successive pulses. The average density of the pulse sequence, in time, returns the quantity to be represented.

As explained, the role of a neuron is to convert a certain analog input into a train of spikes, whereas the role of a synapse could be seen as the conversion of a spike train into an analog signal by convolution. In a certain sense, the data are continuously moved and processed as spikes, but weighted and given in input to the neurons as analog by the synapses. There is a continuous conversion between these two domains during time.

1.3.7 Rate Models

Once neurons, synapses and neural coding have been introduced, a simple method aimed to study the computational properties of neural networks is needed. Within a rate model the spike trains are replaced with firing rates, this provides a simple way to understand how neural networks work.

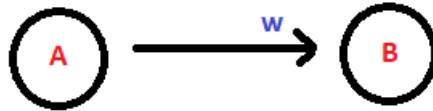


Figure 1.17. Two neurons communicating.

In the simplest case, two neurons connected by a synapse can be considered, as reported in figure 1.17. The input neuron A has some firing rate given by x that can be due to the f-I response to a constant stimulus or to a more generic behaviour as explained in the previous section, whereas the output neuron B has some firing rate given by y . The synaptic current injected into the postsynaptic neuron because of the presynaptic activity is given by eq.1.33, where $G_{syn}(t)$ is given by the eq.1.37.

$$I_{syn}(t) = (V_C - E_{syn}) \int_{-\infty}^{+\infty} G_{max} e^{-\frac{t'}{\tau_{syn}}} S(t - t') dt' \quad (1.41)$$

In general, eq.1.41 can be written. By neglecting synaptic saturation, the postsynaptic current could be considered proportional just to the synaptic conductance G_{syn} . Since G_{max} is a constant it can be moved out from the integral, whereas the exponential which multiplies the input spike train can be considered a kernel.

$$I_{syn}(t) = G_{max} \int_{-\infty}^{+\infty} K(t') S(t - t') dt' \quad (1.42)$$

It has to be remembered that G_{max} depends only on some internal parameters of the synapses, mainly its conductance. It is a sort of trans-conductance weighting the input activity to have the injected current. The idea is to have a device able to tune its trans-conductance using external inputs, so that the weight associated to the synapse can be tuned: that's the basic of learning. Moreover, as described talking about neural coding, the synaptic convolution is doing a temporal average of the input spike train using the kernel of the synapse itself (that has been found with the Magleby-Stevens model, approximately).

$$I_{syn}(t) = wx(t) \quad (1.43)$$

This means that a certain firing rate associated to the activity of the presynaptic neuron will be obtained through a synaptic temporal weighting, then the trans-conductance

will act as a further weight depending just on the synapse itself.

Ultimately, the synaptic current will have the expression reported in eq.1.43.

This current contributes to the charge/discharge of the capacitance associated to the output neuron, which will respond with a certain firing rate given by its f-I curve, during time.

$$y(t) = F[I_{syn}(t)] = F[wx(t)] \quad (1.44)$$

The firing rate of the output neuron will be given by the eq.1.44, where $F[X]$ is just the f-I relation. This is the basic equation of the rate models, which can be easily generalized to multiple inputs.

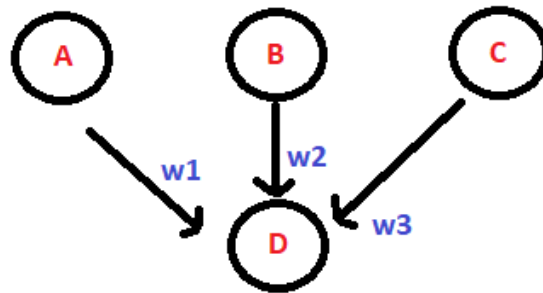


Figure 1.18. A perceptron.

In fig.1.18 it is reported a so called "perceptron" as example: a single output neuron taking a certain number of inputs. Each input has its own synapse which connects it to the output neuron, having a certain weight w_i . The output firing rate will be given by the contributions of all the synaptic currents.

$$y(t) = F[I_{syn1}(t) + I_{syn2}(t) + I_{syn3}(t)] = F[w_1x_A(t) + w_2x_B(t) + w_3x_C(t)] = F[\vec{w} \cdot \vec{x}(t)] \quad (1.45)$$

Because of the parallelism in neural networks, it is common to use vector and matrix (when more output neurons are present) notation.

Chapter 2

PCP-based MolFET: analysis and applications

The purpose of this work is to search for a possible application of the peculiar NDR, observable in the PCP-based MolFET characteristics, in the field of neuromorphic computing. Therefore, a first preliminary analysis of the provided molecule, introduced in chapter 1, has to be done.

2.1 The PCP-based MolFET characteristics

The I-V characteristics and the trans-characteristics can be obtained by connecting a battery between the drain and the source, so that a certain V_{DS} can be forced on the MolFET. At the same time, another battery is connected between the gate and ground, so that a certain V_{GS} can be forced.

All the simulations have been performed using Cadence Virtuoso, then the data have been exported as ".csv" file format on Matlab, so that further analysis were possible. As explained in section 1.2.2, the I-V characteristics regarding the PCP-based MolFET have been obtained by interpolating the data inserted into a Look-Up-Table, extracted by semi-empirical physical ab-initio simulations. This procedure allows to create a proper symbol in Cadence Virtuoso environment, using VerilogA [2].

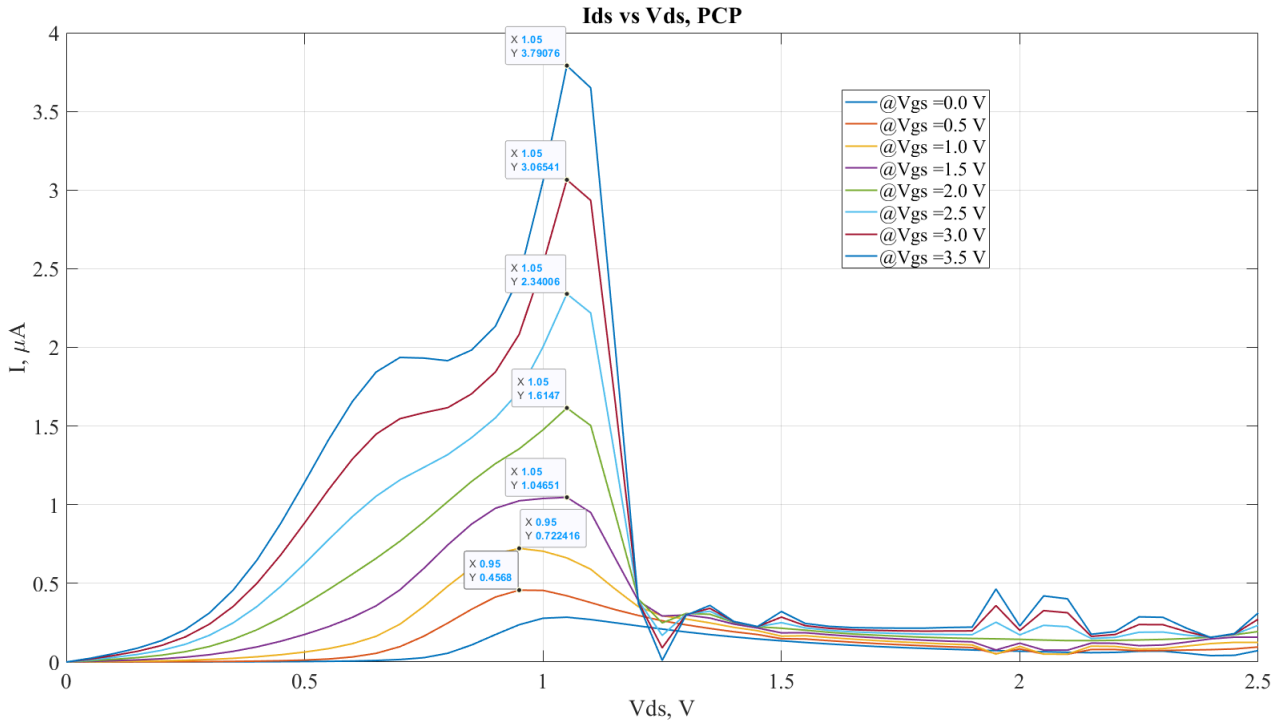


Figure 2.1. PCP-based MolFET I-V characteristics, $V_{DS} > 0$ V and $V_{GS} > 0$ V.

The I-V characteristics reported in figure 2.1 were obtained varying V_{DS} between 0 V and 2.5 V at fixed V_{GS} . The values for V_{GS} go from 0 V to 3.5 V.

All the curves reach their peak around $V_{DS}=1$ V, in particular, the current associated to the peak increases as V_{GS} increases. The order of magnitude is few μA .

Before reaching the peak, the curves having around $V_{GS}=2$ V present a quasi-linear behaviour with respect to V_{DS} , which will be exploited in order to try to have a linearization of the characteristic. A second minor peak is observed around $V_{DS} = 0.6$ V as V_{GS} increases.

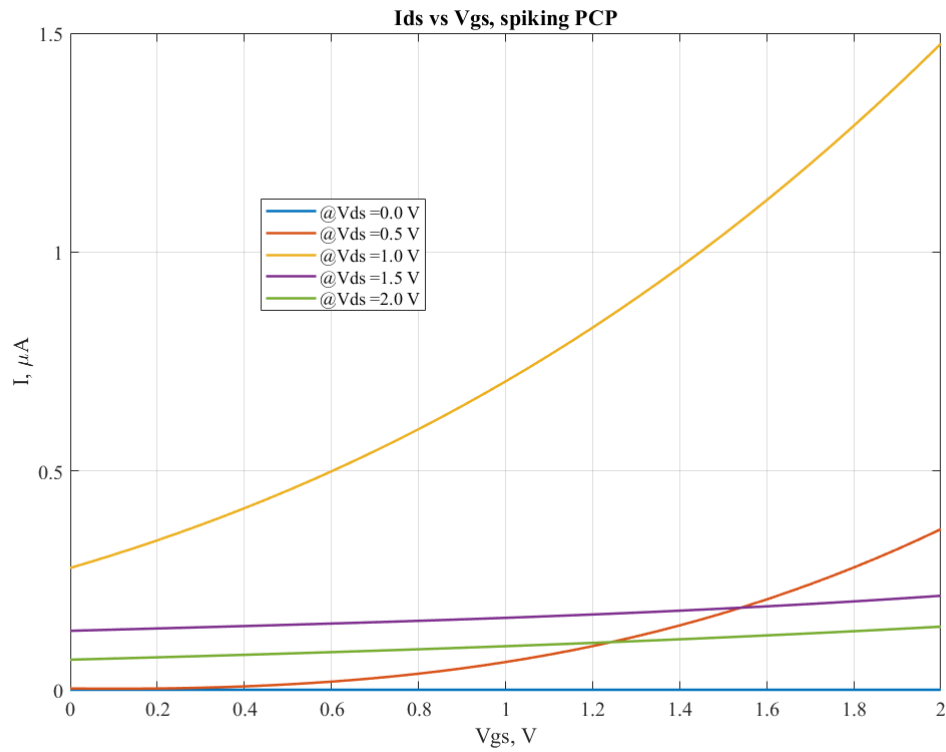


Figure 2.2. PCP-based MolFET I-V trans-characteristics, $V_{DS} > 0$ V and $V_{GS} > 0$ V.

Figure 2.2 reports the trans-characteristics obtained varying V_{GS} between 0 V and 2 V at fixed V_{DS} . In particular, the values of V_{DS} go from 0 V to 2 V. It is noticeable a curve presenting greater values for the current with respect to the other ones for V_{DS} around 1 V, and this is a direct consequence of having all the peaks around $V_{DS}=1$ V in the I-V characteristics.

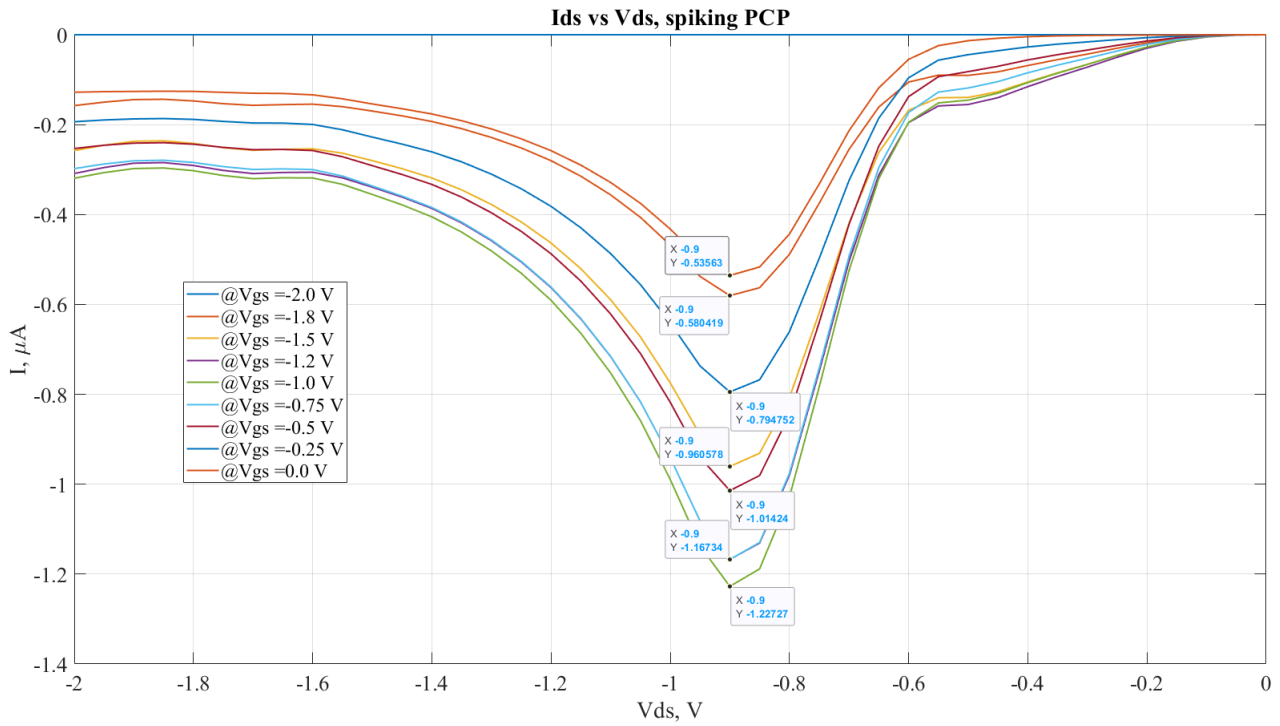


Figure 2.3. PCP-based MolFET I-V characteristics, $V_{DS} < 0$ V and $V_{GS} < 0$ V.

A further analysis can be performed by varying V_{DS} between 0 V and -2 V. In this case, a monotonic behaviour for the amplitude of the peaks is not observed by varying V_{GS} from 0 V to -2 V. In particular, the peaks become more and more negative as V_{GS} approaches -1 V, then they decrease in amplitude again.

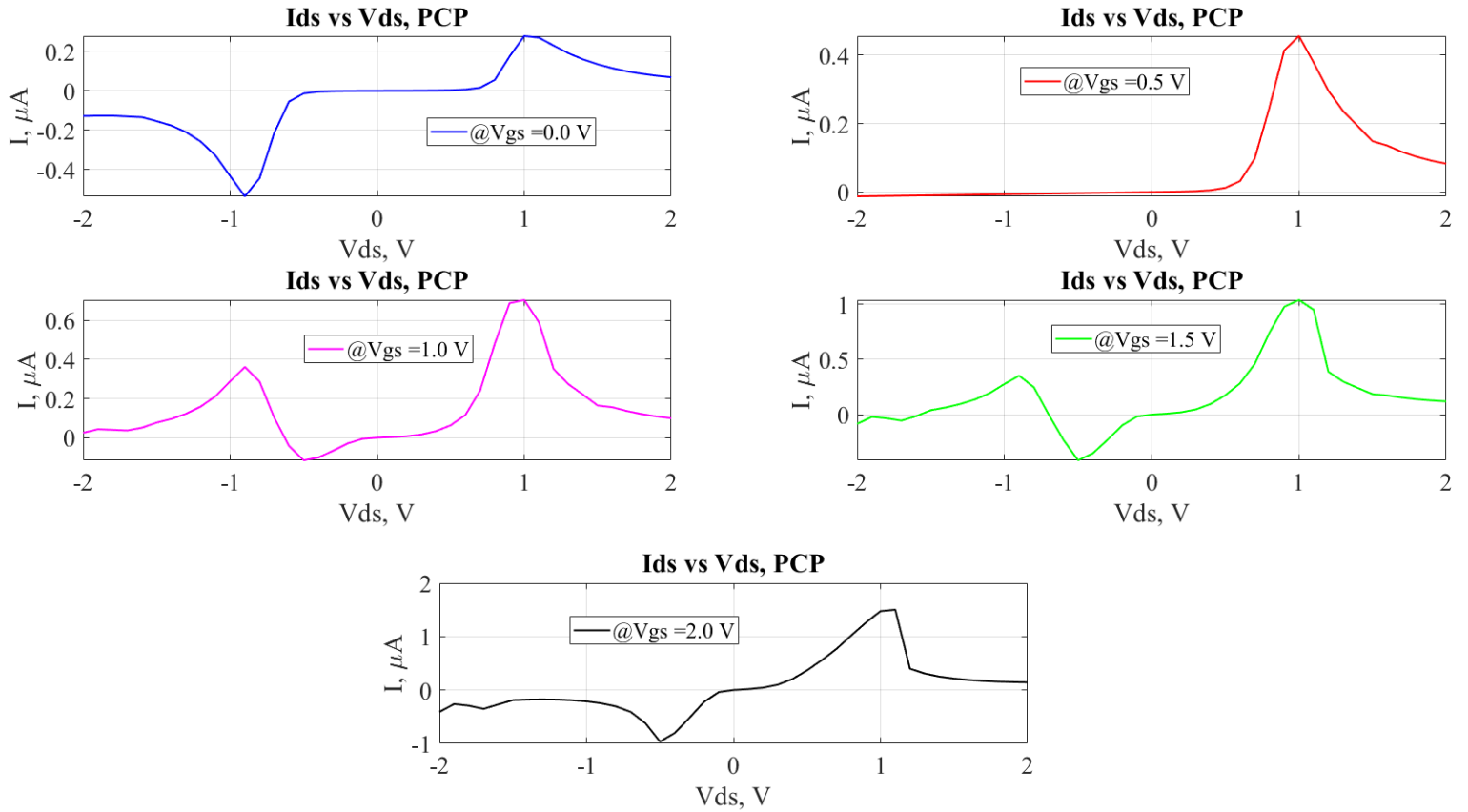


Figure 2.4. PCP-based MolFET I-V characteristics, $V_{GS} > 0$ V.

Another important aspect to be observed is that the I-V characteristics are not symmetric with respect to the origin. In figure 2.4 positive values for V_{GS} have been used. The behaviour of the current for negative V_{DS} depends on the specific V_{GS} value. For example, it can be noticed that:

- Using $V_{GS}=0$ V the negative peak is greater in amplitude than the positive one;
- Using $V_{GS}=0.5$ V the negative peak is absent,
- Using $V_{GS}=1$ V or $V_{GS}=1.5$ V a positive peak is present for negative V_{DS} ;
- Using $V_{GS}=2$ V only a negative peak for negative V_{DS} is present again, lesser in amplitude with respect to the positive one for V_{DS} greater than 0 V.

Once the general analysis were performed to know the behaviour of the PCP-based MolFET, due to the shape of the curves, the initial idea was to use it at circuitual level in order to replicate a spike of current: in this way, exploiting the V_{GS} , a sort of weight could have been introduced since the peak for positive V_{DS} increases as V_{GS} increases. This strategy was not feasible since it should have required a sort of ramp for V_{DS} , moreover, this ramp should have been obtained integrating the different current peaks coming from each input neuron, which is quite difficult due to the impedance coupling.

In order to have an exclusive contribution coming from the NDR, the second idea was to implement some particular stages based on the PCP-based MolFET instead of using the molecule itself. If the behaviour of the stage is exclusive for the PCP, then the request is indirectly satisfied by implementing such stages.

Another important electronic device presenting NDR which is seen during the master degree course is the "Resonant tunneling diode" (RTD) [21]. This is a device which makes use of quantum mechanical tunneling through some resonant states in order to conduct current. The incoming electrons have an energy which is more or less equal to the Fermi level of the injecting metal: when it is aligned with a confined state (generated by using a quantum well) then the state will act as a channel. The alignment is possible by changing the potential barrier structure, applying a certain voltage drop between the electrodes.

A research of possible useful electronic stages, based on RTD, has been done. Then, for each stage, tests have been performed on the PCP in order to try to replicate some results and to understand if such stages could be used for neuromorphic applications. Hopefully, the PCP would show something new with respect to the versions exploiting RTD devices. The results that will be presented in the following pages have been obtained by studying possible applications from articles [22],[23],[24],[25],[26],[27].

2.2 A stage presenting non-linear behaviour

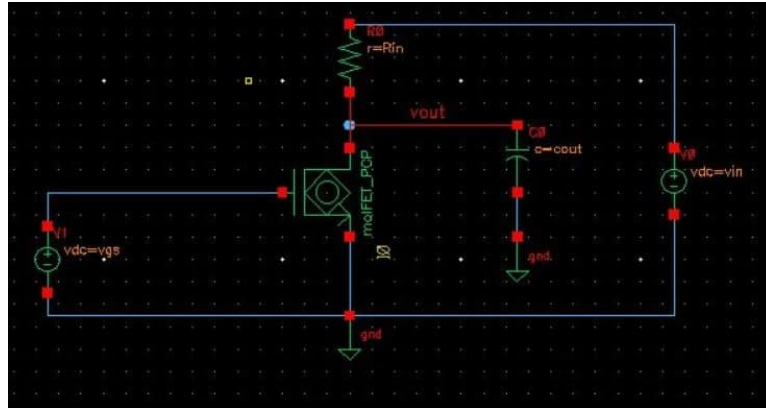


Figure 2.5. Stage presenting non-linear behaviour.

The first stage that will be discussed is reported in figure 2.5. It is based on a series between the PCP-based MoFET and a resistance R_{in} . An input voltage V_{in} is provided between the resistance and the source of the device, V_{GS} instead just sets the amplitude for the current peak of the MoFET.

It is possible to understand in a very easy way the behaviour of this stage by considering a load analysis.

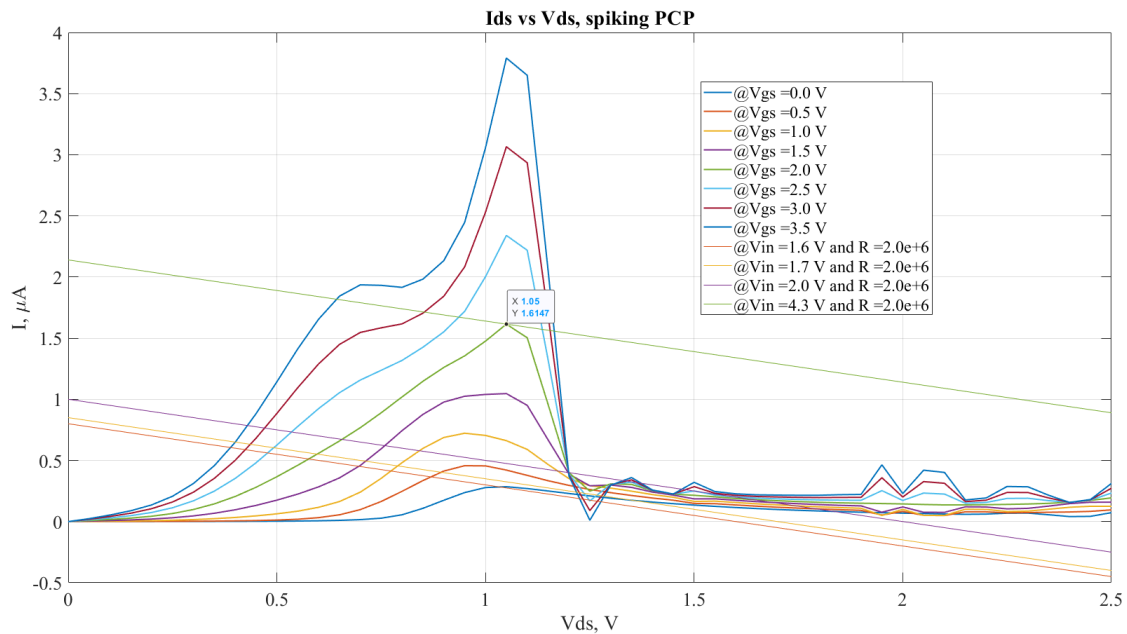


Figure 2.6. Load analysis for the PCP-based mofFET.

In figure 2.18 different lines corresponding to the current which can pass through the resistance, using a certain V_{in} , has been superposed to the MolFET's I-V characteristics ($0\text{ V} < V_{GS} < 3.5\text{ V}$). Since they have been put in series, the current which is passing through the branch will be given by the intersection points. In particular, R_{in} is equal to $2\text{ M}\Omega$. Exploiting the Kirchoff's law for the voltage, the simple relation expressing these lines can be obtained:

$$i_R = \frac{V_{in}}{R_{in}} - \frac{V_{DS}}{R_{in}} \quad (2.1)$$

Therefore, once V_{GS} is fixed, the current passing through the series is equal to the intersection point between the I-V characteristics of the device and the line in equation 2.1. The slope of each of these lines is equal to $-\frac{1}{R_{in}}$ and, because of the NDR, they meet the characteristics in three points: the first point is given by the intersection before the NDR, the second one is given by the intersection with the NDR region of the characteristics whereas the third point is given by the intersection after the NDR. Among these three possible solutions, the one corresponding to the lowest V_{DS} is assumed by the circuit.

This means that until the load line will meet the characteristics before the NDR, then the V_{DS} allowed for the MolFET will be the ones associated to the states on the left of the NDR. If instead the load line does not meet the characteristics before the NDR, then the V_{DS} allowed for the MolFET will be the ones associated to the states on the right of the NDR. The points of the NDR region of the characteristics cannot be assumed, since they are unstable.

What can be expected by increasing V_{in} is an increase of V_{DS} , until this will reach values around 1 V , where all the peaks are positioned. After surpassing the peak, V_{DS} will assume values on the right of the NDR. In particular, it is possible to obtain the last possible stable state on the left of the NDR by imposing $V_{in}=V_{th}$ and $V_{DS}=V_{peak}$.

$$V_{th} = I_{peak}R_{in} + V_{peak} \quad (2.2)$$

Where V_{th} is the value for the voltage V_{in} needed in order to obtain the stable state V_{peak} associated to the peak of the characteristics. I_{peak} is the current associated to the peak, it will change by varying V_{GS} whereas V_{peak} will be more or less the same.

Summarizing:

- Since $V_{peak} \simeq 1\text{ V}$, V_{th} will be always greater than 1 V , independently on the used V_{GS} ;
- Using $V_{in} > V_{th}$ a jump for V_{DS} to higher values will be observed;
- Before reaching the jump for $V_{in} \simeq V_{th}$, V_{DS} will always tend to $V_{peak} \simeq 1\text{ V}$.

It has also to be noticed from equation 2.2 that V_{th} is proportional to V_{GS} because of I_{peak} , and R_{in} .

The final remark is related to the slope of the load lines and the value V_{DS} assumed after the NDR. Since the slope is equal to $-\frac{1}{R_{in}}$, by varying R_{in} also the intersection on the right of the NDR will change.

For example, by increasing R_{in} , the slope will decrease (and so V_{in} will have to be greater in order to reach V_{peak} , this is the reason why V_{th} is proportional to R_{in}) and so the intersection with the MolFET's characteristics will be farther, V_{DS} after having reached V_{th} will be higher.

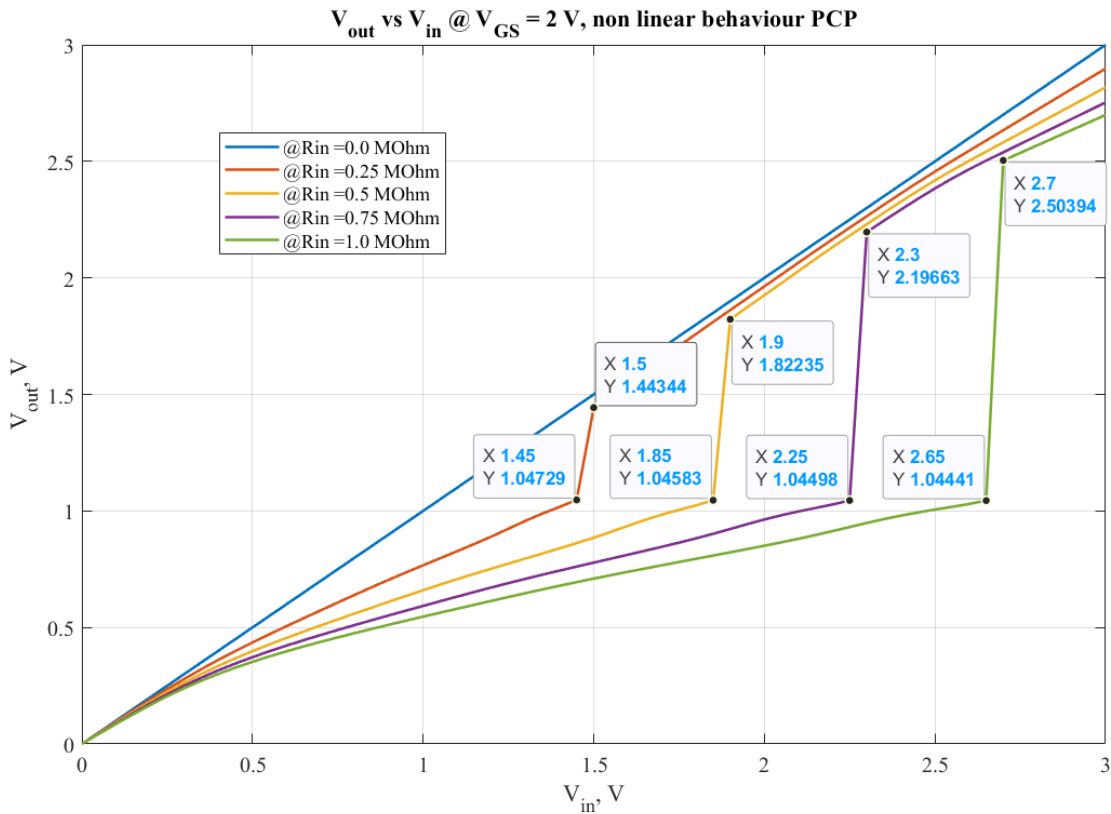


Figure 2.7. Non-linear behaviour, $V_{GS}=2\text{ V}$.

In figure 2.7 the $V_{out}=V_{DS}$ vs V_{in} curves can be observed. These were found by imposing $V_{GS}=2\text{ V}$, whereas R_{in} has been set from $0\ \Omega$ to $1\ \text{M}\Omega$. It can be noticed how by increasing R_{in} , both the amplitude of the jump and the threshold V_{th} increase.

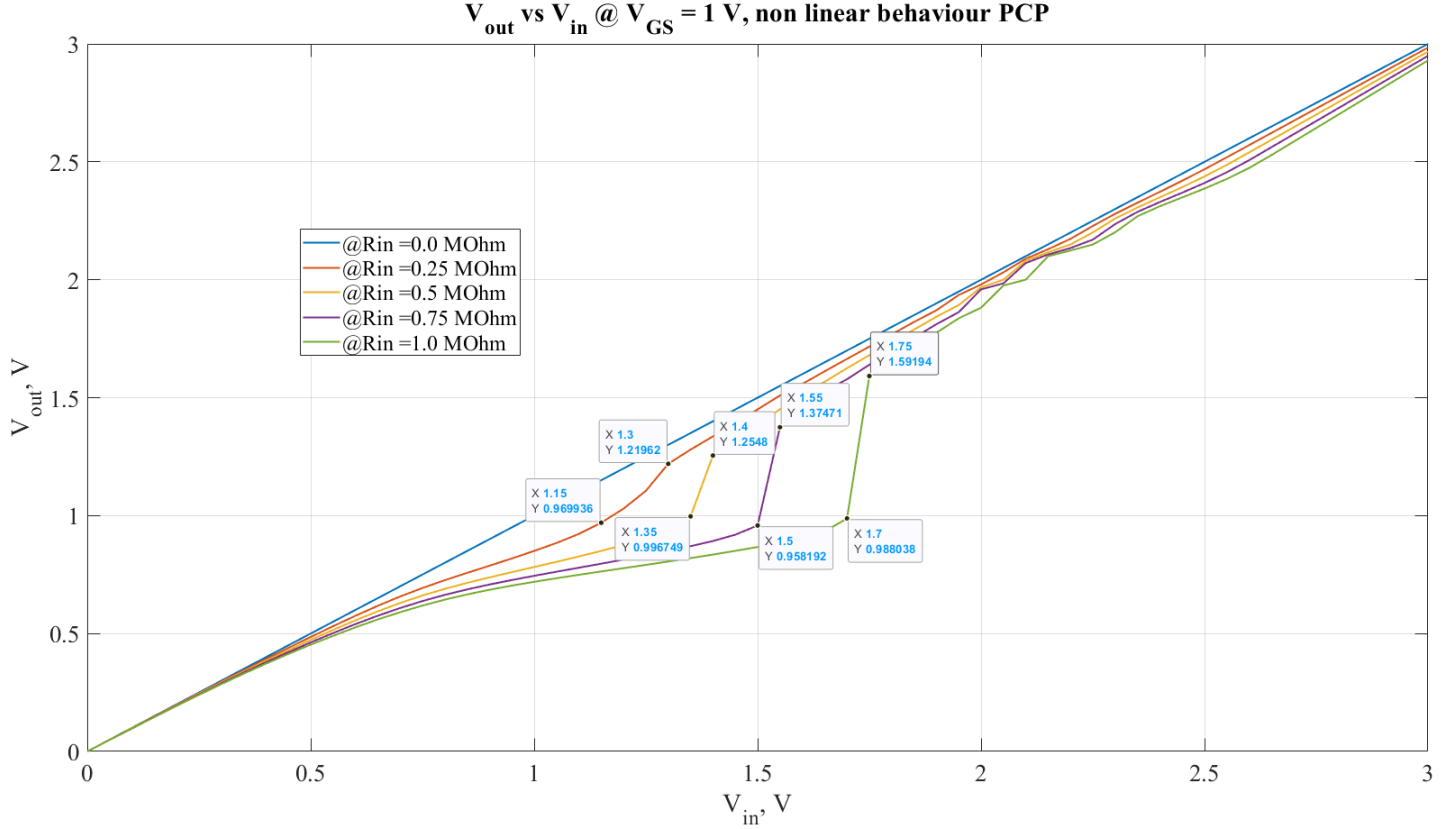


Figure 2.8. Non-linear behaviour, $V_{GS}=1\text{ V}$.

In figure 2.8 the curves obtained fixing $V_{GS}=1\text{ V}$ has been reported, R_{in} varies in the same range. The jumps and the V_{th} are smaller with respect to the ones in figure 2.7 since the current associated to the peak is smaller.

The disadvantage of this circuit consists in the fact that the input voltage is not given on the gate of the MolFET. This could imply problems in terms of impedance decoupling.

2.2.1 The hysteresis loop in the $V_{out}(V_{in})$ curves

The reason why this stage turned out to be very important for this work, is that V_{out} shows a different trend if V_{in} decreases after passing V_{th} .

It is not clear to the author the actual reason of this behaviour. A possible criteria has been searched among the literature concerning RTDs.

I-V characteristics presenting a NDR seem to show hysteresis when the magnitude of the negative differential resistance is lesser than the positive one ([26]). The resistance connected in series increases the positive differential resistance but also decreases the negative one ([27]), this leads to the condition required to have hysteresis.

This is shown in figure 2.9.

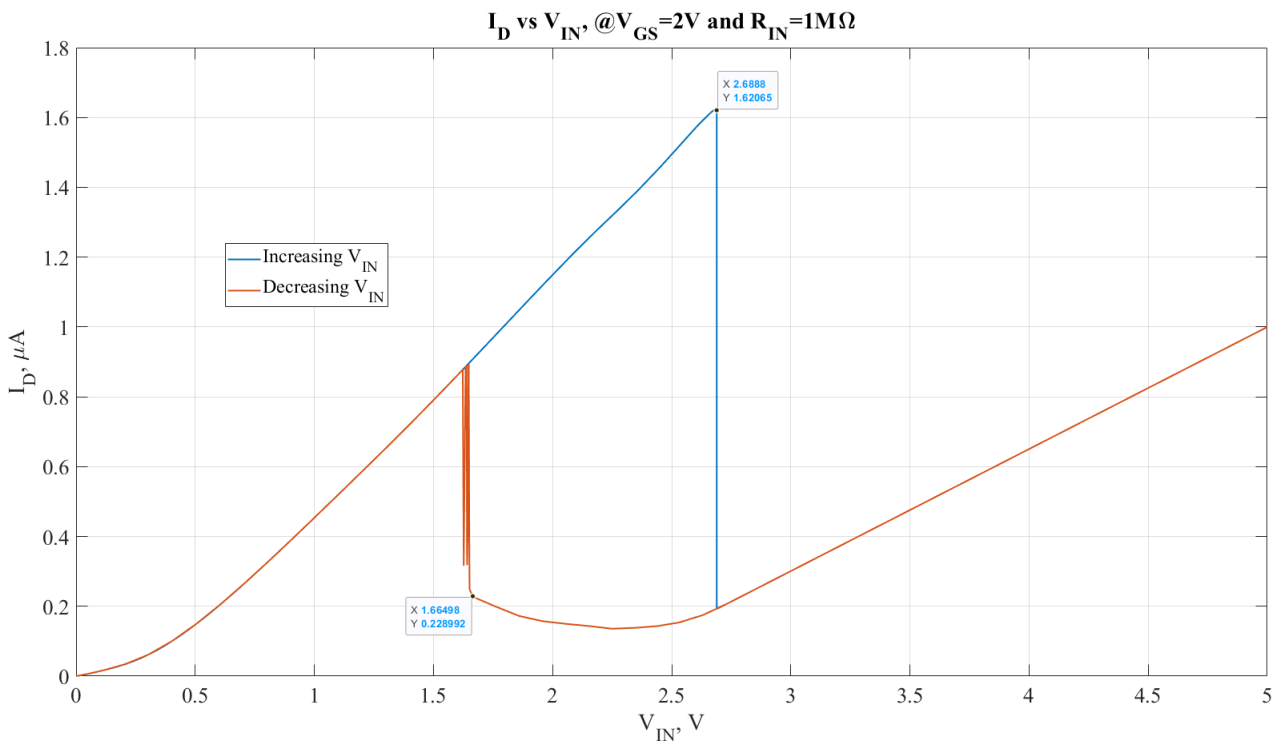


Figure 2.9. Hysteresis loop in the I-V characteristics, $V_{GS}=2\text{ V}$ and $R_{in}=1\text{ M}\Omega$.

Performing some simulations, the critical value required for the resistance in order to have the hysteresis loop seems to be around $150\text{ k}\Omega$, as shown in figure 2.10. In this case V_{GS} has been fixed to 2 V .

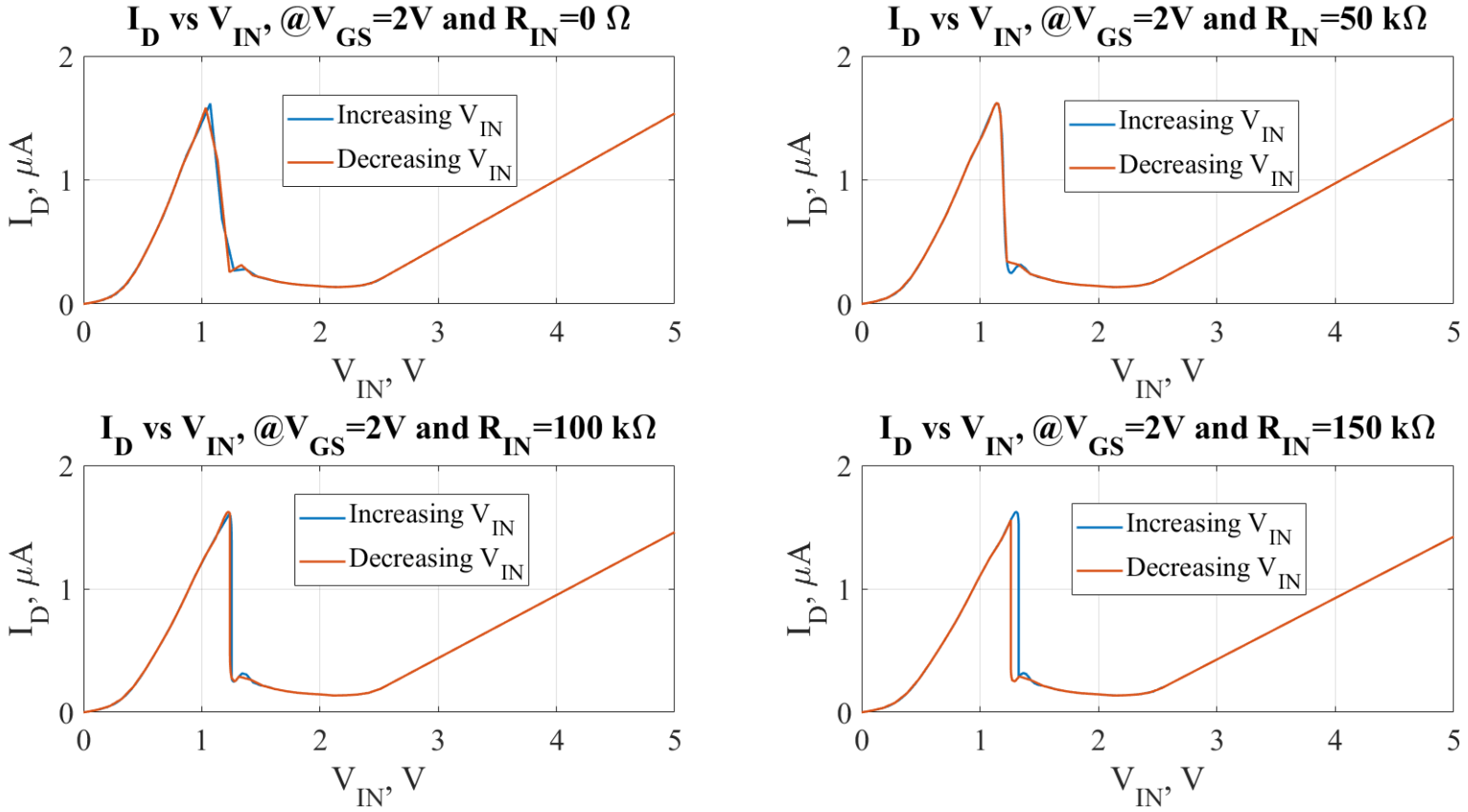


Figure 2.10. Investigation regarding the load resistance required in order to have the hysteresis in the I-V characteristics.

Comparing figure 2.10 with figure 2.9 it can be also noticed that the more R_{in} increases, wider the hysteretic range will be. Moreover, the discontinuity observed for the red curve (the one describing the behaviour going backward) will decrease.

It follows that if the I-V characteristics of the PCP shows a hysteresis, also the V_{out} vs V_{in} will do the same, as shown in figure 2.11.

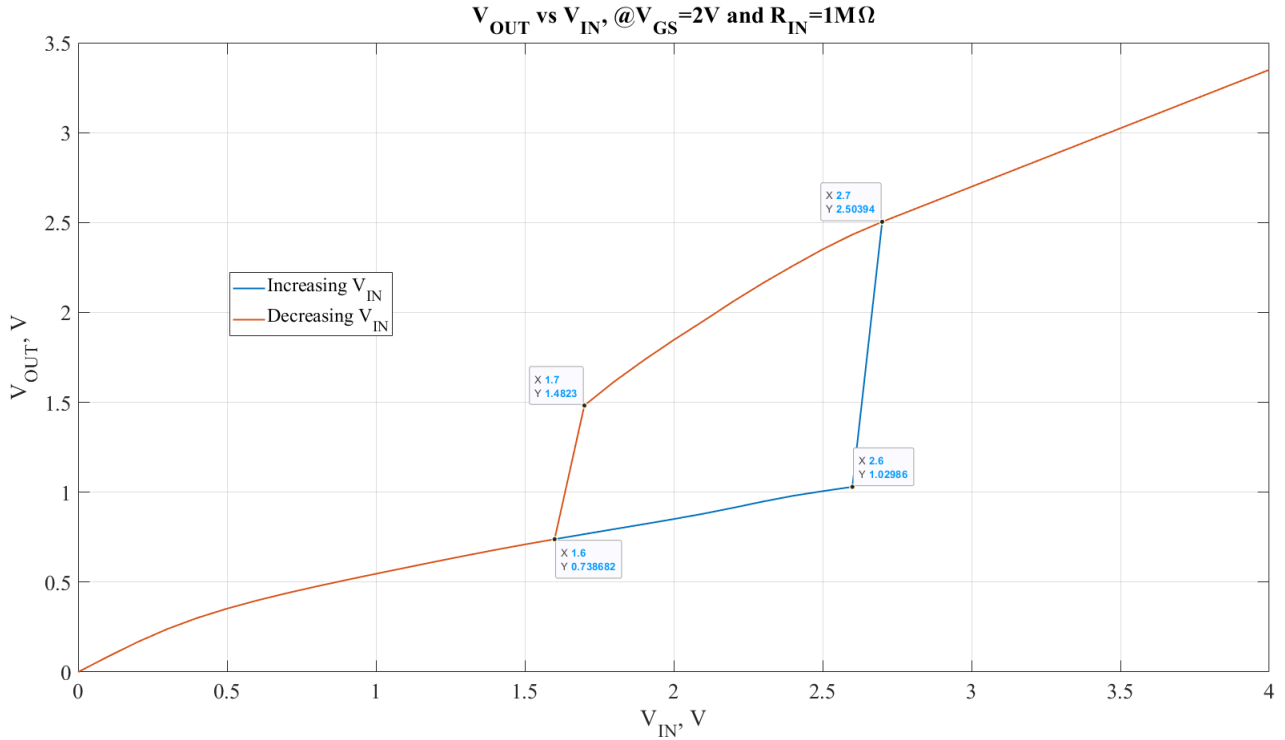


Figure 2.11. Hysteresis loop in the non-linear PCP-based stage, $V_{GS}=2V$ and $R_{in}=1M\Omega$.

These curves have been extracted by fixing $V_{GS}=2V$ and $R_{in}=1M\Omega$.

If V_{in} increases starting from 0 V the forward behaviour will be observed.

A $V_{th}=1.6147\mu A \cdot 1M\Omega + 1.05V = 2.6647V \simeq 2.7V$ will be present. When it is reached, the voltage drop V_{DS} will abruptly go from 1.03 V to 2.5 V.

At this point, decreasing V_{in} the V_{out} will not follow the same curve. Higher values will be assumed until $V_{in} \simeq 1.7V$, where V_{out} abruptly passes to 0.74 V starting from 1.5 V. Of course, also for the V_{out} vs V_{in} curve, if R_{in} increases the hysteretic range will increase and the discontinuity of the backward behaviour will decrease. The discontinuity of the forward behaviour increases if R_{in} increases, as explained in the previous section.

The important thing that can be noticed is that the V_{out} obtained decreasing the V_{in} (0.74 V) is lesser than the last value obtained before the V_{th} get reached (1.03 V).

Imagining to provide firstly a linear V_{in} to this circuit increasing in time, and then decreasing in time, from a temporal point of view a sort of spike will be obtained.

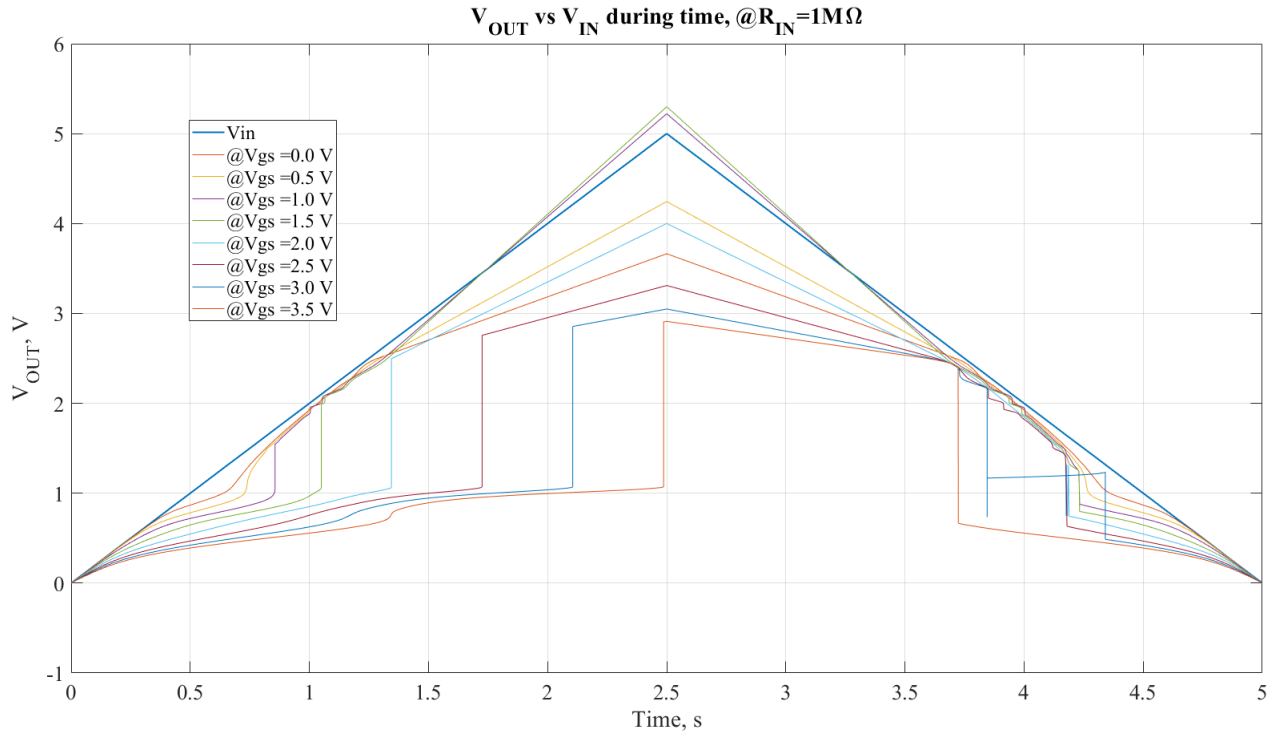


Figure 2.12. Analysis during time of the hysteresis.

The idea will be more developed talking about the neuron. In principle, the hysteresis loop in time could be used to implement a refractory period, since the V_{out} reached decreasing the voltage is lesser than the one before V_{th} . Figure 2.12 has been obtained by providing a linear V_{in} in time, initially going from 0 V to 5 V and then going from 5 V to 0 V. R_{in} is fixed to 1 M Ω whereas V_{GS} changes from 0 V to 3.5 V.

For V_{GS} lesser than 3 V the second threshold seems to be more or less the same, for higher voltages the trend changes.

It is important to notice that, since the simulations are based on the static model of the PCP molecule, all these results are valid only if the response time of the molecule is order of magnitudes smaller than the simulation time scale. However, since the response time has magnitude of ps the results obtained in the range of s or ms will hold [2].

2.2.2 Observations: parallel and cascade of non-linear stages

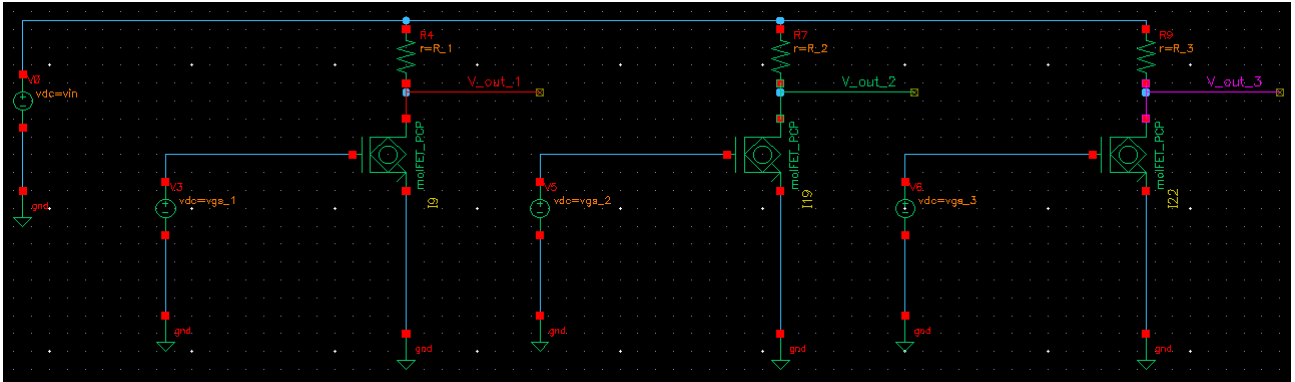


Figure 2.13. Parallel of non-linear stages based on PCP.

Considering a parallel of multiple branches implementing different non-linear stages, using PCP molfets, the behaviour described in the previous section can be observed for each V_{DS} once V_{GS} and R_{in} are fixed. This allows to have a stage presenting multiple thresholds, one for each V_{DS} .

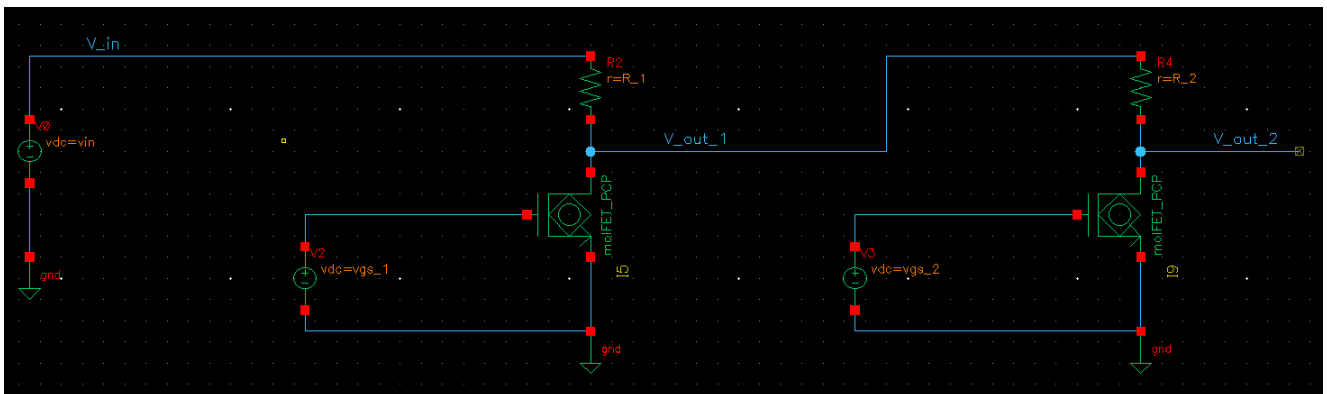


Figure 2.14. Cascade of non-linear stages based on PCP.

Considering a cascade of PCP non-linear stages as reported in figure 2.14, it is possible to obtain multiple thresholds on a single node as reported in 2.15.

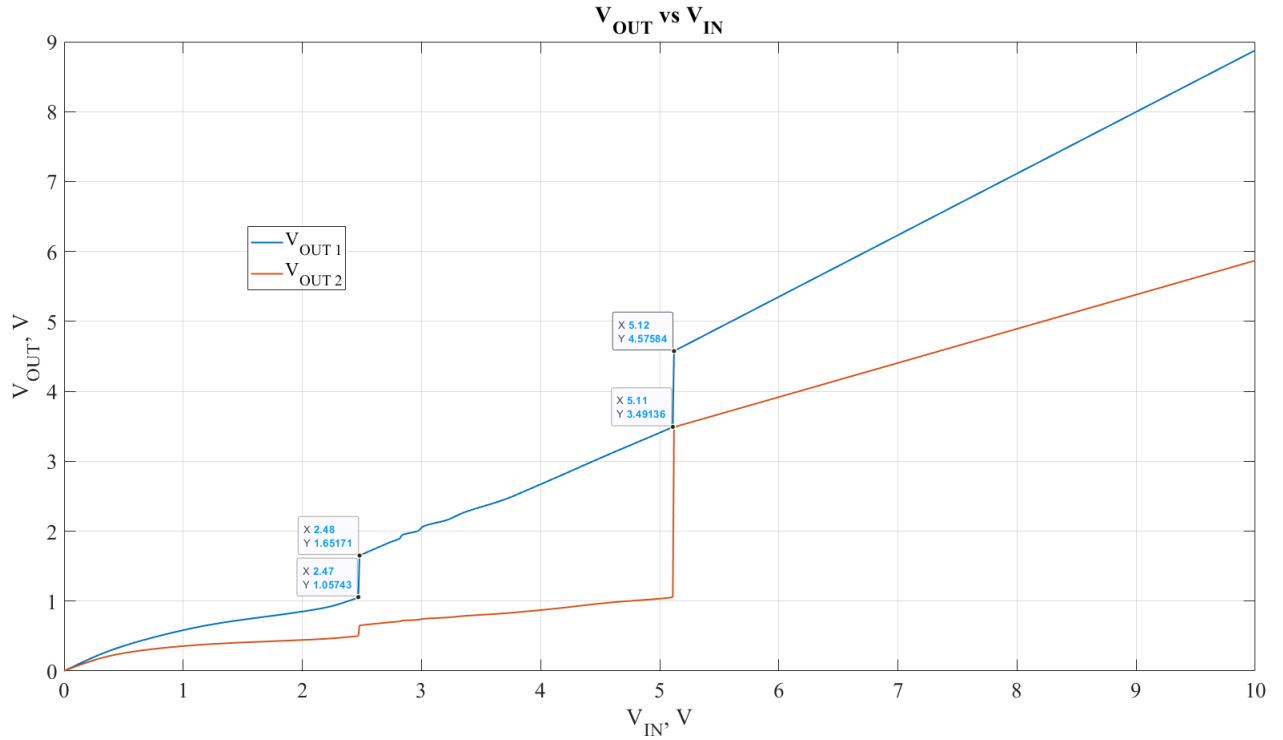


Figure 2.15. Multiple thresholds observed for a cascade of non-linear stage.

These results have been obtained using $R_1=1\text{ M}\Omega$, $R_2=1.5\text{ M}\Omega$, $V_{GS1}=1.5\text{ V}$ and $V_{GS2}=2\text{ V}$. It can be noticed that the first threshold at 2.47 V , associated to R_1 and V_{GS1} , is greater than the one obtained by using this branch alone, around 2.1 V . The second threshold at 5.11 V , due to R_2 and V_{GS2} , results to be more or less equal to $V_{peak2} + I_{peak2} \cdot (R_1 + R_2)$. In particular, the threshold associated to the first branch has to be lower with respect to the one associated to the second branch.

This trend can be generalized to more branches in cascade, introducing more steps for V_{OUT1} . However, for some combinations of the parameters, this behaviour seems to be not respected.

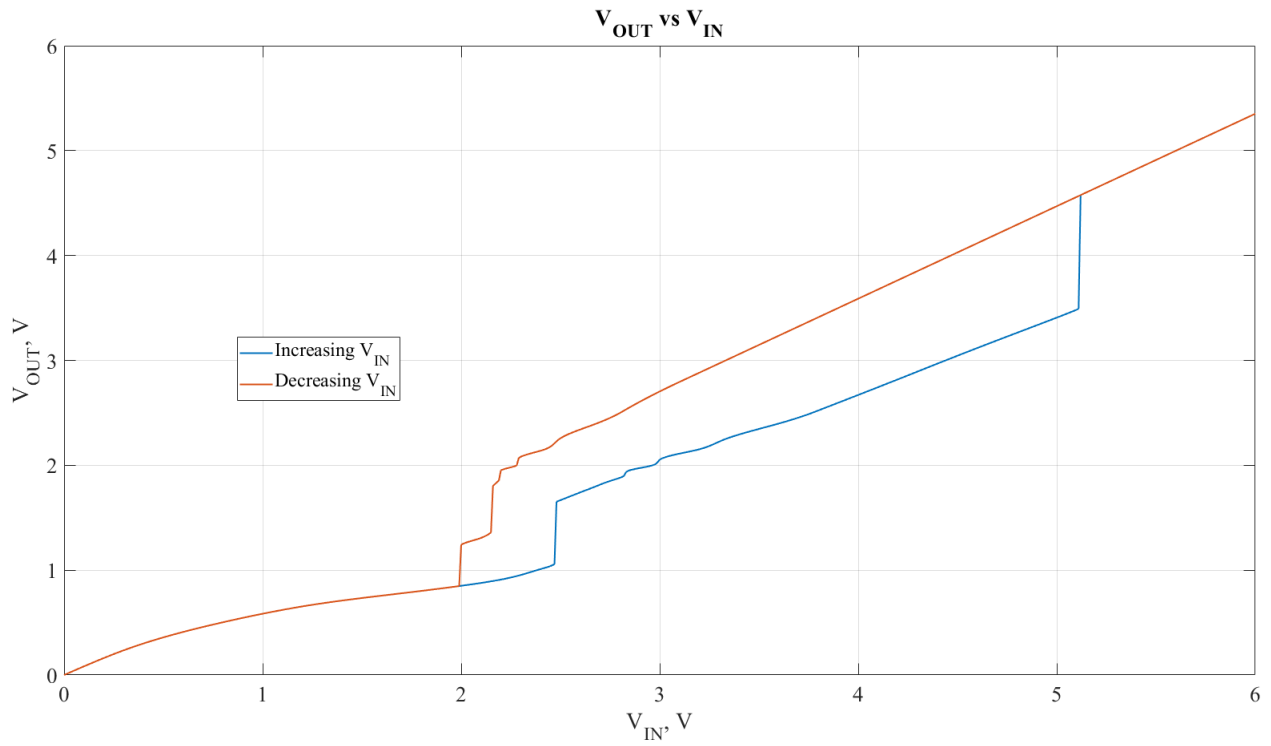


Figure 2.16. Hysteresis in multiple thresholds observed for a cascade of non-linear stage.

Hysteresis is still present, in figure 2.16 only V_{OUT1} has been reported. Maybe, this stage could be used for multilevel memory circuits.

2.3 PCP MolFETs based TRAM

In literature, the acronym "TRAM" refers to a tunneling-based random access memory ([23]).

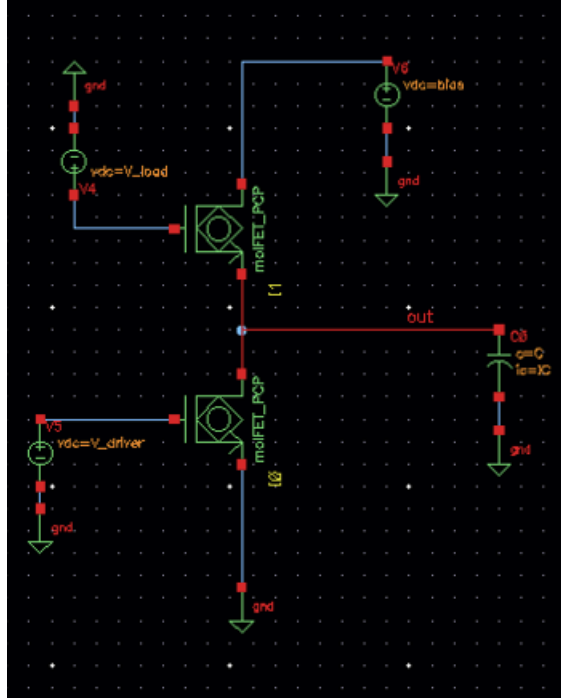


Figure 2.17. TRAM stage.

The circuit in figure 2.17 presents two PCP-based MolFETs in series, the top one is generally called "Load" whereas the bottom one is called "Driver". A constant positive bias voltage is applied to the drain of the load. A capacitance C is connected between the two PCP and ground, having a certain initial condition "IC".

The V_{DS} of the driver is equal to V_C , whereas the V_{DS} of the load is equal to $(V_{bias} - V_C) = -(V_C - V_{bias})$. This means that in principle, the I-V characteristics for the load can be plotted in the same I-V graph for the driver by reversing it with respect to the y-axis, afterwise, a shift for such characteristics towards right of an amount $V_{bias} > 0$ is performed.

Another thing to take into account is that the peaks of the I-V characteristics will reduce as it shifts with V_{bias} , therefore, V_{GS} for the load has to be increases in order to recover the peak's amplitude.

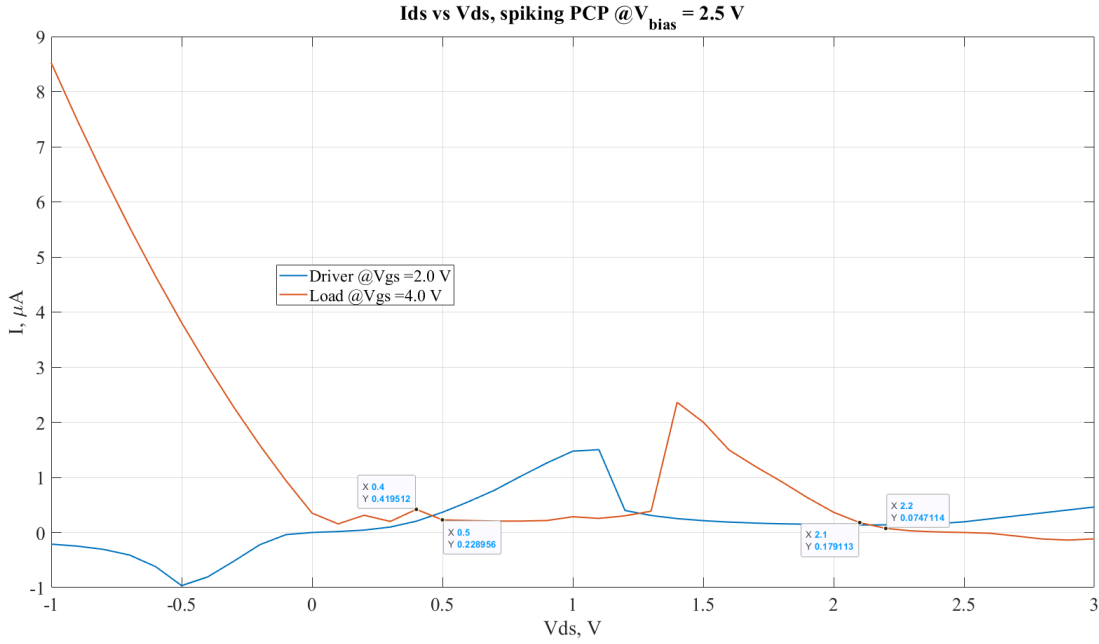


Figure 2.18. Load analysis using a PCP MolFET as load.

The results reported in figure 2.18 have been obtained by imposing $C=100$ pF, $V_{bias}=2.5$ V, $V_{load}=4$ V and $V_{driver}=2$ V.

As reported in [24], V_{bias} has to be greater than $2V_{peak}$ in order to obtain a shift able to provide two stable states. This is because, only in that case, two intersections can be obtained between the characteristics (the one in the middle due to the NDRs is not considered, since it is no stable).

As consequence, the only available voltages for the capacitance will be given by the two allowed stable states. Concerning the example in figure 2.18, these stable states are around 0.4 V-0.5 V and 2.1 V-2.2 V.

This means that, once the capacitance is charged towards one of these two states, the circuit will compensate eventual losses due to the leak from the capacitance, bringing back the voltage to the stable state: this can be exploited to implement RAMs, it is a refresh mechanism.

If the voltage increases, then the driver will discharge the capacitance until the stable state is reached again. If the voltage decreases, then the load will inject some current in the capacitance to recover the stable state, compensating the leaks.

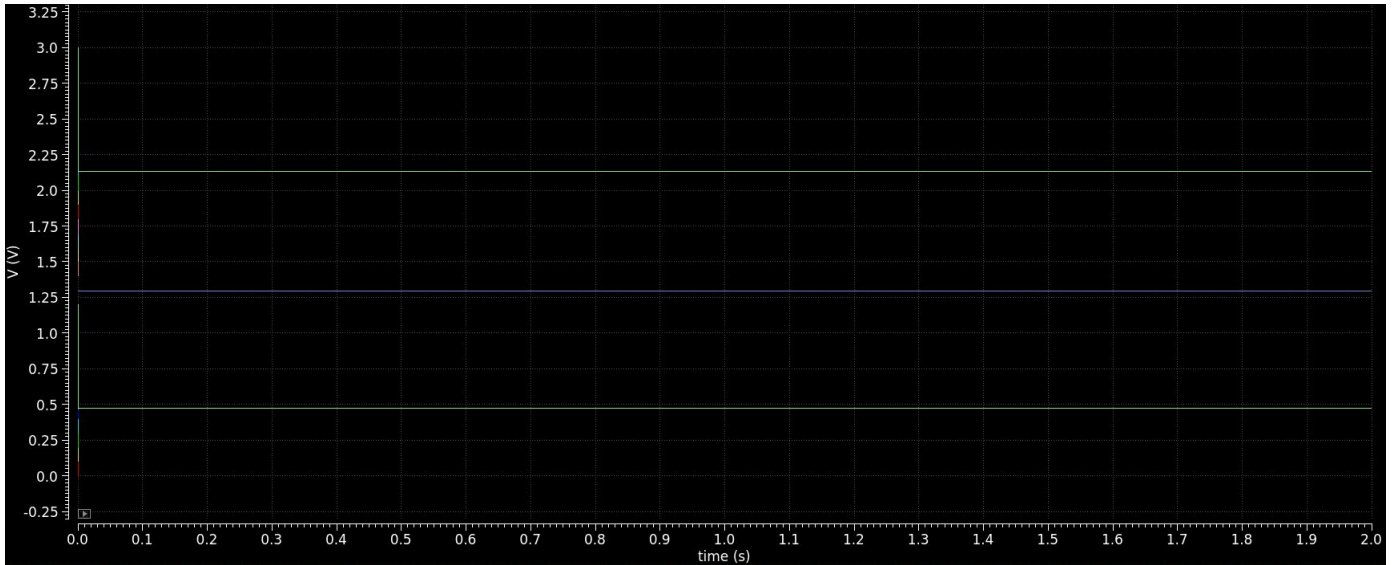


Figure 2.19. Time analysis: V_C vs time starting from different initial conditions.

Figure 2.19 reports a time analysis obtained letting V_C relaxing towards one of the two stable states, starting from an initial condition IC which has been changed as parameter.

Going from 0 V to around 1.2 V, the relaxation happens towards 471 mV, quite coherent with the load analysis. If IC=1.25 V then this voltage will be kept, since it corresponds to the unstable state due to the intersection near the NDRs. Finally, going from around 1.3 V to 3 V, the relaxation happens towards 2.13347 V, again coherent with the load analysis.

The ranges for which a convergence to one of the two states happens, are evidently different: for the state corresponding to 471 mV, the convergence range is equal to 1.2 V whereas for the one corresponding to 2.13347 V, it is equal to 1.7 V.

This is due to the difference between the peaks of the I-V characteristics present in the load analysis, it turns out that the state near the greatest peak is favoured with respect the other one. This is not observed in RTD-based TRAM, since the characteristics are symmetric with respect to the origin, therefore the amplitude of the peaks are the same.

2.4 PCP-based MOBILE

Another application deriving from the stable states allowed by the TRAM stage is the MOBILE one (see [25]). It stays for "Monostable-Bistable Transition Logic Element". The circuit is the same as figure 2.17, however, this time the bias voltage is not fixed but consists in a square wave. The usage of the square wave allows to have a transition from a monostable configuration (only one intersection between the characteristics of driver and load) to a bistable configuration (two intersections between the characteristics of driver and load, due to the shift introduced by V_{bias}).

Theoretically, the output voltage V_C should be forced by the peak presenting a greater amplitude, when V_{bias} is such that a bistable configuration can be assumed. This means that when the condition $V_{bias} > 2V_{peak}$ is met, V_C will assume the high voltage value if the driver's peak is lower than the load one, otherwise the low voltage value will be assumed. When $V_{bias} < 2V_{peak}$, the stable state get reset.

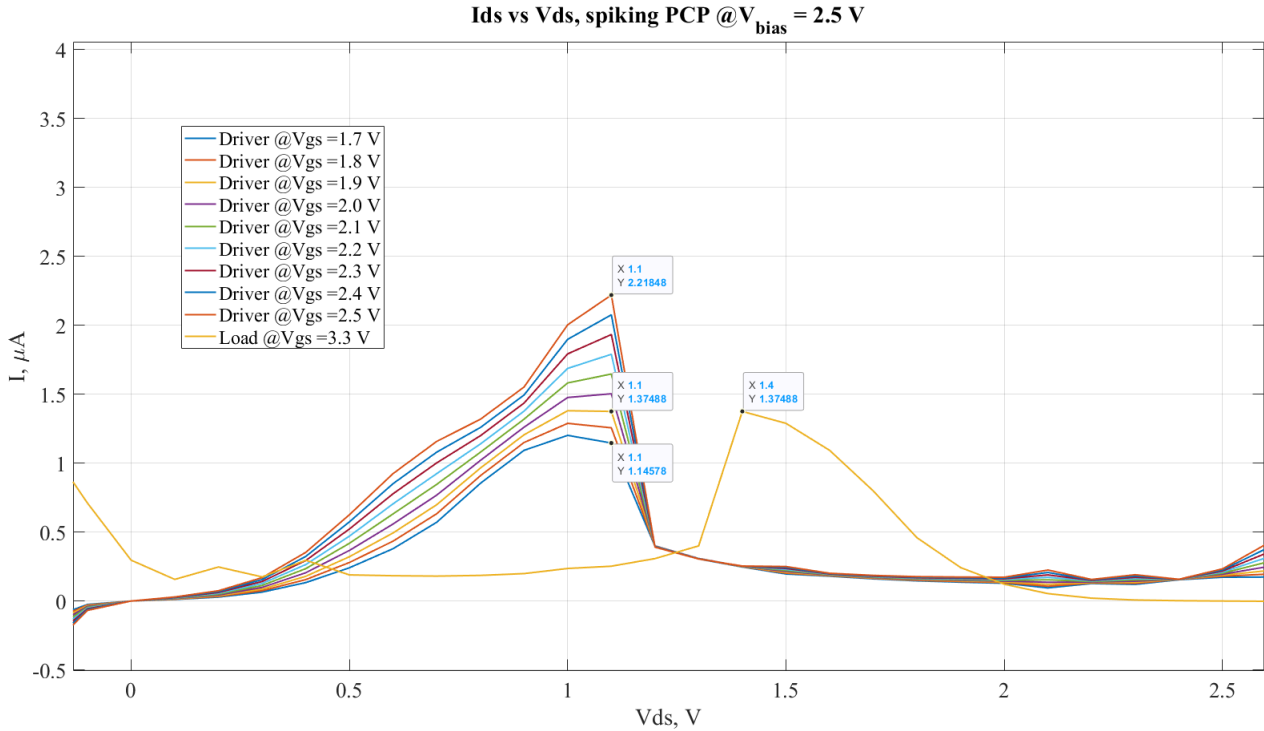


Figure 2.20. MOBILE load analysis.

In figure 2.20 a load analysis using different values for V_{GS} of the driver is reported.

- $V_{load}=3.3\text{ V}$;
- V_{bias} goes from 0 V to 2.5 V, the period of its square wave is 2 μs whereas the pulse width is 1 ms;

- V_{driver} goes from 1.7 V to 2.4 V, the period of its square wave is 4 μ s whereas the pulse width is 1 ms;
- $C=100$ aF.

Since the value of the current peak for the driver is equal to the one of the load for $V_{driver}=1.9$ V a threshold around this voltage was expected.

From simulations, it turned out to be around 2.4 V, therefore the lower voltage is favoured only when V_{driver} reaches this value and V_{bias} is 2.5 V. If instead V_{bias} is 2.5 V but V_{driver} is lesser than 2.4 V, then the higher voltage state will be assumed by V_C . The two stable states are coherent with the ones provided by the load analysis in figure 2.20.

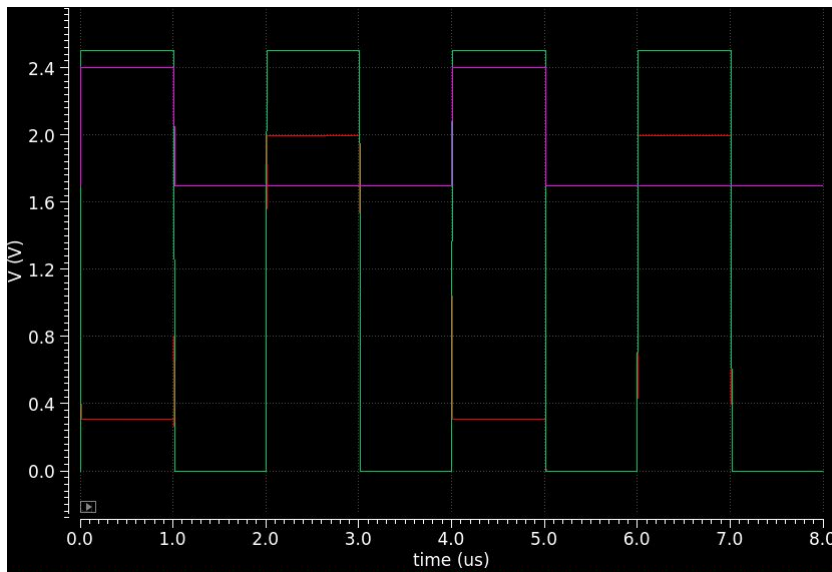


Figure 2.21. Results for the MOBILE stage: V_C in red, V_{driver} in purple and V_{bias} in green.

Of course, when $V_{bias}=0$ V the only stable state obtained is for $V_C=0$ V since the curves meet just in the origin.

This overestimation for the voltage needed to have the switch from one stable state to the other one, can be due to the shape of the characteristics of the PCP MolFET.

In fact, using RTD, the shape is the same for all the curves and what change are just the peaks of current. Concerning PCP MolFETs, the characteristics of the driver and the load are different because of the shift. This may says that what matters is not really the difference in amplitude of the peaks, but the difference in area underlying each curve.

In any case, the behaviour is met apart from the overestimation for the threshold voltage.

2.4.1 MOBILE as threshold mechanism

A possible application for such stage could be the implementation of a threshold mechanism. This could be useful for some applications of the PCP MolFETs in the neuro-morphic field.

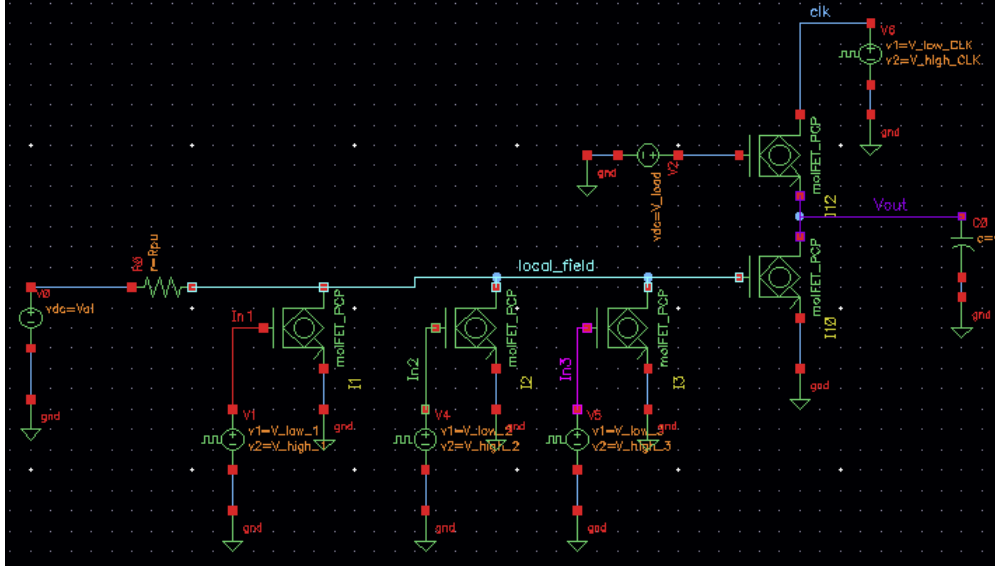


Figure 2.22. Threshold mechanism using PCP molecules.

The solution for the implementation of a neuron proposed in [2] uses MolFETs in order to reduce the V_{DS} dropping on them, so that when a certain value is reached, a voltage comparator changes its output. Maybe, a threshold mechanism implemented with a PCP-based MOBILE could bring to a full PCP implementation for the proposed artificial neuron.

Referring to the circuit in figure 2.22, the following parameters have been set:

- A clock signal is given as square wave to provide the bias going from 0 V to 2.5 V, the pulse width is 1 μ s, the period is 2 μ s;
- V_{al} is fixed to 1.2 V;
- R_{PU} is fixed to 90 k Ω , so that when at least two MolFETs conduct, the threshold is reached;
- The pulses arriving on the three gates go from 600 mV to 1.7 V, the pulse width is equal to 1 μ s and the periods are such that different combinations can be tested;
- V_{load} is set to 2 V;
- $C = 100$ aF.

From figure 2.22 the relation giving the V_{DS} can be obtained through Kirchhoff for the voltage. In particular, $V_{DS} = V_{al} - i_R \cdot R_{PU}$, where i_R is the total current passing through the resistance R_{PU} .

The current i_R depends on how much current the MolFETs conduct. The idea is to exploit this current in order to let the MOBILE stage to assume one of the two stable states, when V_{bias} is high, by varying the voltage on the gate of the driver. Of course the presence of a clock signal limits the applicability of this solution, however, it is still a solution full PCP-based which allows also a decoupling from the input MolFETs.

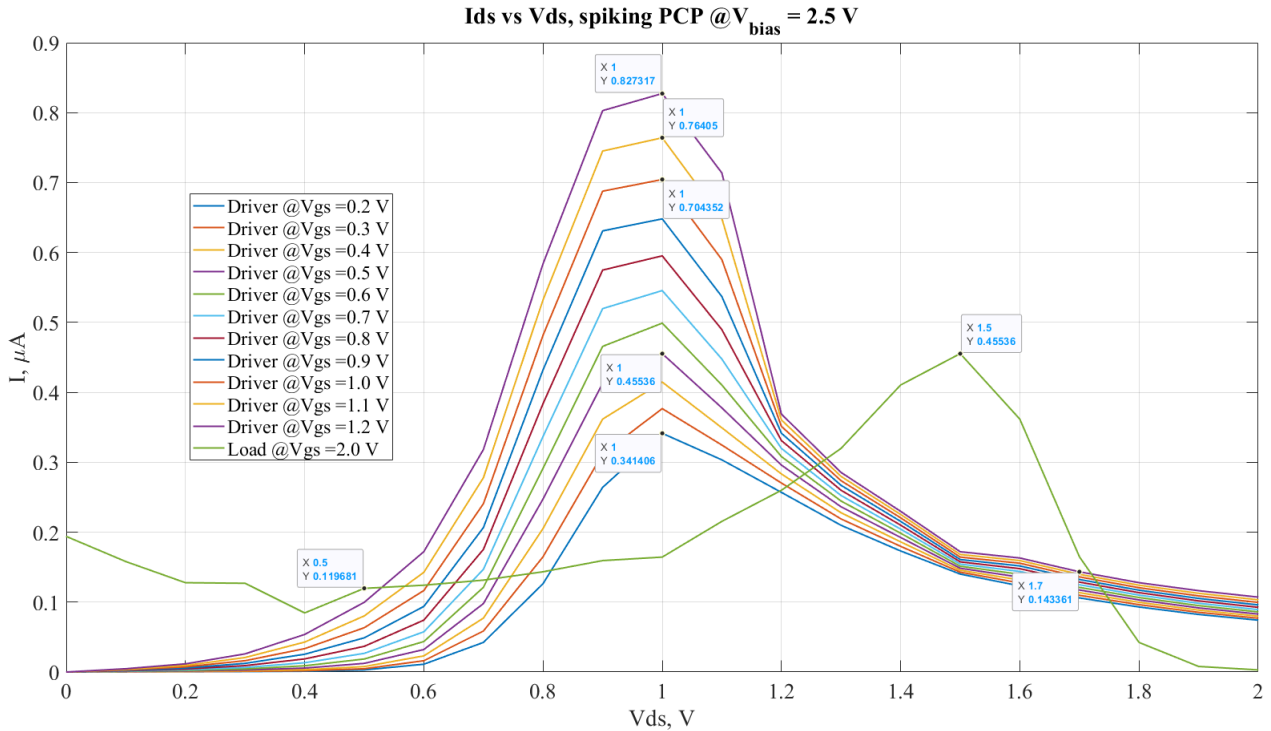


Figure 2.23. Load analysis for the MOBILE threshold mechanism.

The threshold voltage results to be around 0.9 V. If all the MolFETs are switched OFF, V_{DS} is equal to V_{al} . Only when two or more PCP MolFETs are active the V_{DS} reaches the threshold and V_{out} goes from 0.62 V to 1.72 V, as shown in figure 2.24.

The parameters have been optimized in order to have similar input and output levels, so that multiple stages can follow in cascade.

It has also to be noticed that this stage is inverting the output voltage with respect to the input one.

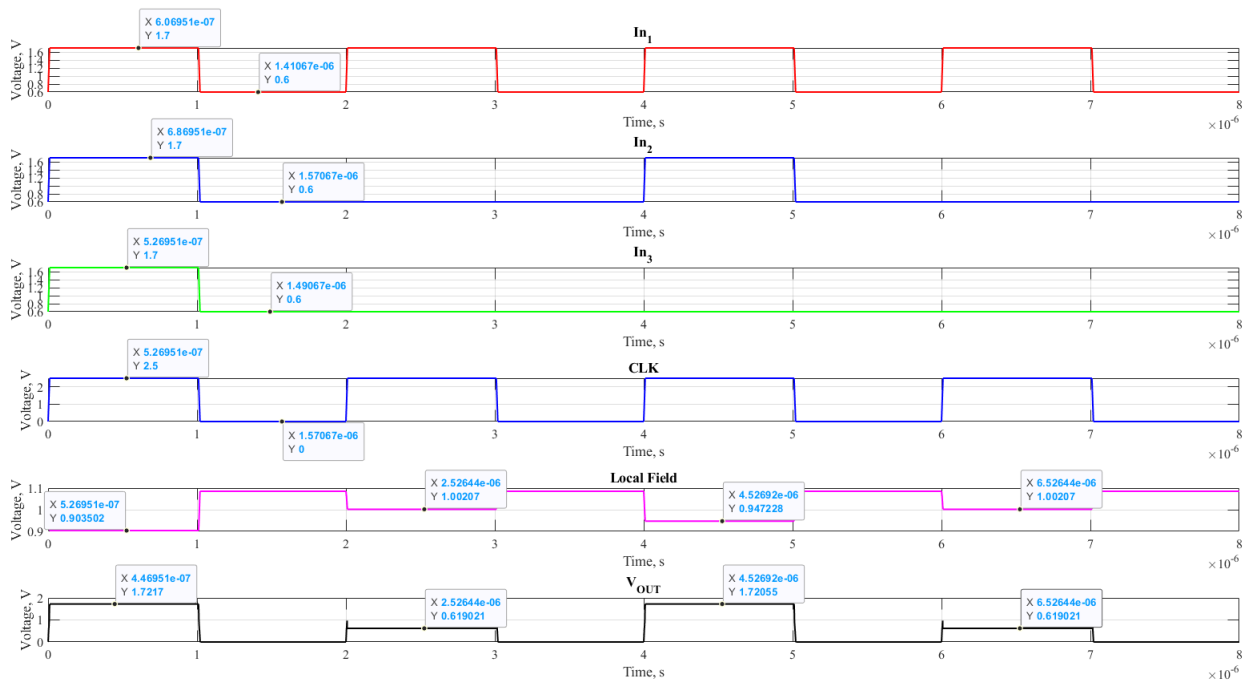


Figure 2.24. Results for the MOBILE threshold mechanism.

A final consideration needs to be done concerning the behaviour required for the clock, in order to have this stage working correctly.

- It is necessary to reset the stable state for the output, so that the next one can be assumed;
- The input voltages need to switch to their higher value together with the clock, this means that the period of the input signals has to be a multiple of the clock's period;
- An input which has switched to its higher value must return to its lower value before the clock returns to its lower value, or in the same time;
- An input which has switched to its lower value can maintain it, there are not conditions such as for the switches to the higher value.

2.5 Conclusion

This concludes the discussion about the possible general applications for the PCP-based MoFETs in electronic circuits. The stages are exploiting the presence of stable states, originated by the interaction between different loads and the NDR in the MoFET I-V characteristics.

Chapter 3

Artificial neurons based on PCP MolFETs

In this chapter, a possible molecular implementation for artificial neurons, based on the theory presented in chapter 2, will be proposed and commented.

The idea is to exploit an exclusive contribution coming from the NDR in the I-V characteristics of the PCP, this is possible by using the non-linear stage presented in chapter 3.

3.1 Molecular-FET based soma

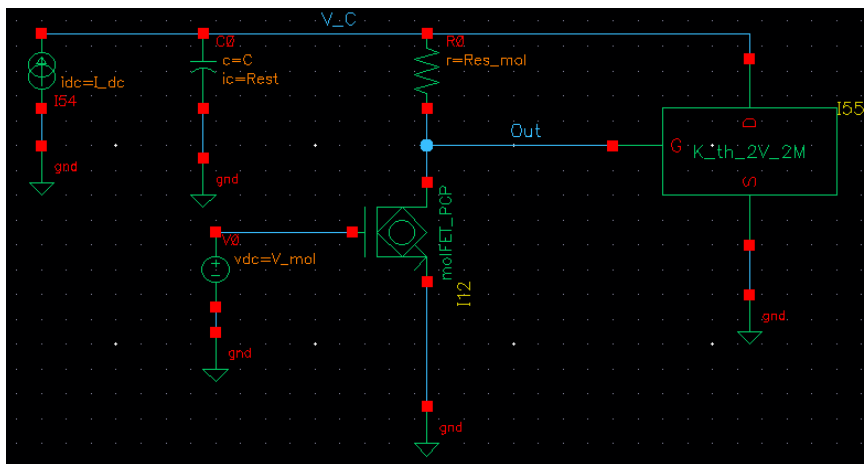


Figure 3.1. Implementation of a soma based on NDR.

Talking about the model of Hodgkin and Huxley, introduced in chapter 2, it has been explained how the collective action of the ionic channels brings to the generation of an action potential: V_C charges up until it activates the sodium channel, which

then brings to the activation of the potassium channel, that finally discharges the capacitance again. Concerning the Integrate and Fire model, this whole mechanism is somehow hidden in the spike generator block, which just takes into consideration a V_{th} to overcome in order to generate a spike.

The circuit in figure 3.1 presents a PCP MolFET in series with a resistance Res_{mol} , which implements a non-linear stage. A constant current generator (I_{dc}) is charging the capacitance C during time. When V_C reaches a certain threshold V_{th} fixed by Res_{mol} and V_{mol} , the V_{DS} dropping on the PCP will increase abruptly and this will increase the current passing through the block "K_th_2V_2M". In particular, the V_{DS} dropping on the PCP is the V_G dropping on this second block. This block is playing the role of the K-channel, in the view of Hodgkin and Huxley model. This means that, once it is activated, it must discharge the capacitance C so that V_C can reach the value required from the non-linear stage in order to have the second threshold (the one allowing a jump toward a smaller voltage for V_{DS} , coming from the hysteresis), then the K-channel block will stop to conduct again.

The non-linear stage and the K-channel block implement the spike generator, under the Integrate and Fire perspective. In particular, the node "Out" will present the generation of voltage spikes during time.

3.1.1 The theoretical K-channel

Supposing to have the possibility to work on different molecules, searching for a specific behaviour, it is possible to understand how the I-V characteristics of the block should be, to let the neuron work correctly. This is not a limit, since, as explained in chapter 1, one of the advantages of the molecular technology is the versatility in terms of I-V characteristics.

Let's fix $V_{mol}=2V$, so that the quasi-linear behaviour before the peak in the I-V characteristics of the PCP can be used to have some qualitative information about the equivalent resistance for the PCP. Then $Res_{mol}=2M\Omega$ allows to have a non-linear stage with a well defined jump, this will be around $V_C=V_{th}=4.3V$ because of the considerations done in chapter 3. The name "K_th_2V_2M" just refers to the fact that this theoretical block should allow the neuron to work correctly using $V_{mol}=2V$ and $Res_{mol}=2M\Omega$. Once the idea is demonstrated, then it could be extended using different Res_{mol} and V_{mol} .

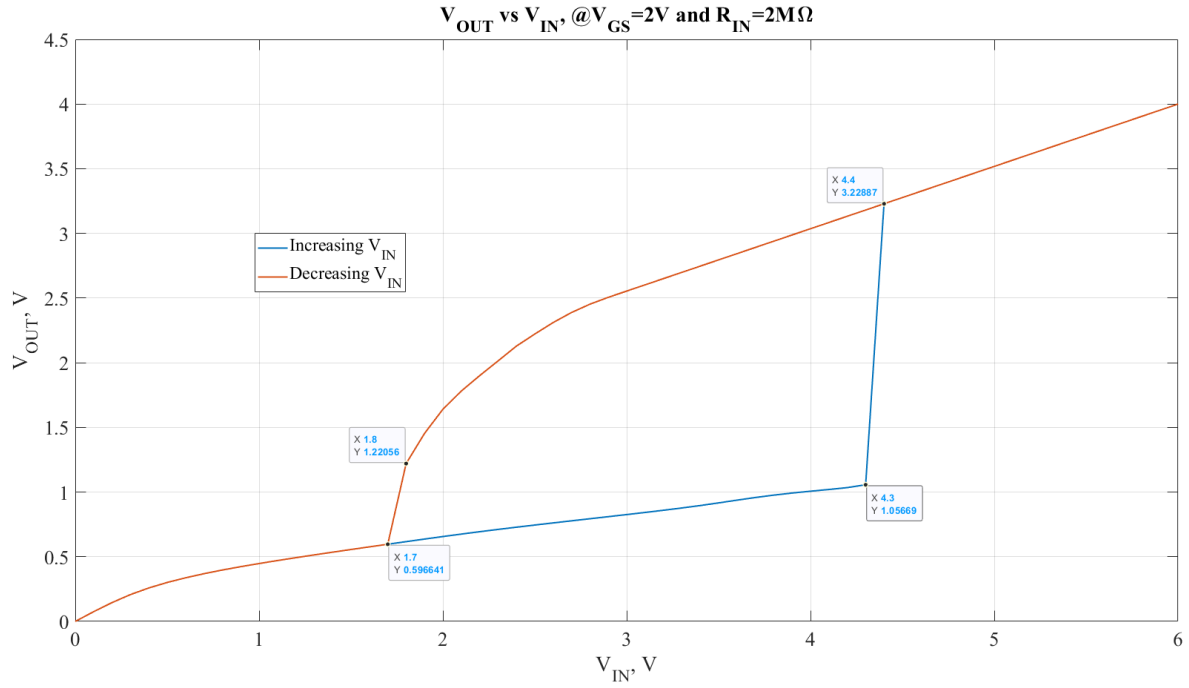


Figure 3.2. Hysteresis of the non-linear stage using $V_{mol}=2\text{ V}$ and $Res_{mol}=2\text{ M}\Omega$.

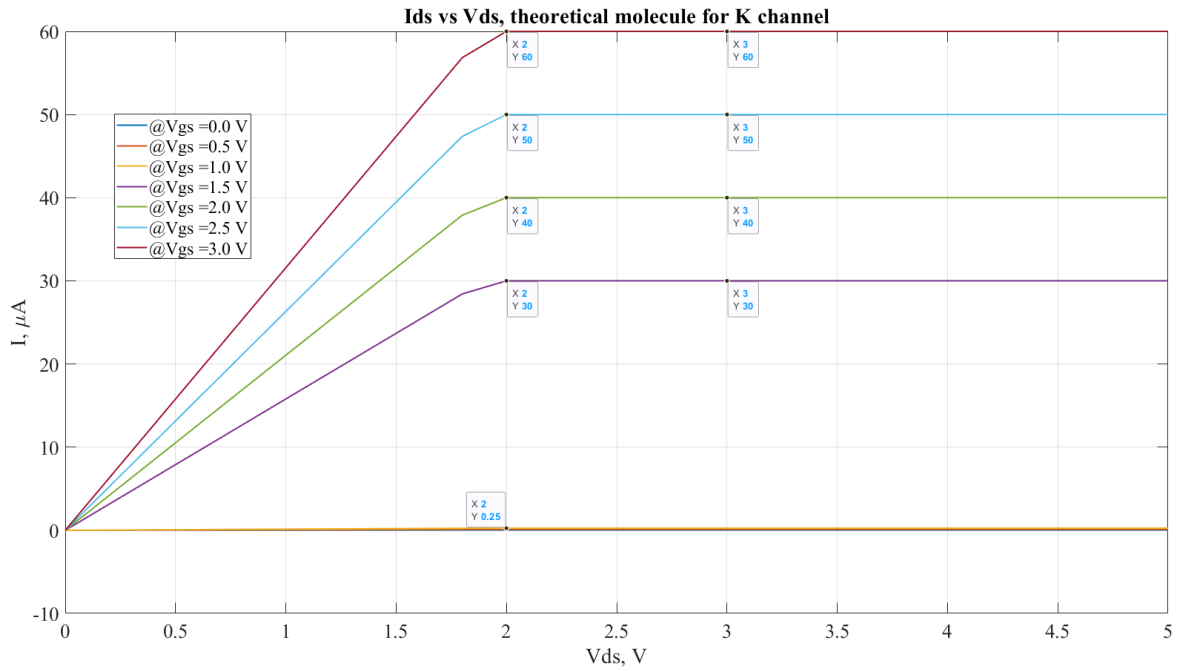


Figure 3.3. I-V characteristics for the hypothetical molecule implementing the K-channel.

Taking into account the non-linear stage, from figure 3.2 can be noticed a first jump for the "Out" node from 1.06 V to 3.23 V once V_C reaches 4.3 V, then, decreasing V_C a second jump will be observed from 1.22 V to 0.6 V once V_C reaches around 1.7 V.

This means that the hypothetical MolFET should use a molecule which is not able to conduct at all for V_{GS} between 0 V and around 1 V. However, it must be able to conduct a lot if V_{GS} is between 1.22 V and 3.22 V.

Concerning the $V_{DS}=V_C$, the "K MolFET" should be able to maintain a high current going from around $V_C=4.4$ V to around $V_C=1.8$ V, therefore we could think about a sort of saturation in this range.

A possible I-V characteristics for such theoretical molecule is reported in figure 3.3.

The maximum current is fixed to 60 μ A when V_C is around 3 V.

It is a nmos-like characteristics and actually it is also very similar to the behaviour of the current passing through potassium channel in time. It has been created in Matlab (Appendix B), then imported on Cadence Virtuoso in order to simulate the circuit.

3.1.2 Estimation of the time constant τ

As can be noticed from figure 3.1, while $V_C < V_{th}$ this circuit is implementing a parallel RC. The differential equation describing its charging will be similar to eq. 1.11, having eq. 1.12 as solution since the input current is constant.

The first thing to do in order to make an estimation for the time constant of this circuit, is to study the equivalent resistance for the PCP MolFET before the NDR occurrence.

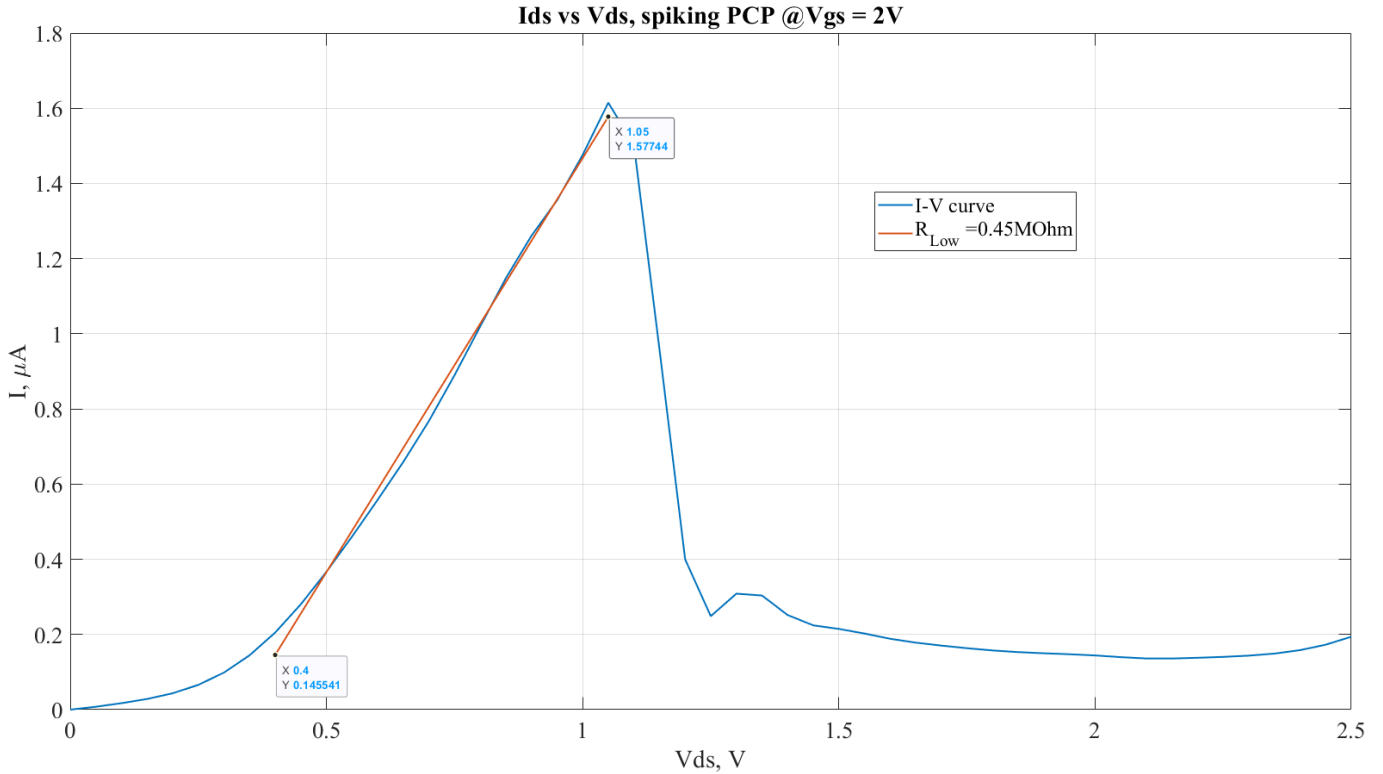


Figure 3.4. Estimation for the equivalent resistance for the PCP molecule before the current peak, $V_{mol} = V_{GS} = 2$ V.

Exporting the I-V characteristics from Cadence Virtuoso to Matlab, it is possible to interpolate the linear range before the peak of current. The linear behaviour is evident going from around $V_{DS} = 0.4$ V to $V_{peak} = 1.05$ V.

This resistance turns out to be around $R_{LOW} = 0.45$ M Ω and can be used to estimate the global resistance before the jump due to the non-linear stage, when injecting current into the neuron. Performing the linear approximation in this range it should be also considered a battery, having value determined by the intersection between the line and the voltage axis. This battery should be in series to the resistance, implementing a sort of E_{Leak} . However, its contribution in V_{∞} will be neglected, since it is around 0.334 V.

From figures 3.2 and 3.3, it is possible to notice that if $V_C < V_{th}$ then $V_{DS} \lesssim 1\text{ V}$, therefore the K-channel will not conduct at all (hundreds of nA).

A resistance having value around $0.45\text{ M}\Omega + Res_{mol} = 2.45\text{ M}\Omega$ will be obtained. This resistance can be considered as the R_{Leak} , both present in "Hodgkin and Huxley" and "Integrate and Fire" models, at least until the occurrence of V_{th} . This implies that the value of the capacitance needs to be some nF in order to have $\tau = RC$ of some ms. Arbitrarily, the capacitance C has been fixed to 1 nF.

An important point to be highlighted is that the choices taken for this circuit are not necessarily the best ones for emulating the biological behaviour, this work just wants to set the basis in order to verify the feasibility of the idea of exploiting the neural computational principles with MolFETs.

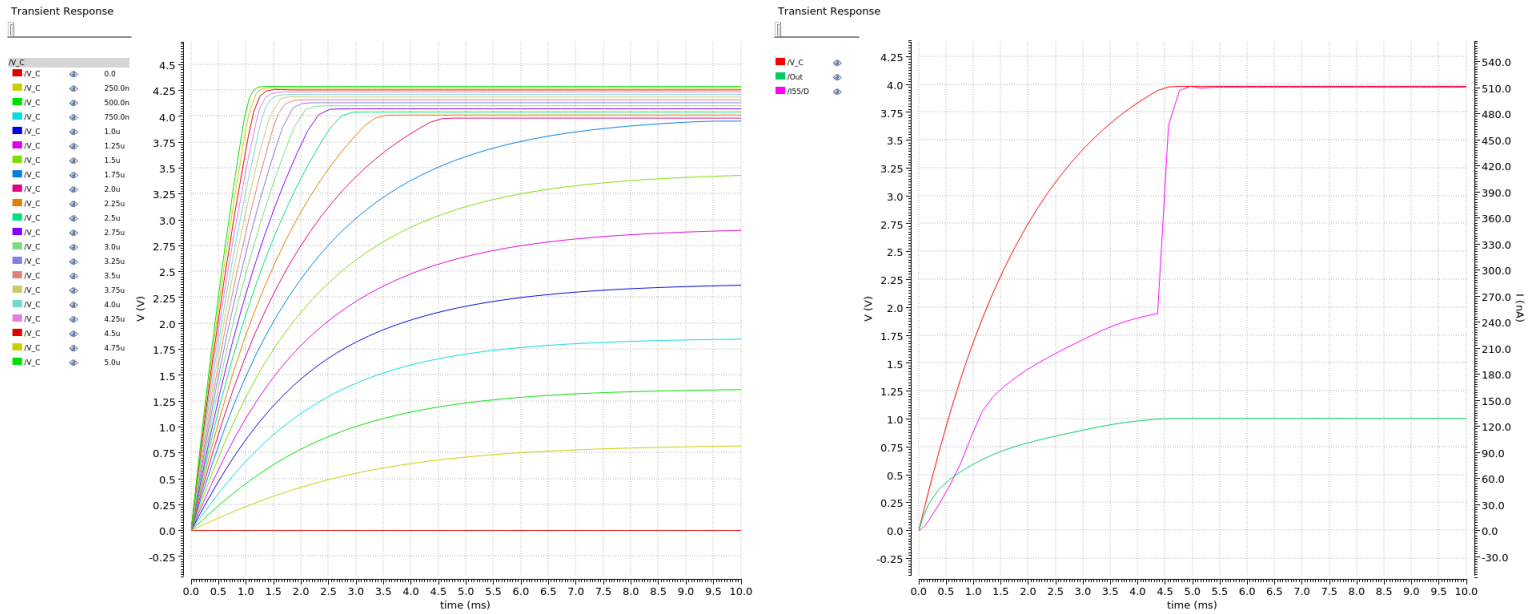


Figure 3.5. RC charging in time of the proposed neuron using:
 1) $0\text{ }\mu\text{A} \leq I_{in} \leq 5\text{ }\mu\text{A}$ 2) $I_{in} = 2\text{ }\mu\text{A}$ (Green = V_{out} , Red = V_C , Pink = I_{DS} of the K-channel).

The RC charging in fig.3.5a) is quite respected until the injected current reaches values around $2\text{ }\mu\text{A}$. In such condition the exponential behaviour is lost when V_C is more or less equal to 4 V , therefore when it approaches V_{th} . This is due to the fact that in this range V_{out} reaches values around 1 V , enabling the K-channel MolFET to conduct instantaneously a certain amount of current, proportional to V_C and different from $0.25\text{ }\mu\text{A}$ kept below threshold. As can be noticed from the example in fig.3.5b), for this range of input currents, the K-channel is not able to discharge the capacitance, but can delay the reaching of the threshold.

3.1.3 Patterns of spikes vs constant injected current

When $V_C = V_{th}$ a single voltage spike is generated at the output node, whereas V_C get reset by a spike of current passing through the "K-channel", to a value $V_{reset} \approx 1.8\text{ V}$. If no input currents are present, V_C will relax back to $E_{Leak} = 0\text{ V}$. All of this will adapt to the spike generator block used by the integrate and fire model.

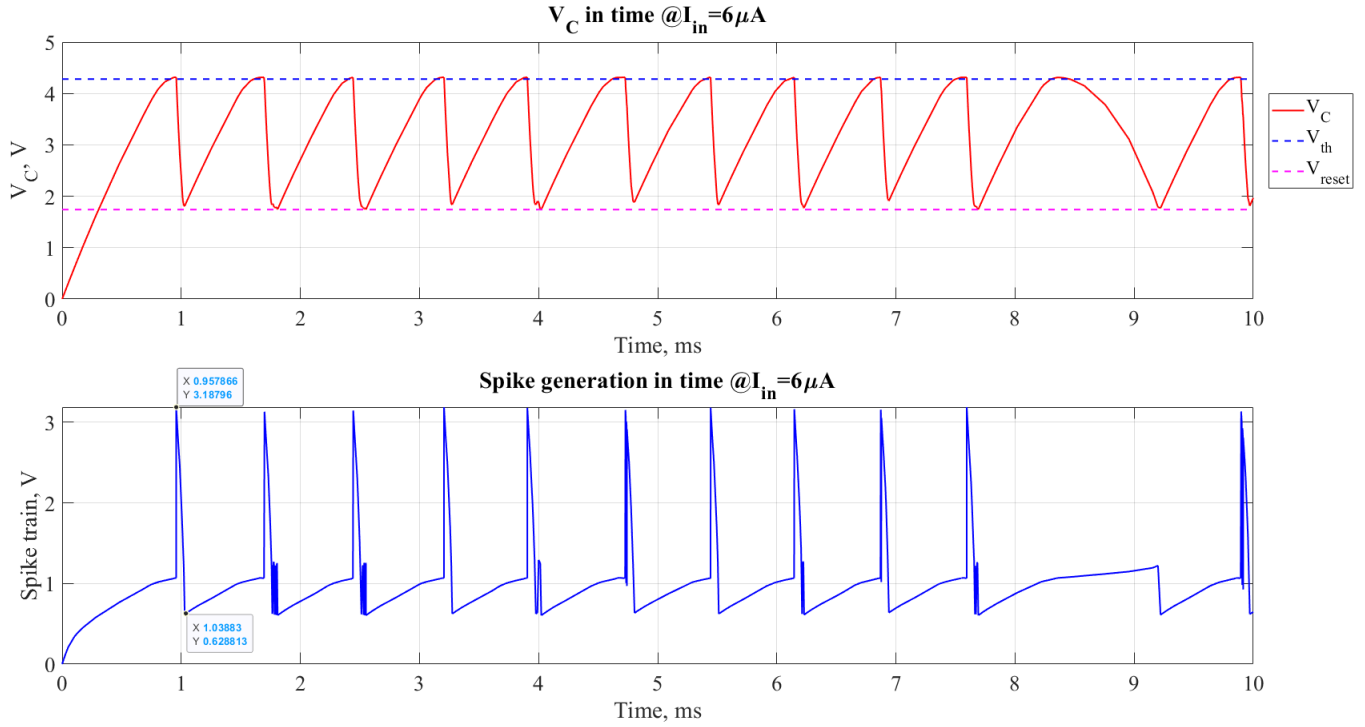


Figure 3.6. V_C and spike generation in time, injecting $I_{in}=6\text{ }\mu\text{A}$.

The spikes generated by this circuit present a peak of about 3.18 V , the minimum due to the hysteresis in the non-linear stage is around 628 mV . By injecting $I_{in} = 6\text{ }\mu\text{A}$, the refractory period is around 0.63 ms while the frequency of the spike train is around 1.34 kHz .

The generation of the patterns starts from $6\text{ }\mu\text{A}$ and stops around $12\text{ }\mu\text{A}$, value for which the K-channel is no more able to discharge the capacitance because of the constant input injection. This provides a range of about $6\text{ }\mu\text{A}$ in which the frequency changes with the constant injected current.

The idea is to use some sensors able to provide some information through a constant current, therefore, a possible "frequency encoding" of the input can be obtained and processed further with other neuron layers.

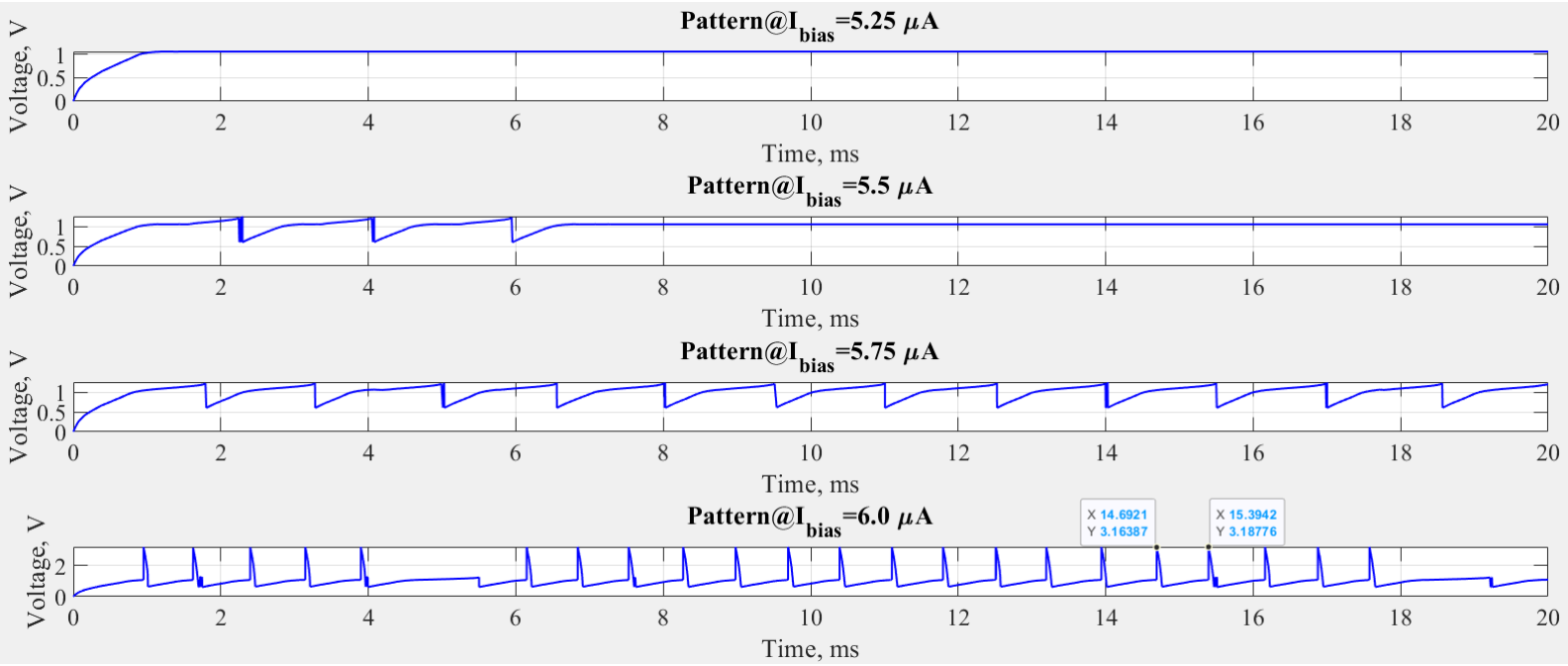


Figure 3.7. Patterns generated using $5.25 \mu A < I_{dc} < 6 \mu A$.

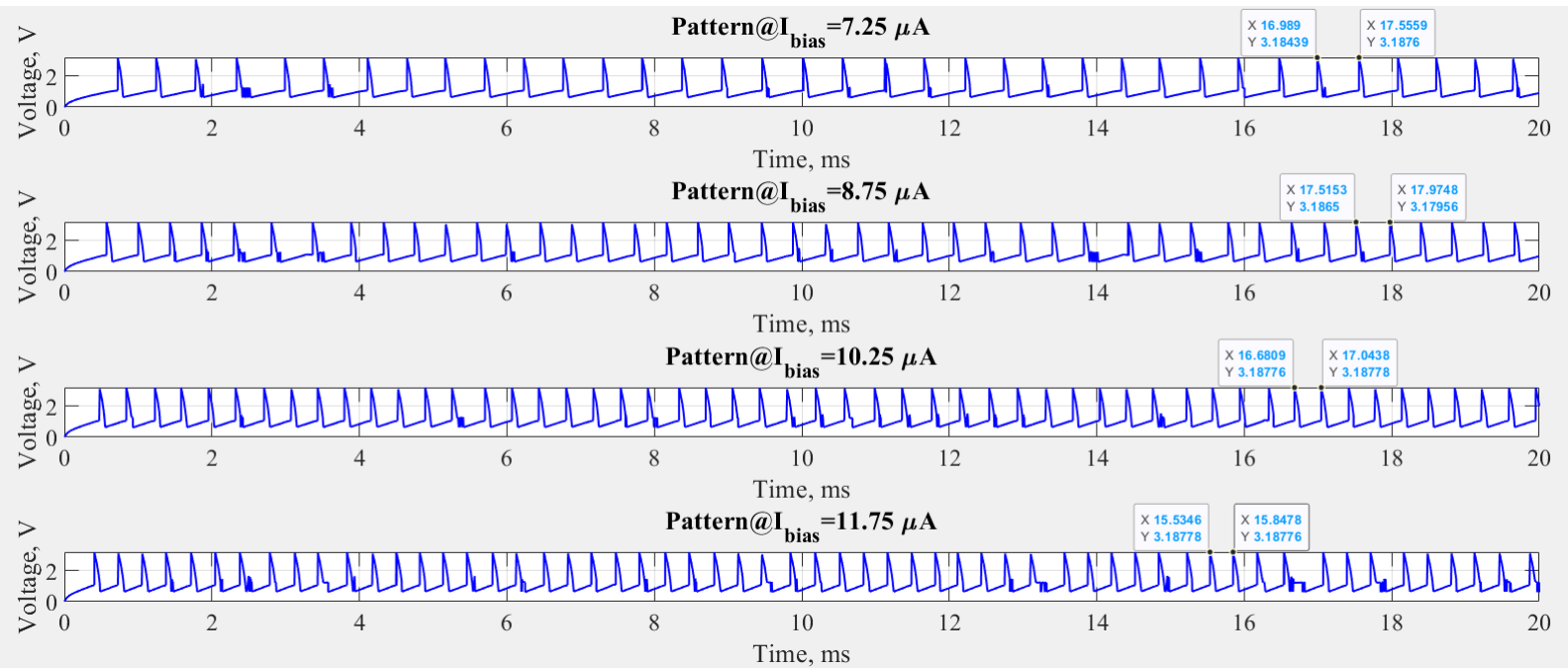


Figure 3.8. Some patterns generated using $7 \mu A < I_{dc} < 12 \mu A$.

The patterns presented in fig.3.7 and 3.8 are more or less periodic and so it is reasonable to extract a frequency in order to have an idea of how it changes by changing the injected current. In particular, the refractory period is decreasing by increasing the injected current since a faster charge for the capacitance will be achieved. This implies an increase of the frequency for the pattern by increasing the injected current, coherently with the integrate and fire model.

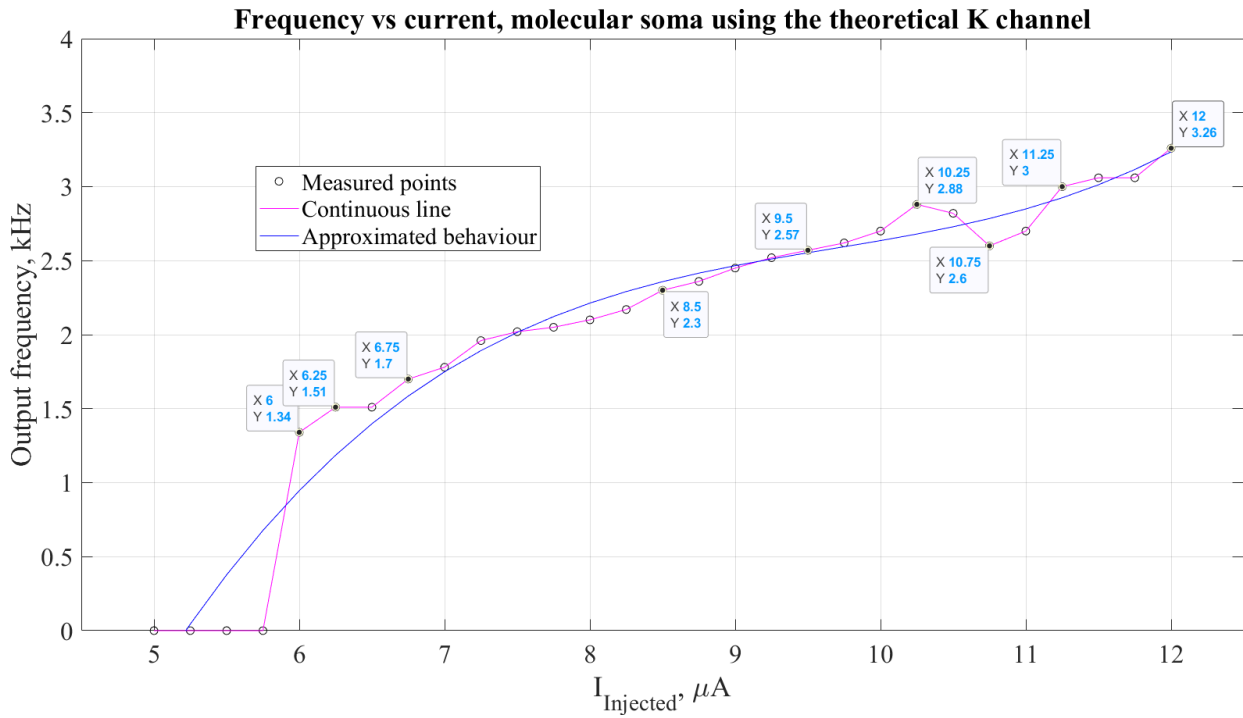


Figure 3.9. f-I curve.

In fig.3.9 the frequency vs current curve of this neuron is presented. A rheobase I_{th} can be recognized, but the frequencies involved are in the order of kHz, quite high if compared with the biological ones (Hz).

3.2 Response to the synaptic injection

A good implementation for the synapses is the most critical part for neuromorphic circuits. There are a lot of possibilities, depending on the biophysical mechanisms taken into account. In this work both paired pulse facilitation and synaptic plasticity will be not considered, but simpler synapses will be proposed as a starting point for further investigations. In particular, the TRAM proposed in chapter 3 could be used to make some refreshing mechanism in order to obtain blocks implementing the Hebbian rule ([7], [6]).

The different circuits implementing the synapses are based on the results presented in [18], [19] and [7], which use CMOS solutions.

3.2.1 Spiking synapses

The most simple version of synapses has to provide an injection mechanism based on the input spike train and a way to implement a synaptic weight. For sake of simplicity also injection on the dendritic part will be neglected, however, it could be easily implemented basing on the results obtained in chapter 2.

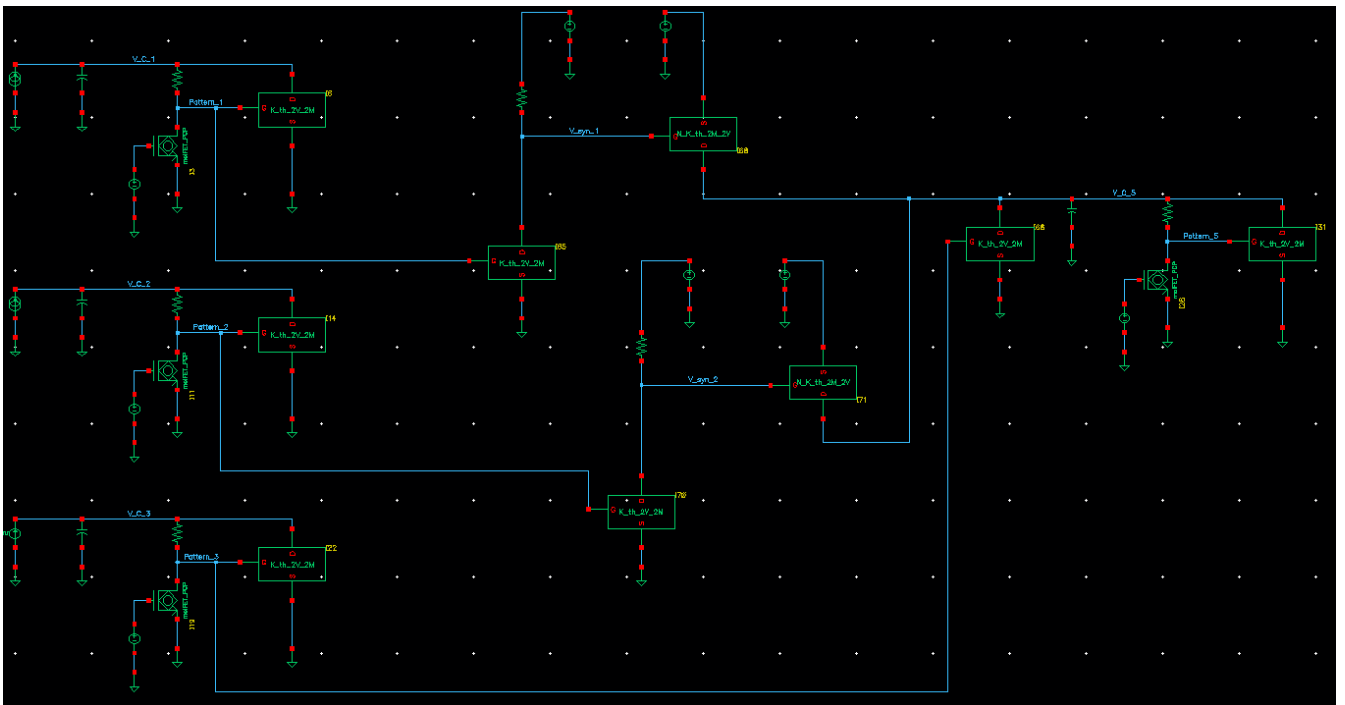


Figure 3.10. A simple 3-1 SNN.

In figure 3.10 a spiking neural network using 3 input neurons and 1 output neuron has been reported. In particular, the third neuron is inhibitory for the output one. An inhibitory synapse can be implemented by using a nmos-like device, like the one supposed to have the K-channel. When an input spike arrives on the gate, the molfet will conduct a certain current and the difference between V_{th} and V_C will increase: each neuron presents $C=1$ nF, $V_{mol}=2$ V and $Res_{mol}=2$ M Ω , therefore $V_{th} \simeq 4.3$ V whereas the synapse tend to discharge C towards ground. The spikes generated in output have the same features with respect to the ones seen in the previous section, since the parameters involved have the same values.

The first and the second neurons are excitatory for the output one. This means that, once a spike arrives, they should reduce the difference between V_C and V_{th} . E_{syn} has been chosen to be 5 V, so that the excitatory synapses can allow V_C to reach $V_{th} \simeq 4.3$ V. However, a pmos-like device is needed in order to inject current into the output neuron.

A pmos-version of the theoretical K-channel block has been proposed (Appendix C). This is the second hypothesis introduced in this work.

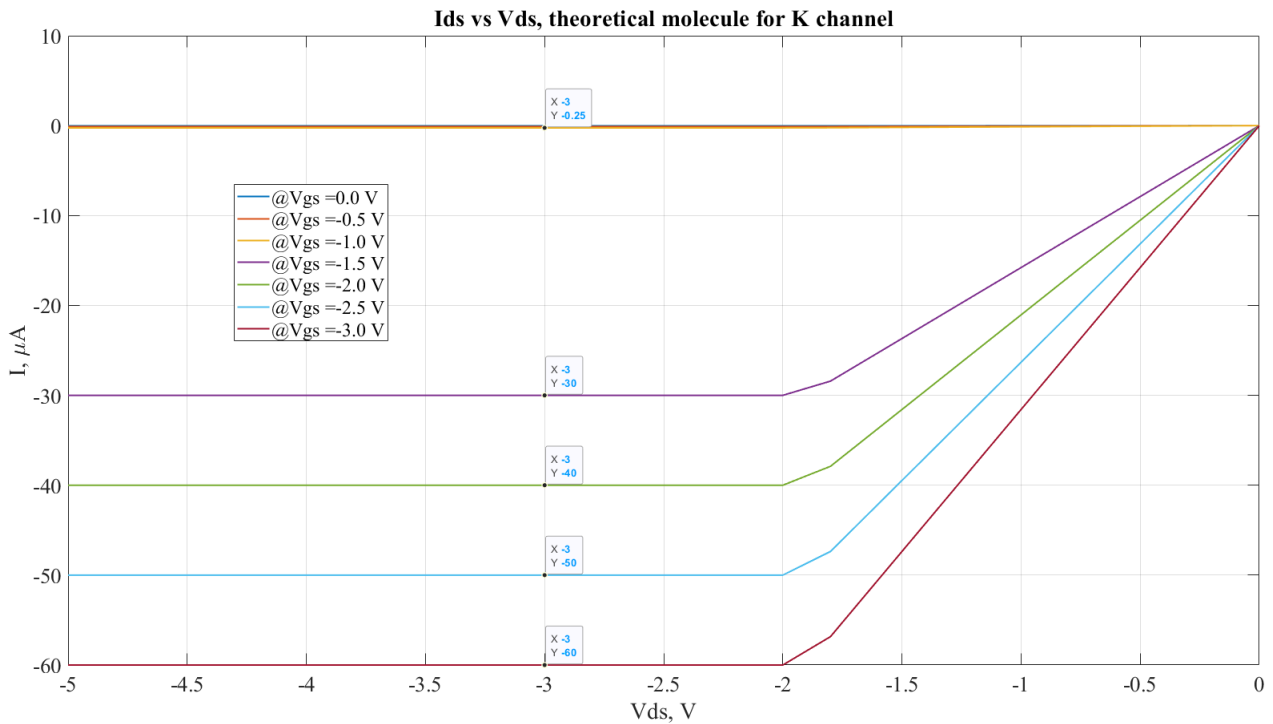


Figure 3.11. p-like version of the I-V characteristics for the hypothetical K-channel.

Again, this is just to demonstrate the idea. The relative block is " $N_K_th_2M_2V$ ", where "N" stays for "negative".

Since this requires a negative spike to inject a current, a "*K_th_2V_2M*" block in series with a resistance R_{syn} is used as inverter. In particular, $R_{syn}=55\text{ k}\Omega$ so that a spike having a peak around 3.18 V can be converted into a V_{DS} around 1.8 V. Then, V_{GS} for the "*N_K_th_2M_2V*" is around -3.18 V when a spike arrives. In both cases, the weight can be easily implemented by acting on the back-gate voltage of the injecting MoFET, introducing an off-set for its gate voltage and this is a big advantage coming from the molecular technology. The back-gate node can be set manually after an offline training or by the circuit, during an online training (maybe using the voltage V_C of the TRAM stage, if used to implement the Hebbian learning).

At this point, different cases can be commented and discussed.

- $I_1 \neq 0, I_2 = 0, I_3 = 0$

In this case, only the first neuron is injecting into the soma of the output one.

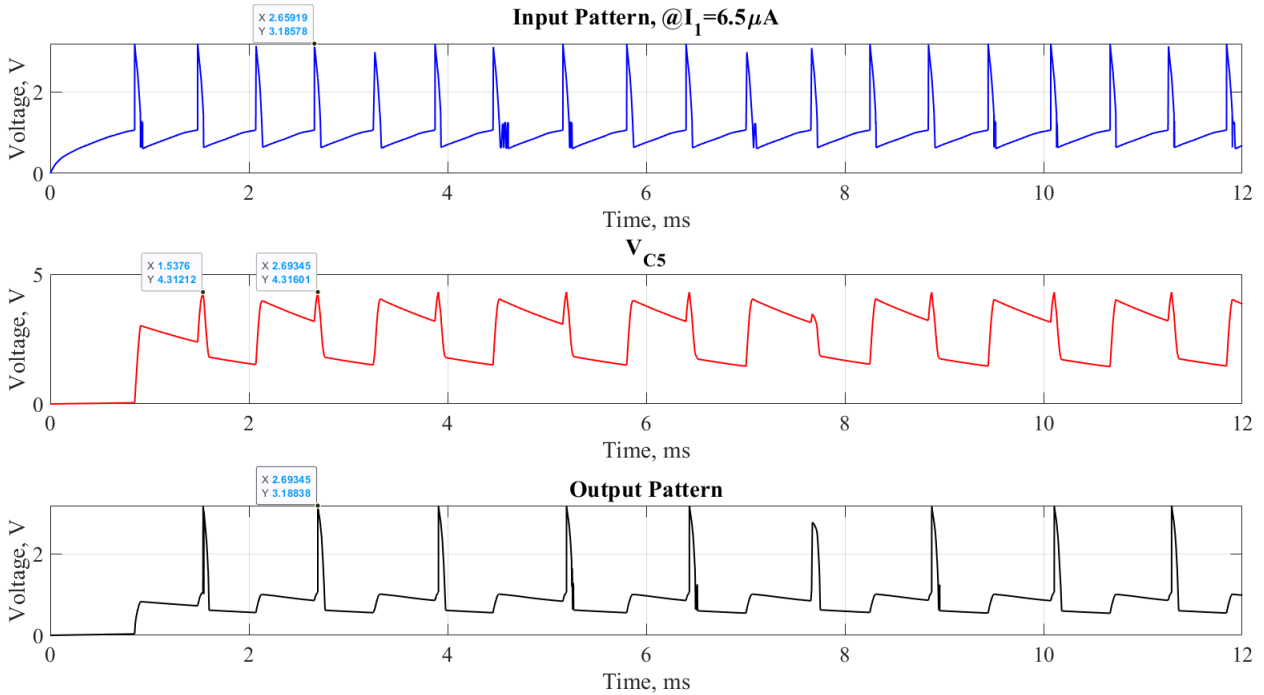


Figure 3.12. Response to an injected train of spikes.

An input spike train coming from the first neuron, at frequency 1.51 kHz and generated by a current of $6.5\text{ }\mu\text{A}$, injects a current made by a train of spikes into the soma of the output neuron. Since the input current provided to the soma is made by pulses, a convolution in time for V_C will be observed. Only when the value of V_C provided by the convolution reaches a value around 4.3 V, an output spike will be generated.

Using this input current, the output pattern presents a frequency of about 0.82 kHz. It is possible to decrease or increase such frequency by acting on the injected current for each spike, therefore, acting on the back-gate voltage of the synapse (weight). Moreover, changing the input current I_1 the number of input spikes will change, and so also the convolution giving V_C in time. This means that, the frequency of the output spike train depends both on the synaptic weight and on the frequency of the input spike train: the injection must consider both current amplitude and frequency.

- $I_1 \neq 0, I_2 \neq 0, I_3 = 0$

In this case, both the excitatory synapses are injecting into the output neuron.

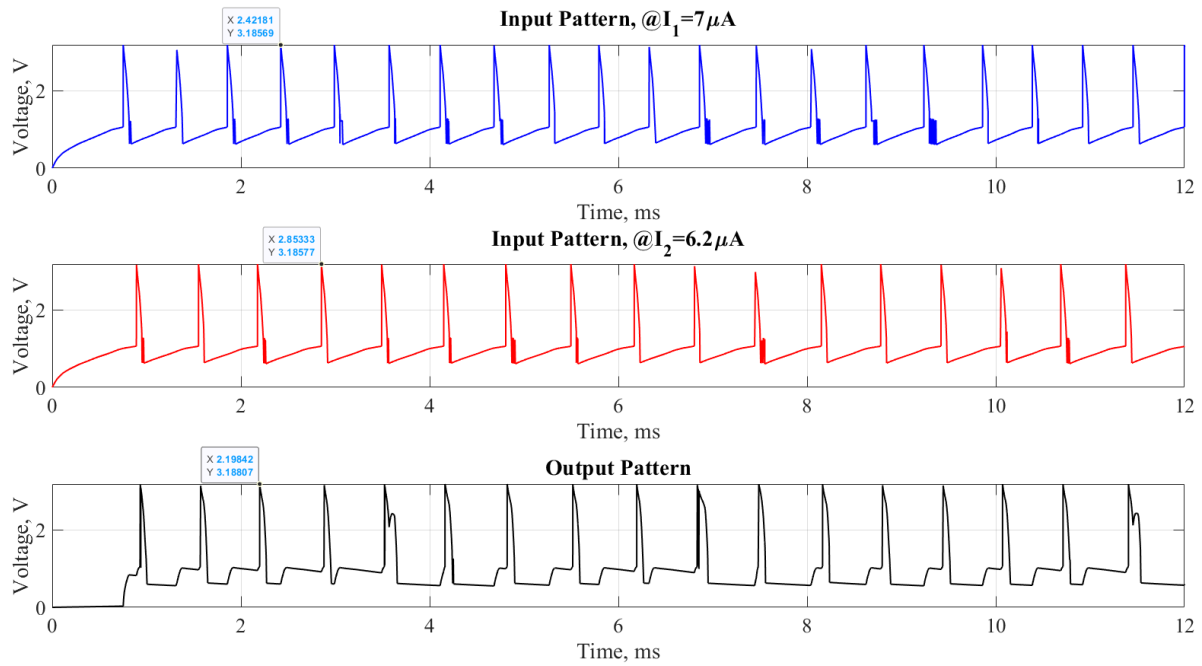


Figure 3.13. Response to two injected trains of spikes.

The first train of spikes is generated by an injected current equal to $I_1=7\mu\text{A}$ and has a frequency of about 1.78 kHz. The second one is generated by an injected current equal to $6.2\mu\text{A}$ and has a frequency around 1.5 kHz. In figure 3.14 the global train of current spikes given in input to the output neuron is provided: this is the superposition between the current coming from the first and the second excitatory synapses, having same weight. It is possible to notice a decrease in amplitude due to the synaptic saturation (V_{DS} dropping on the synapses decreases, if V_C increases).

The global input presents more frequent pulses with respect to the previous case, where a single excitatory synapse was used, therefore the frequency for the output train of spike will increase. This will depend on both the synaptic weights and the frequencies for the input patterns, given by I_1 and I_2 .

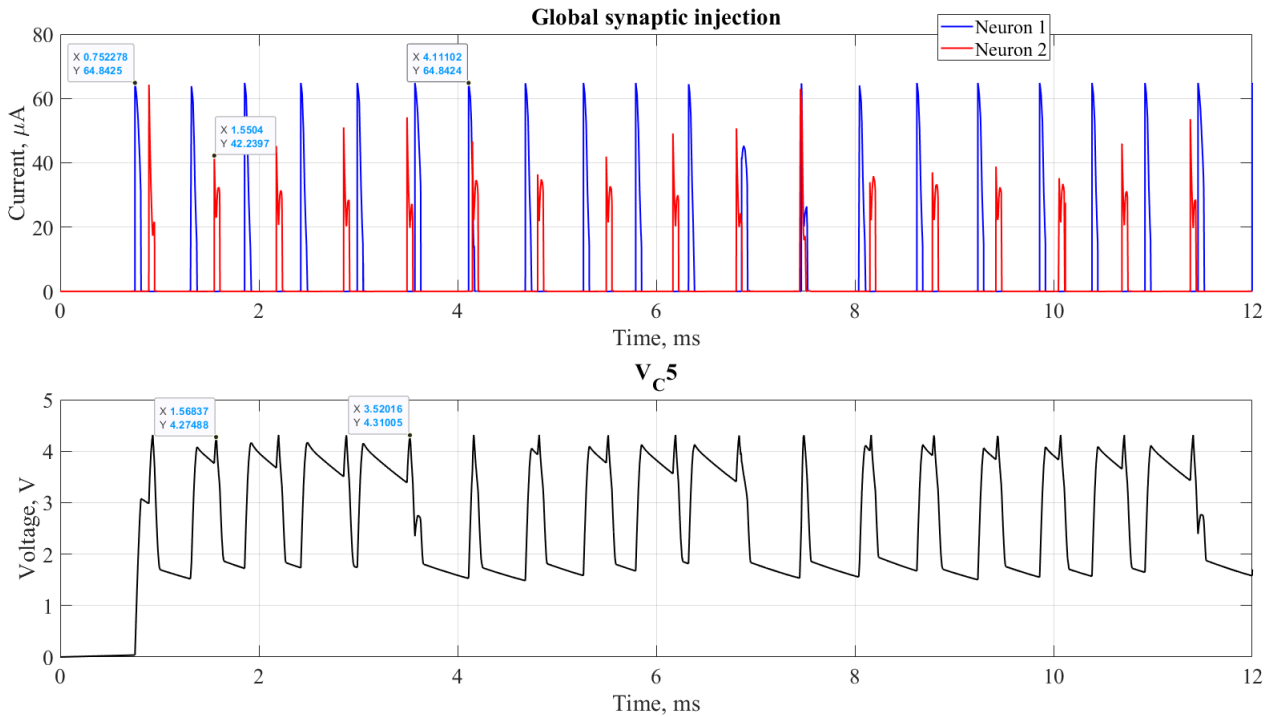


Figure 3.14. Global current injected from the two trains of spikes.

The "Temporal coherence" takes into consideration the distance between nearest spikes in the global pattern, obtained by the superposition of the inputs. The convolution will reach higher values if the spikes are near between each other in time, otherwise it will decay.

The output pattern is doing data compression with respect to the input ones, this encodes some kind of information depending on the application (and so on the training, fixing the weights).

- $I_1 \neq 0, I_2 \neq 0, I_3 \neq 0$

At this point, the contribution from the inhibitory neuron can be considered.

In figure 3.15 three patterns are shown. The first one is generated by injecting $8 \mu\text{A}$ into the first excitatory neuron, the second one is generated by injecting $6.2 \mu\text{A}$ into the second excitatory neuron whereas the third one is generated by injecting $9 \mu\text{A}$ into the inhibitory neuron. The weight for the three synapses is the same for all the input neurons, however, the inhibitory one present a higher frequency with respect to the other two. The pattern for the output neuron will present a lesser number of spikes with respect to the previous cases, due to the negative current induced by the third neuron's activity.

In figure 3.16 the global train of current spikes (with positive and negative terms) and the behaviour in time for the membrane potential have been reported.

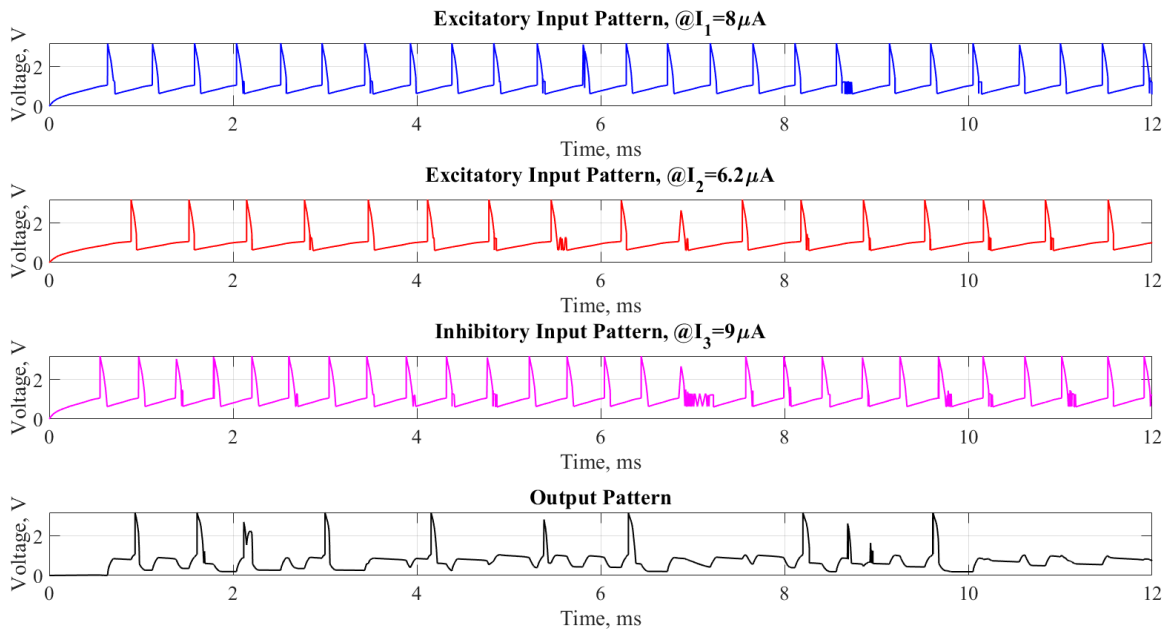


Figure 3.15. Response to three injected trains of spikes, 2 excitatory and 1 inhibitory.

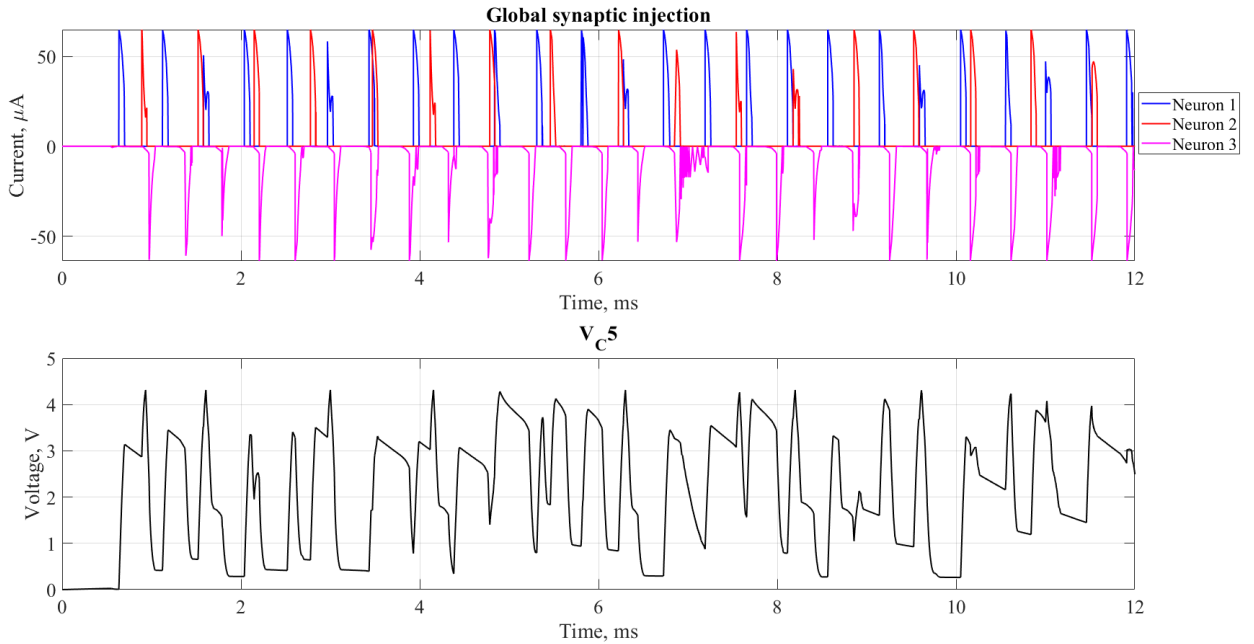


Figure 3.16. Global current injected from the three trains of spikes, 2 excitatory and 1 inhibitory.

3.2.2 Introducing the synaptic response

Equation 1.37 describes the response of a synapse to a train of spikes impinging on the pre-synaptic terminal. The synaptic conductance is given by a convolution between the input spike train and the impulse response $K(t)$. An intuition for such behaviour can be obtained by considering the differential equation 1.34.

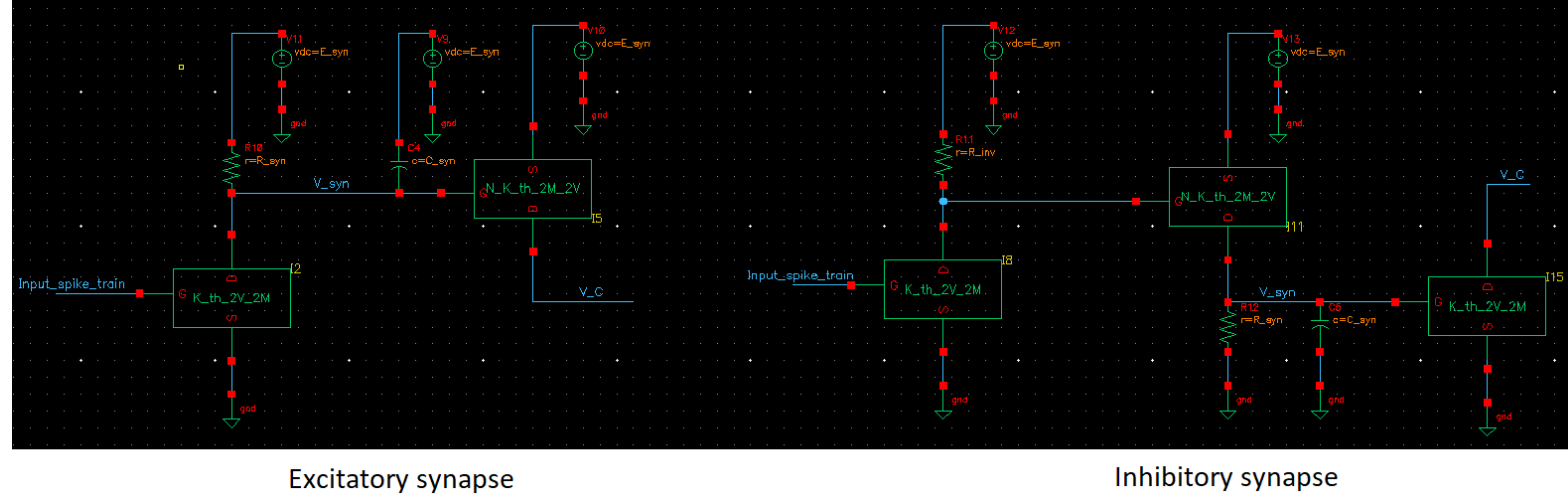


Figure 3.17. Excitatory and inhibitory synapses showing time dependence.

In figure 3.17 a possible implementation for excitatory (left) and inhibitory (right) synapses having a response in time to an input spike train is shown.

- Excitatory synapse: if no spike arrives on the synaptic input, V_{syn} will be equal to E_{syn} , otherwise it will decrease until $V_{syn}-E_{syn}$ is such that a current can be injected into the neuron membrane through the pmos-like molfet. The capacitance C_{syn} allows the presence of a time constant $\tau_{syn}=R_{syn} C_{syn}$;
- Inhibitory synapse: a first stage made by a nmos-like molfet and a resistance R_{inv} is used as inverter in order to have negative spikes, these are used as synaptic input to raise V_{syn} so that the last nmos-like molfet can conduct a current towards ground. Also in this case, the capacitance C_{syn} allows the presence of a time constant $\tau_{syn}=R_{syn} C_{syn}$.

In both cases the gate voltage provided to the injecting MolFETs is given by a convolution due to the RC circuit, the idea is to use it in order to replicate the behaviour of equation 1.37. The synaptic weights are still fixed by the back-gate voltages applied to the injecting molfets, they are supposed to be all the same.

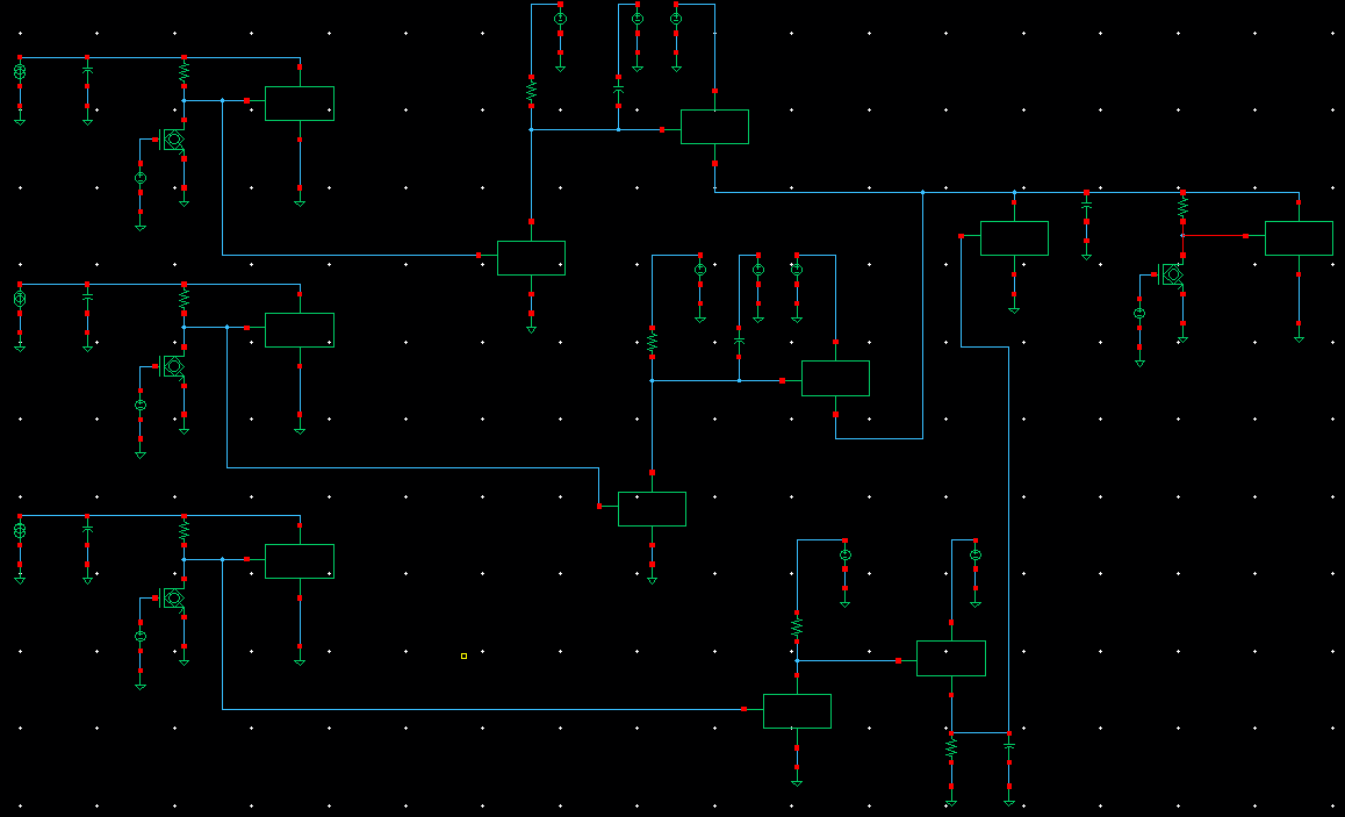


Figure 3.18. 3-1 SNN exploiting synaptic responses.

In figure 3.18 the molecular spiking neural network has been proposed again, using these new synapses. In particular R_{syn} has been fixed to 110 k Ω whereas C_{syn} has been fixed to 5 nF. This implies a τ_{syn} around 0.55 ms.

$R_{inv}=55$ k Ω so that a negative spike having peak around -3.18 V is obtained as V_{GS} for the pmos-like MolFET of the inhibitory synapse, when a positive spike arrives from the pre-synaptic neuron.

In figure 3.19 an example of EPSC has been reported. The input pattern is generated by injecting 5.9 μ A into the first neuron, the convolution obtained for the synaptic response is indicated as V_{syn1} . The pmos-like MolFET injects a current depending on $V_{syn1}-E_{syn}$.

Figure 3.20 presents an example of IPSC, this has been obtained by using $I_1=11$ μ A, $I_2=10$ μ A and $I_3=9$ μ A. In particular, the excitatory neurons are injecting since it is the only way to increase V_C , allowing the inhibitory neuron to conduct when a certain activity is present on its pre-synaptic terminal.

Finally, an example for the output pattern is reported in figure 3.21. This has been obtained by using $I_1=11$ μ A, $I_2=10$ μ A and $I_3=7.5$ μ A.

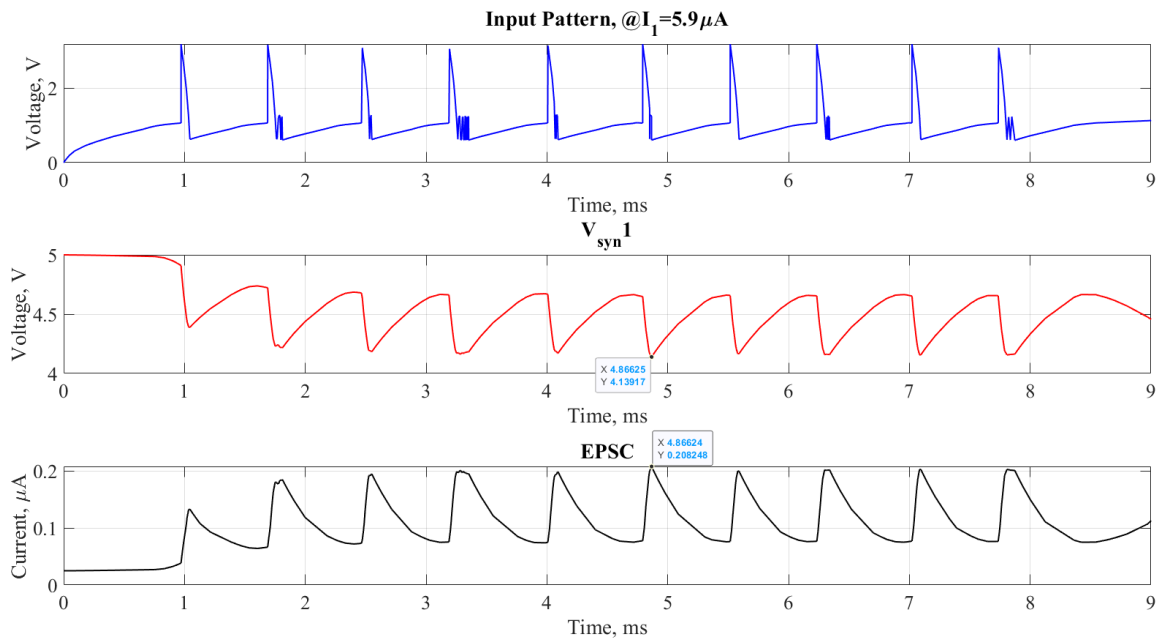


Figure 3.19. Example of excitatory post-synaptic current.

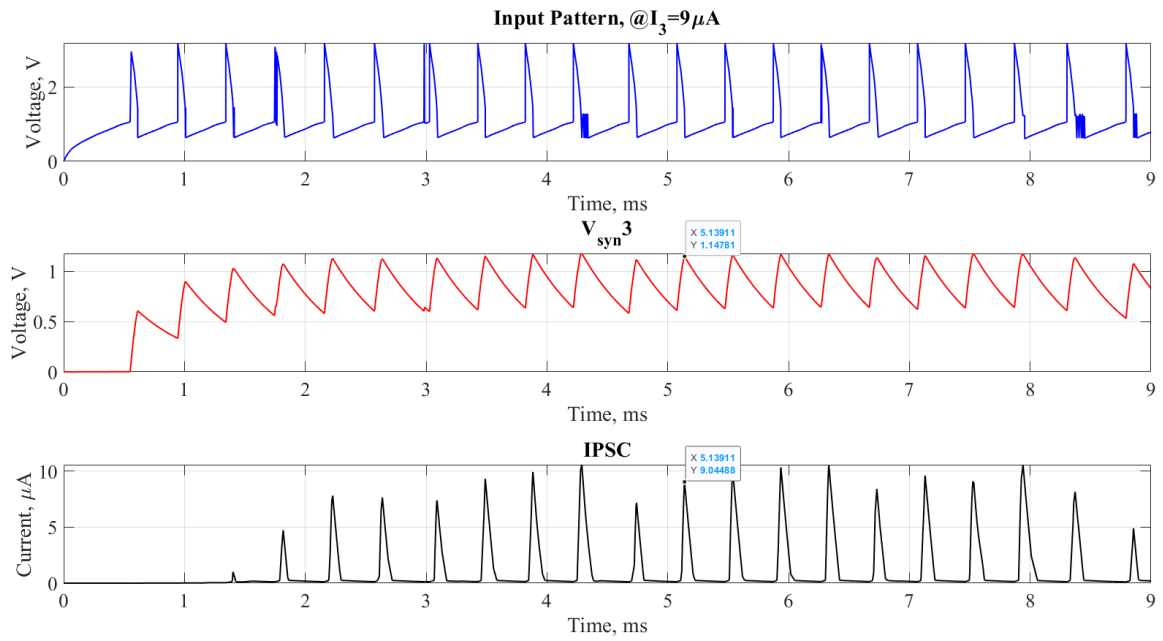


Figure 3.20. Example of inhibitory post-synaptic current.

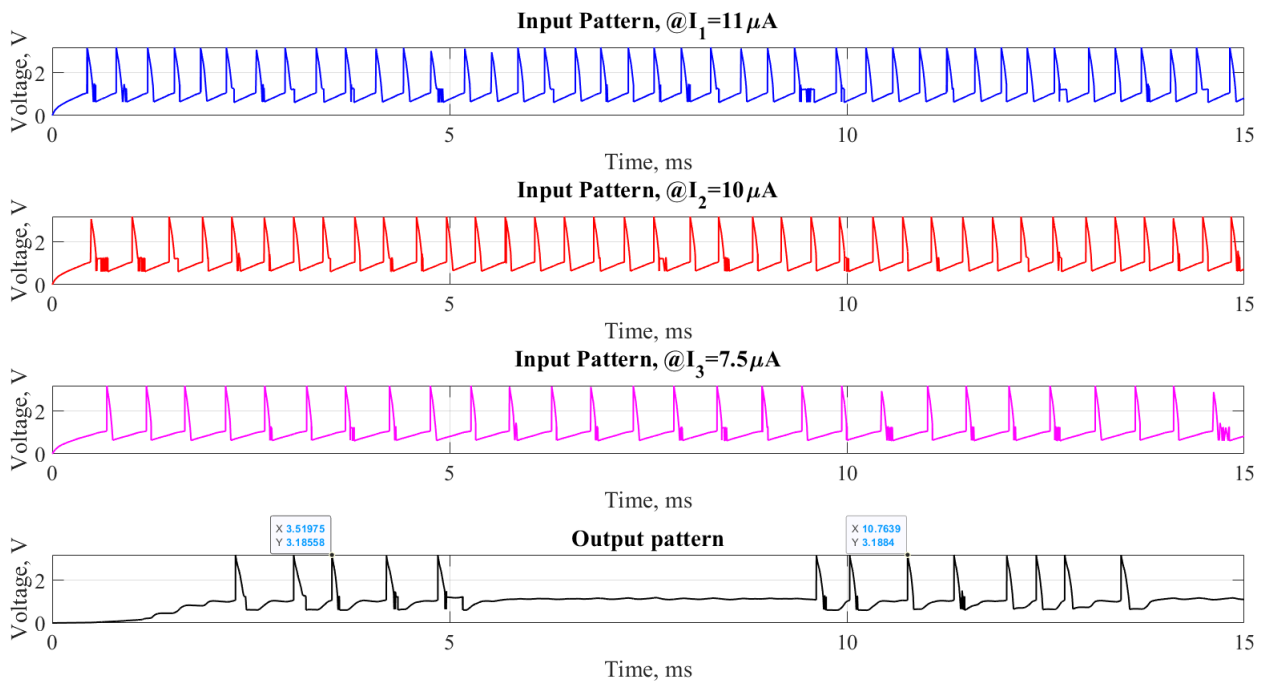


Figure 3.21. Example of output pattern.

Chapter 4

Conclusions and future works

The exploration of a possible implementation of neuromorphic circuits using molecular technology has been presented. Initially, all the important aspects related to the theory used in this work have been explained. Then, some stages based on the NDR of the PCP MolFET have been introduced, in particular:

1. The stage presenting non-linear behaviour based on emerging hysteresis effect;
2. The PCP-based TRAM, having tunable stable states allowed for the system;
3. The PCP-based MOBILE, also used as threshold mechanism.

Finally, they have been used in order to try to replicate at least some basic biological neural functions, aimed to emulating the computational principles of the brain.

This thesis provides a beginning in such exploration and a lot of work is still needed to obtain real applications, even if, through a bottom-up approach, it has been proved that patterns of spikes can be obtained using the PCP (both providing constant currents and trains of spikes).

However, some obstacles must be faced:

- The study of a MolFET having the I-V characteristics required to implement the K-channel is a must, not necessarily it has to be the same used to implement synapses;
- The neuron itself can be ameliorated, so that more biophysical functions can be discussed and comprised (for example, bursting, adaptation and so on);
- The weights for the proposed synapses are implemented using the back-gate voltage of the MolFETs. Technologically speaking, this may be a great advantage with respect to CMOS solutions because a single MolFET would be sufficient for both injection and weighting mechanisms, but not all the molecular I-V trends could be accepted. The investigation for possible molecules able to provide in a good way the synaptic weights through their back-gate voltage is needed. In

this thesis it has not been faced, since the molecule used to implement them was supposed. The aim was just to give some ideas regarding architectures and links with the theoretical background;

- Learning is a concept characterizing the neural networks. This should be faced once having a reliable molecular neural network presenting all the main biological characteristics exposed in the previous points. In particular, the weights could be firstly found offline by using learning algorithms for spiking neural networks and then implemented through the back-gates (in a way which depends on the molecules used as synapses). This could also provide a validation for the whole molecular neuromorphic system, maybe trying to fit some results obtained with the algorithm. Finally, the stage based on the series of two PCPs (TRAM) could find an application in plasticity-based synapses, so that a complete online training can be achieved.

Appendices

Appendix A

Matlab: "Integrate and fire" model

```
clc;
close all;
clear all;
format long;

%Parameters

R_Leak = 10^8; %ohm
C = 10^(-10); %F
tau = R_Leak*C; %sec

E_Leak = -50e-3; %V
V_th = 10e-3; %V
V_reset = -70e-3; %V

%Time and Current set
I_max = 2; %nA
number_currents = 15;
I_values = linspace(0, I_max, number_currents)*1e-9; %A

time_steps = 20000;
t_max = 200; % msec
time = linspace(0, t_max, time_steps)*1e-3; %sec
t1_index = round(time_steps/5);
t1 = time(t1_index); %sec
t2_index = round(time_steps/1.2);
t2 = time(t2_index); %sec
t0 = 0; %sec
```

```

% Time of injection
for t_i = 1:time_steps
    injection_range(t_i) = heaviside(time(t_i)-t1) -...
                        heaviside(time(t_i)-t2);
end

%V_inf
for I_i = 1:number_currents
    for t_i = 1:time_steps
        V_inf(I_i,t_i) = E_Leak +...
                        injection_range(t_i)*I_values(I_i)*R_Leak; %V
    end
end

% Spike generation in time

V_C_Spikes = zeros(number_currents, time_steps);

for I_i = 1:number_currents
    Initial_cond = E_Leak; %V
    Spike = 0; %Flag
    Spikes_time_index (I_i,1) = 0;
    for t_i = 1:time_steps

        if time(t_i) < t1 %Before the injection

            V_C_Spikes(I_i,t_i) = V_inf(I_i,t_i) + (Initial_cond -...
                V_inf(I_i,t_i))*exp(-(time(t_i)-t0)/tau); %V

        elseif (time(t_i) >= t1) && (time(t_i) < t2) %During the injection

            if Spike == 0
                Initial_cond = V_C_Spikes(I_i,t1_index-1); %V
                Initial_time = t1;
            else
                Initial_cond = V_reset;
                Initial_time = time(Spikes_time_index(I_i,end));
            end

            V_C_Spikes(I_i,t_i) = V_inf(I_i,t_i) + ...

```

```

        (Initial_cond - V_inf(I_i, t_i))...
        *exp(-(time(t_i)-Initial_time)/tau); %V

elseif time(t_i) >= t2 % After the injection

    Initial_cond = V_C_Spikes(I_i, t2_index-1); %V

    V_C_Spikes(I_i, t_i) = V_inf(I_i, t_i) +...
        (Initial_cond - V_inf(I_i, t_i))...
        *exp(-(time(t_i)-t2)/tau); %V
end

if V_C_Spikes(I_i, t_i) >= V_th

    V_C_Spikes(I_i, t_i) = V_reset;
    Spikes_time_index(I_i, end+1) = t_i;
    Spike = 1; %Flag, it means we had a spike

end

end
end

% Charging in time

V_C = zeros(number_currents, time_steps);

for I_i = 1:number_currents
    Initial_cond = E_Leak; %V

    for t_i = 1:time_steps

        if time(t_i) < t1 %Before the injection

            V_C(I_i, t_i) = V_inf(I_i, t_i) +...
                (Initial_cond - V_inf(I_i, t_i))*exp(-(time(t_i)-t0)/tau); %V

        elseif (time(t_i) >= t1) && (time(t_i) < t2) %During the injection

            Initial_cond = V_C(I_i, t1_index-1); %V
            Initial_time = t1;

```

```

        V_C(I_i,t_i) = V_inf(I_i,t_i) +...
            (Initial_cond - V_inf(I_i,t_i))...
            *exp(-(time(t_i)-Initial_time)/tau); %V

    elseif time(t_i) >= t2 % After the injection

        Initial_cond = V_C(I_i,t2_index-1); %V

        V_C(I_i,t_i) = V_inf(I_i,t_i) +...
            ( Initial_cond - V_inf(I_i,t_i))...
            *exp(-(time(t_i)-t2)/tau); %V
    end
end
end

% Spike trains visualization in time
Spikes_generation = zeros(number_currents, time_steps);
for I_i = 1:number_currents
    for t_i = 1:time_steps
        if ismember(t_i, Spikes_time_index(I_i,:))
            Spikes_generation(I_i,t_i) = 1;
        end
    end
end

%Frequency vs Current curve
I_th = (R_Leak^-1*(V_th - E_Leak))*1e9; %nA
I_max_fI = 2; %nA
number_fI_current = 140000;
I_values_fI = linspace(I_th, I_max_fI, number_fI_current)*1e-9; %A
for I_i=1:number_fI_current
    V_inf_fI = E_Leak + I_values_fI(I_i)*R_Leak; %V
    f_I_and_F(I_i)=(tau*log((V_inf_fI-V_reset)/(V_inf_fI-V_th)))^-1; %Hz
end
linear_f =(I_values_fI - I_th*1e-9)/(C*(V_th-V_reset)); %Hz

%Plot
E_Leak_vec = E_Leak*ones(1,time_steps); %V
Vth_vec = V_th*ones(1,time_steps); %V
Vreset_vec = V_reset*ones(1,time_steps); %V

```

```

figure
subplot(2,1,1)
plot(time*1e3,V_C_Spikes(8,:)*1e3,'b');
hold on
plot(time*1e3,V_C(8,:)*1e3,'b--');
plot(time*1e3,E_Leak_vec*1e3,'m--');
plot(time*1e3,Vth_vec*1e3,'r--');
plot(time*1e3,Vreset_vec*1e3,'k--');
set(gca,'FontSize',20,'FontName','Times New Roman', ...
        'XScale','lin','YScale','lin','box','on')
xlabel('Time, ms');
ylabel('V_{C}, mV');
grid on;
title('Integrate and fire model')
legend('V_{C}','Charging in time','E_{Leak}','V_{th}','V_{reset}')

subplot(2,1,2)
plot(time*1e3,Spikes_generation(8,:),'r');
set(gca,'FontSize',20,'FontName','Times New Roman', ...
        'XScale','lin','YScale','lin','box','on')
xlabel('Time, ms');
ylabel('Events');
grid on;
title('Spike train due to the injection with the I&F model')

figure
plot(I_values_fI*1e9,f_I_and_F,'b');
hold on
plot(I_values_fI*1e9,linear_f,'r');
set(gca,'FontSize',20,'FontName','Times New Roman', ...
        'XScale','lin','YScale','lin','box','on')
xlabel('I_{Injected}, nA');
ylabel('Output frequency, Hz');
xlim([0,I_max_fI]);
grid on;
title('Frequency vs Current, Integrate and fire model')
legend('Real behaviour','Approximation for large I_{in}')

```


Appendix B

Matlab: n-type hypothetical molecule used as K-channel and for synaptic injection

```
clc;
clear all;
close all;

I_min = 30; %uA
I_max = 60; %uA

Vds_points = [0, 1.9, 4.6];

Ids_Vgs_0 = [0; 0.025; 0.025]*1e-6; %A
Ids_Vgs_0p5 = [0; 0.10; 0.10]*1e-6; %A
Ids_Vgs_1 = [0; 0.25; 0.25]*1e-6; %A
Ids_Vgs_1p5 = [0; I_max-30; I_max-30]*1e-6; %A
Ids_Vgs_2 = [0; I_max-20; I_max-20]*1e-6; %A
Ids_Vgs_2p5 = [0; I_max-10; I_max-10]*1e-6; %A
Ids_Vgs_3 = [0; I_max; I_max]*1e-6; %A

Ids_th = [ Ids_Vgs_0, Ids_Vgs_0p5, Ids_Vgs_1, Ids_Vgs_1p5, Ids_Vgs_2, ...
           Ids_Vgs_2p5, Ids_Vgs_3 ];

figure
for i=1:length(Ids_th)
plot (Vds_points, Ids_th(:,i)*1e6, 'o-')
hold on
```

```

xlabel('Vds, V')
ylabel('Ids, \muA')
grid on
end

%%%%

Vds = [0:0.2:5];
Vgs = [0:0.5:3];

for i=1:1:length(Ids_th)
p = polyfit(Vds_points(1:2),Ids_th((1:2),i),1);
I_drain((1:11),i) = polyval(p,Vds(1:11)); %uA
I_drain(11:26,i) = Ids_th(3,i);
labels_Vgs(i,:) = strcat('@Vgs = ',string(vpa(Vgs(i),3)), ' V');
end

figure
for i=1:1:length(Ids_th)
plot(Vds,I_drain(:,i)*1e6,'LineWidth',1.5);
hold on
end
set(gca,'FontSize',20,'FontName','Times New Roman', ...
        'XScale','lin','YScale','lin','box','on')
xlabel('Vds, V');
ylabel('I, \muA');
grid on;
title('Ids vs Vds, theoretical molecule for K channel')
legend(labels_Vgs)

% export as .txt

file_row = 1;
for i = 1:1:length(Vgs)
    for j = 1:1:length(Vds)
        matrix_to_export(file_row,(1:3)) = [Vgs(i), Vds(j), I_drain(j,i)];
        file_row = file_row+1;
    end
end

writematrix(matrix_to_export,'K_th_2V_2M_LUT.txt','Delimiter','space')

```

Appendix C

Matlab: p-type hypothetical molecule used for synaptic injection

```
clc;
clear all;
close all;

I_min = 30; %uA
I_max = 60; %uA

Vds_points = [0, 1.9, 4.6];

Ids_Vgs_0 = [0; 0.025; 0.025]*1e-6; %A
Ids_Vgs_0p5 = [0; 0.10; 0.10]*1e-6; %A
Ids_Vgs_1 = [0; 0.25; 0.25]*1e-6; %A
Ids_Vgs_1p5 = [0; I_max-30; I_max-30]*1e-6; %A
Ids_Vgs_2 = [0; I_max-20; I_max-20]*1e-6; %A
Ids_Vgs_2p5 = [0; I_max-10; I_max-10]*1e-6; %A
Ids_Vgs_3 = [0; I_max; I_max]*1e-6; %A

Ids_th = [ Ids_Vgs_0, Ids_Vgs_0p5, Ids_Vgs_1, Ids_Vgs_1p5, Ids_Vgs_2, ...
           Ids_Vgs_2p5, Ids_Vgs_3 ];

figure
for i=1:length(Ids_th)
plot (Vds_points, Ids_th(:,i)*1e6, 'o-')
hold on
xlabel('Vds, V')
ylabel('Ids, \muA')
```

```

grid on
end

%%%%

Vds = [0:0.2:5];
Vgs = [0:-0.5:-3];

for i=1:length(Ids_th)
p = polyfit(Vds_points(1:2),Ids_th((1:2),i),1);
I_drain((1:11),i) = polyval(p,Vds(1:11)); %uA
I_drain(11:26,i) = Ids_th(3,i);
I_drain(:,i) = -flip(I_drain(:,i));
labels_Vgs(i,:) = strcat('@Vgs = ',string(vpa(Vgs(i),3)), ' V');
end

figure
Vds = [-5:0.2:0];
for i=1:length(Ids_th)
plot(Vds,I_drain(:,i)*1e6,'LineWidth',1.5);
hold on
end
set(gca,'FontSize',20,'FontName','Times New Roman', ...
'XScale','lin','YScale','lin','box','on')
xlabel('Vds, V');
ylabel('I, \muA');
grid on;
title('Ids vs Vds, theoretical molecule for K channel')
legend(labels_Vgs)

% export as .txt
file_row = 1;
for i = 1:length(Vgs)
    for j = 1:length(Vds)
        matrix_to_export(file_row,(1:3)) = [Vgs(i), Vds(j), I_drain(j,i)];
        file_row = file_row+1;
    end
end

writematrix(matrix_to_export,'Negative_K_th_2V_2M_LUT.txt','Delimiter',...
'space')
```

Bibliography

- [1] John von Neumann, "The Computer & the Brain", Foreword by Ray Kurzweil, Yale university press.
- [2] Mo, Fabrizio Spano, Chiara Ardesi, Yuri Piccinini, Gianluca Graziano, Mariagrazia. (2021). Beyond-CMOS Artificial Neuron: A simulation-based exploration of the molecular-FET. *IEEE Transactions on Nanotechnology*. 1-1. 10.1109/TNANO.2021.3133728.
- [3] 2022 Roadmap on Neuromorphic Computing and Engineering (arXiv:2105.05956)
- [4] Zou, X., Xu, S., Chen, X. et al. Breaking the von Neumann bottleneck: architecture-level processing-in-memory technology. *Sci. China Inf. Sci.* 64, 160404 (2021). <https://doi.org/10.1007/s11432-020-3227-1>
- [5] International Roadmap for Devices and Systems
<https://irds.ieee.org/>
- [6] Fusi S, Annunziato M, Badoni D, Salamon A, Amit DJ. Spike-driven synaptic plasticity: theory, simulation, VLSI implementation. *Neural Comput.* 2000 Oct;12(10):2227-58. doi: 10.1162/089976600300014917. PMID: 11032032.
- [7] E. Chicca et al., "A VLSI recurrent network of integrate-and-fire neurons connected by plastic synapses with long-term memory," in *IEEE Transactions on Neural Networks*, vol. 14, no. 5, pp. 1297-1307, Sept. 2003, doi: 10.1109/TNN.2003.816367
- [8] Paven Thomas Mathew, Fengzhou Fang, *Advances in Molecular Electronics: A Brief Review*, Engineering, Volume 4, Issue 6, 2018, Pages 760-771, ISSN 2095-8099, <https://doi.org/10.1016/j.eng.2018.11.001>. (<https://www.sciencedirect.com/science/article/pii/S2095809918306453>)
- [9] Li HB, Tebikachew BE, Wiberg C, Moth-Poulsen K, Hihath J. A Memristive Element Based on an Electrically Controlled Single-Molecule Reaction. *Angew Chem Int Ed Engl.* 2020 Jul 6;59(28):11641-11646. doi: 10.1002/anie.202002300. Epub 2020 Apr 21. PMID: 32222017.
- [10] Goswami, S., Pramanick, R., Patra, A. et al. Decision trees within a molecular memristor. *Nature* 597, 51–56 (2021). <https://doi.org/10.1038/s41586-021-03748-0>

- [11] Marc Baldo. 6.701 Introduction to Nanoelectronics. Spring 2010. Massachusetts Institute of Technology: MIT OpenCourseWare, <https://ocw.mit.edu>. License: Creative Commons BY-NC-SA.
- [12] Zahir, Ali Pulimeno, Azzurra Graziano, Mariagrazia Ruo Roch, Massimo Masera, Guido Piccinini, Gianluca. (2016). EE-BESD: Molecular FET Modeling for Efficient and Effective Nanocomputing Design. *Journal of Computational Electronics*. 1. 1. 10.1007/s10825-015-0777-y.
- [13] Chuancheng Jia, Marjan Famili, Marco Carlotti, Yuan Liu, Peiqi Wang, Iain M. Grace, Ziyang Feng, Yiliu Wang, Zipeng Zhao, Mengning Ding, Xiang Xu, Chen Wang, Sung-Joon Lee, Yu Huang, Ryan C. Chiechi, Colin J. Lambert, and Xiangfeng Duan. Quantum interference mediated vertical molecular tunneling transistors. *Science Advances*, 4(10), 2018.
- [14] Michale Fee, and Daniel Zysman. 9.40 Introduction to Neural Computation. Spring 2018. Massachusetts Institute of Technology: MIT OpenCourseWare, <https://ocw.mit.edu>. License: Creative Commons BY-NC-SA.
- [15] Neuronal Dynamics From single neurons to networks and models of cognition and beyond, Wulfram Gerstner, Werner M. Kistler, Richard Naud and Liam Paninski
- [16] W. Yi, K. K. Tsang, S. K. Lam, X. Bai, J. A. Crowell and E. A. Flores, "Active Memristor Neurons for Neuromorphic Computing," 2019 IEEE International Electron Devices Meeting (IEDM), 2019, pp. 22.7.1-22.7.4, doi: 10.1109/IEDM19573.2019.8993550.
- [17] Li, Y. and Ang, K. (2021), Hardware Implementation of Neuromorphic Computing Using Large-Scale Memristor Crossbar Arrays. *Adv. Intell. Syst.*, 3: 2000137. <https://doi.org/10.1002/aisy.202000137>
- [18] Indiveri Giacomo, Linares-Barranco Bernabe, Hamilton Tara, van Schaik André, Etienne-Cummings Ralph, Delbruck Tobi, Liu Shih-Chii, Dudek Piotr, Häfliger Philipp, Renaud Sylvie, Schemmel Johannes, Cauwenberghs Gert, Arthur John, Hynna Kai, Folowosele Fopefolu, SAÏGHI Sylvain, Serrano-Gotarredona Teresa, Wijekoon Jayawan, Wang Yingxue, Boahen Kwabena, Neuromorphic Silicon Neuron Circuits, *Frontiers in Neuroscience*, volume 5, 2011, <https://www.frontiersin.org/article/10.3389/fnins.2011.00073>, DOI 10.3389/fnins.2011.00073, ISSN 1662-453X
- [19] Bartolozzi, Chiara Indiveri, Giacomo. (2007). Synaptic dynamics in analog VLSI. *Neural computation*. 19. 2581-603. 10.1162/neco.2007.19.10.2581.
- [20] Zidan, M.A., Strachan, J.P. Lu, W.D. The future of electronics based on memristive systems. *Nat Electron* 1, 22–29 (2018). <https://doi.org/10.1038/s41928-017-0006-8>, DOI

- <https://doi.org/10.1038/s41928-017-0006-8>
- [21] Jian Ping Sun, G. I. Haddad, P. Mazumder and J. N. Schulman, "Resonant tunneling diodes: models and properties," in Proceedings of the IEEE, vol. 86, no. 4, pp. 641-660, April 1998, doi: 10.1109/5.663541.
 - [22] T. Akeyoshi, H. Matsuzaki, T. Itoh, T. Waho, J. Osaka and M. Yamamoto, "Applications of resonant-tunneling diodes to high-speed digital ICs," Conference Proceedings. Eleventh International Conference on Indium Phosphide and Related Materials (IPRM'99) (Cat. No.99CH36362), 1999, pp. 405-410, doi: 10.1109/ICIPRM.1999.773719.
 - [23] D. Akinwande and H. -. P. Wong, "A Composite Circuit Model for NDR Devices in Random Access Memory Cells," in IEEE Transactions on Electron Devices, vol. 54, no. 4, pp. 776-783, April 2007, doi: 10.1109/TED.2007.892356.
 - [24] P. Mazumder, S. Kulkarni, M. Bhattacharya, Jian Ping Sun and G. I. Haddad, "Digital circuit applications of resonant tunneling devices," in Proceedings of the IEEE, vol. 86, no. 4, pp. 664-686, April 1998, doi: 10.1109/5.663544.
 - [25] K. Maezawa, T. Akeyoshi and T. Mizutani, "Functions and applications of monostable-bistable transition logic elements (MOBILE's) having multiple-input terminals," in IEEE Transactions on Electron Devices, vol. 41, no. 2, pp. 148-154, Feb. 1994, doi: 10.1109/16.277386.
 - [26] TaiHaur Kuo, Hung C. Lin, Robert C. Potter, and Dave Shupe, "Analysis of the hysteresis in the IV characteristics of vertically integrated, multi-peaked resonant-tunneling diodes", Journal of Applied Physics 68, 2496 (1990); doi: 10.1063/1.346513.
 - [27] H. C. Lin, "Resonant tunneling diodes for multi-valued digital applications," Proceedings of 24th International Symposium on Multiple-Valued Logic (ISMVL'94), 1994, pp. 188-195, doi: 10.1109/ISMVL.1994.302201.
 - [28] Agarap, A.F. (2018). Deep Learning using Rectified Linear Units (ReLU). ArXiv, abs/1803.08375.